

Solid-supported biomimetic membranes based on amphiphilic block copolymers

Inauguraldissertation

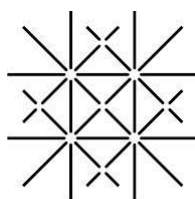
zur

Erlangung der Würde eines Doktors der Philosophie

vorgelegt der

Philosophisch-Naturwissenschaftlichen Fakultät

der Universität Basel



U N I
B A S E L

von

Justyna Kowal

aus Kraków, Polen

Basel, 2015

Original document stored on the publication server of the University of Basel

edoc.unibas.ch



This work is licenced under the agreement

„Attribution Non-Commercial No Derivatives – 3.0 Switzerland“ (CC BY-NC-ND 3.0 CH). The complete

text may be reviewed here:

creativecommons.org/licenses/by-nc-nd/3.0/ch/deed.en

Genehmigt von der Philosophisch-Naturwissenschaftlichen Fakultät auf Antrag von

Prof. Dr. Wolfgang Meier

und

Prof. Dr. Corinne Nardin

Basel, den 17. Februar 2015

Prof. Dr. Jörg Schibler

Dekan



Namensnennung-Keine kommerzielle Nutzung-Keine Bearbeitung 3.0 Schweiz
(CC BY-NC-ND 3.0 CH)

Sie dürfen: Teilen — den Inhalt kopieren, verbreiten und zugänglich machen

Unter den folgenden Bedingungen:



Namensnennung — Sie müssen den Namen des Autors/Rechteinhabers in der von ihm festgelegten Weise nennen.



Keine kommerzielle Nutzung — Sie dürfen diesen Inhalt nicht für kommerzielle Zwecke nutzen.



Keine Bearbeitung erlaubt — Sie dürfen diesen Inhalt nicht bearbeiten, abwandeln oder in anderer Weise verändern.

Wobei gilt:

- **Verzichtserklärung** — Jede der vorgenannten Bedingungen kann aufgehoben werden, sofern Sie die ausdrückliche Einwilligung des Rechteinhabers dazu erhalten.
- **Public Domain (gemeinfreie oder nicht-schützbares Inhalte)** — Soweit das Werk, der Inhalt oder irgendein Teil davon zur Public Domain der jeweiligen Rechtsordnung gehört, wird dieser Status von der Lizenz in keiner Weise berührt.
- **Sonstige Rechte** — Die Lizenz hat keinerlei Einfluss auf die folgenden Rechte:
 - Die Rechte, die jedermann wegen der Schranken des Urheberrechts oder aufgrund gesetzlicher Erlaubnisse zustehen (in einigen Ländern als grundsätzliche Doktrin des fair use bekannt);
 - Die **Persönlichkeitsrechte** des Urhebers;
 - Rechte anderer Personen, entweder am Lizenzgegenstand selber oder bezüglich seiner Verwendung, zum Beispiel für Werbung oder Privatsphärenschutz.
- **Hinweis** — Bei jeder Nutzung oder Verbreitung müssen Sie anderen alle Lizenzbedingungen mitteilen, die für diesen Inhalt gelten. Am einfachsten ist es, an entsprechender Stelle einen Link auf diese Seite einzubinden.

Table of Contents

Table of Contents.....	- 1 -
Acknowledgements.....	- 5 -
Abbreviations.....	- 7 -
1. Scope of the Thesis	- 11 -
2. Introduction.....	- 13 -
2.1. Biological membranes	- 13 -
2.2. Biomimetic membranes.....	- 14 -
2.2.1. Amphiphilic block copolymers and general aspects of self-assembly	- 14 -
2.2.2. 2D and 3D polymeric membranes	- 16 -
2.2.3. Hybrid materials	- 19 -
2.3. Langmuir monolayers.....	- 21 -
2.3.1. Langmuir technique.....	- 21 -
2.3.2. Properties of the monolayers at the air-water interface	- 22 -
2.4. Solid-supported polymer membranes.....	- 24 -
2.4.1. Strategies for planar solid-supported membranes preparation	- 24 -
2.4.2. Membranes prepared by surface-initiated polymerization	- 25 -
2.4.3. Membranes prepared by vesicle spreading.....	- 26 -
2.4.4. Membranes prepared by monolayer transfer from the air-water interface	- 29 -
2.4.5. Functionalization of solid-supported membranes.....	- 32 -
3. Results and Discussion.....	- 35 -
3.1. Surface engineering by insertion of membrane proteins into solid-supported polymer membranes.....	- 35 -
3.1.1. Polymer modification and characterization	- 36 -
3.1.2. Labeling of the protein with fluorescent dye.....	- 38 -
3.1.3. Polymer at the air water interface.....	- 41 -
3.1.4. Functionalization of the solid support with amino groups	- 44 -
3.1.5. Preparation of solid-supported membranes	- 46 -
3.1.6. Incorporation of membrane protein into polymer membrane.....	- 49 -
3.1.7. Summary.....	- 54 -

Table of Contents

3.2.	Hybrid polymer-lipid materials as platforms for directed membrane protein insertion....	- 55 -
3.2.1.	Surface pressure – area isotherms of pure amphiphiles	- 56 -
3.2.2.	Surface pressure-area isotherms of mixed monolayers.....	- 61 -
3.2.3.	Formation of domains at low surface pressures	- 64 -
3.2.4.	Formation of domains at high surface pressures.....	- 66 -
3.2.5.	Distribution of the protein in the polymer-lipid mixed film	- 69 -
3.2.6.	Summary	- 73 -
3.3.	Asymmetric triblock copolymer-based active surfaces	- 74 -
3.3.1.	Characterization of the PEG- <i>b</i> -PMCL- <i>b</i> -PDMAEMA triblock copolymer.....	- 75 -
3.3.2.	PEG- <i>b</i> -PMCL- <i>b</i> -PDMAEMA triblock copolymer at the air-water interface	- 77 -
3.3.3.	Solid-supported monolayers formed from PEG ₄₅ - <i>b</i> -PMCL ₁₀₁ - <i>b</i> -PDMAEMA _x	- 82 -
3.3.4.	Bilayers formed from PEG ₄₅ -PMCL ₁₀₁ -PDMAEMA ₂₇	- 85 -
3.3.5.	Adsorption of enzyme on PEG ₄₅ -PMCL ₁₀₁ -PDMAEMA _x films	- 87 -
3.3.6.	Generation of active surfaces	- 90 -
3.3.7.	Laccase activity assays with DMP.....	- 94 -
3.3.8.	Summary	- 95 -
4.	Conclusions and Outlook	- 97 -
5.	Materials and Methods.....	- 100 -
5.1.	Materials	- 100 -
5.2.	Methods.....	- 100 -
5.2.1.	Polymers	- 100 -
5.2.2.	Lipids	- 101 -
5.2.3.	MloK1 expression, labeling, and purification.....	- 101 -
5.2.4.	Surface-pressure – area isotherms.....	- 102 -
5.2.5.	Substrate preparation.....	- 102 -
5.2.6.	Langmuir-Blodgett (LB) and Langmuir-Schaefer (LS) transfers	- 102 -
5.2.7.	Protein incorporation.....	- 103 -
5.2.8.	Immobilization of the laccase to polymer films.....	- 103 -
5.2.9.	Activity of the immobilized enzyme.....	- 104 -
5.3.	Characterization techniques	- 104 -
5.3.1.	¹ H NMR	- 104 -
5.3.2.	Brewster angle microscope (BAM)	- 104 -
5.3.3.	Atomic force microscopy (AFM).....	- 105 -
5.3.4.	Ellipsometry	- 105 -

Table of Contents

5.3.5.	Static contact angle	- 105 -
5.3.6.	ATR-Fourier transform infrared spectroscopy (ATR-FTIR)	- 106 -
5.3.7.	Confocal laser scanning microscopy (CLSM).....	- 106 -
5.3.8.	Fluorescence correlation spectroscopy (FCS)	- 107 -
5.3.9.	Electrical conductance	- 107 -
5.3.10.	Quartz crystal microbalance with dissipation (QCM-D).....	- 107 -
5.3.11.	Circular dichroism (CD).....	- 108 -
6.	Appendix	- 109 -
7.	References	- 116 -
	Curriculum Vitae	- 128 -

Acknowledgements

There are a lot of people whom I would like to thank for their contribution to this thesis and for their support during all the time I have spent in Basel.

First of all, I want to thank my parents Alicja and Wojciech without whom, I would not be in the place in which I am today. Thank you for all the motivation, for supporting my choices, and for instilling me with lots of passions in my life.

I would especially like to thank my advisor, Prof. Dr. Wolfgang Meier for giving me the opportunity to do my PhD in his laboratories, giving me a lot of trust and freedom in my research.

I am grateful to Prof. Dr. Cornelia G. Palivan for supervising my work, for constructive discussions, and constant support and motivation.

I thank Prof. Dr. Corinne Nardin for her interest in my research and co-refereeing my PhD thesis.

Dr. Anja Car is acknowledged for careful reading of my thesis and helpful discussions. I thank Dr. Niamh Murray, for editing my thesis and for all the time we spent together, performing LB experiments. Dr. Mariana Spulber, for reading my thesis and for all the positive energy she is always sending around.

I am greatly indebted to Dr. Agnieszka Tajchert, who introduced me into “the world of monolayers”. She was irreplaceable during my first months in Basel. She helped me not only to start my projects in the lab, but also to accommodate and feel well in my new environment.

Prof. Dr. Camelia Draghici is thanked for a very profitable collaboration in the project concerning triblock copolymers. I learned a lot through our long-lasting discussions and common work. I am grateful for her strong support, faith, and all the inspiring words she could find in the moments of doubts.

I thank my sister, Dr. Julia Kowal not only for fruitful collaboration, but also for being a good example for me and for her unceasing support.

Acknowledgements

I would like to thank all the people, who were involved in my projects: Dr. Dalin Wu, Dr. Yves Matters, Viktoria Mikhalevich, Raphael Wagner, Dr. Mathias Wipf, Dr. Wangyang Fu, Dr. Xiaoyan Zhang, Dr. Katarzyna Kita-Tokarczyk, and Alina Darjan.

Many thanks go to former and present group members for the great working atmosphere. Especially I would like to thank Dr. Karolina Langowska, Juan Liu, Fabian Ite, Patric Baumann, Dr. Katarzyna Makyla, Martin Rother, Evgeniia Konisheva, Bernadetta Gajewska, Severin Sigg, and Dr. Sindhu Menon for all the help and good times we had at different stages of my PhD.

This thesis would not be possible without the support of my friends: Magda, Monika, Agata, Karolina, Ala and Ola.

I would especially like to thank Clément for his endless optimism and patience, and for all the time we have spent together.

Finally, I thank the Swiss National Science Foundation, NCCR Molecular Systems Engineering, and the University of Basel for financial support.

Abbreviations

7-ADCA	7-aminodesacetoxycephalosporanic acid
α -He	α -hemolysin
A	absorbance
AFM	atomic force microscopy
APTES	3-aminopropyltriethoxysilane
ATR-FTIR	attenuated total reflection Fourier transform infrared spectroscopy
ATRP	atom transfer radical polymerization
AUT	11-amino-1-undecanethiol hydrochloride
BAM	Brewster angle microscopy
BICINE	2-(bis(2-hydroxyethyl)amino)acetic acid
C_s^{-1}	compressibility modulus
cAMP	3',5'-cyclic adenosine monophosphate
CD	circular dichroism
$CDCl_3$	deuterated chloroform
cGMP	cyclic guanosine monophosphate
CLSM	confocal laser scanning microscopy
CMC	critical micelle concentration
CNBD	cyclic nucleotide binding domain
d	thickness
DM	<i>n</i> -decyl- β -D-maltopyranoside
DMP	2,6-dimethoxyphenol
DMF	dimethyl formamide
DMSO	dimethyl sulfoxide
DOPC	1,2-dioleoyl- <i>sn</i> -glycero-3-phosphocholine
DOPS	1,2-dioleoyl- <i>sn</i> -glycero-3-phospho-L-serine
DOTAP	N-[1-(2,3-dioleoyloxy)]-N,N,N-trimethylammonium propane
DPPC	1,2-dipalmitoyl- <i>sn</i> -glycero-3-phosphocholine
DPPE	1,2-dipalmitoyl- <i>sn</i> -glycero-3-phosphoethanolamine

Abbreviations

f	frequency
FCS	fluorescence correlation spectroscopy
G	electrical conductance
GPC	gel permeable chromatography
HOPG	highly ordered pyrolytic graphite
I	electrical current
L	liquid (state)
LB	Langmuir-Blodgett (transfer)
LC	liquid-condensed (state)
LE	liquid-expanded (state)
LS	Langmuir-Schaefer (transfer)
k	extinction coefficient
MCL	γ -methyl- ϵ -caprolactone
MloK1	cyclic nucleotide-modulated potassium channel
M_n	number average molecular weight
M_w	weight average molecular weight
Mma	mean molecular area
MWCO	molecular weight cut-off
n	refractive index
NaN ₃	sodium azide
NHS	<i>N</i> -hydroxysuccinimide
NMR	nuclear magnetic resonance
OmpA	outer membrane protein A
OmpF	outer membrane protein F
Π	surface pressure
P	molecular packing parameter
PBMA	poly(<i>n</i> -butyl methacrylate)
PBO	poly(butylene oxide)
PBS	phosphate-buffered saline
PDMAEMA	poly(2,2-dimethylaminoethyl methacrylate)
PDI	polydispersity index

Abbreviations

PDMS	poly(dimethylsiloxane)
PEG	poly(ethylene glycol)
PEO	poly(ethylene oxide)
PGME	phenylglycine methyl ester
PHEMA	poly(2-hydroxyethyl methacrylate)
PLA	poly(L-lactic acid)
PMCL	poly(γ -methyl- ϵ -caprolactone)
PMOXA	poly(2-methyl-2-oxazoline)
POPC	1-palmitoyl-2-oleoyl- <i>sn</i> -glycero-3-phosphocholine
POPE	1-palmitoyl-2-oleoyl- <i>sn</i> -glycero-3-phosphoethanolamine
PVP	poly(2-vinylpyridine)
QCM-D	quartz crystal microbalance with dissipation
R _a	average roughness
ROP	ring-opening polymerization
S	solid (state)
SDS-PAGE	sodium dodecyl sulfate polyacrylamide gel electrophoresis
SPR	surface plasmon resonance spectroscopy
SRB	sulforhodamine B
SUV	small unilamellar vesicles
T	temperature
TMS	trimethylsilane
Tris	2-amino-2-hydroxymethyl-propane-1,3-diol
UV/Vis	ultraviolet-visible spectrophotometry
V	voltage

1. Scope of the Thesis

Planar artificial membranes based on amphiphilic block copolymers are of high interest due to their potential applications in catalysis, drug screening, sensing, *etc.* Such polymeric membranes can successfully mimic biological membranes, providing high robustness and stability, which makes them good candidates to be developed in direction of applications. Even though solid-supported polymer membranes have been already investigated to a certain extent, it is still an emerging area.

This thesis presents a new generation of biomimetic solid-supported membranes and hybrid polymer-lipid materials, based on amphiphilic block copolymers: poly(dimethylsiloxane)-*block*-poly(2-methyl-2-oxazoline) (PDMS-*b*-PMOXA) and poly(ethylene glycol)-*block*-poly(γ -methyl- ϵ -caprolactone)-*block*-poly[(2-dimethylamino) ethyl methacrylate] (PEG-*b*-PMCL-*b*-PDMAEMA). The scope was preparation of stable solid-supported membranes and development of different strategies for insertion/attachment of biomolecules into such membranes.

These main goals of the thesis were approached through:

- i) development of solid-supported membranes having bilayer, hydrophilic-hydrophobic-hydrophilic structure,
- ii) functional insertion of membrane protein into such polymer membrane,
- iii) investigation of protein distribution in hybrid materials composed of mixture of polymer and lipid,
- iv) preparation of asymmetric polymer films with adsorbed active enzyme for potential applications in sensing.

Block copolymers were firstly investigated in respect of behavior at the air-water interface. Deposition of the films on different solid supports (silica wafers, glass and gold slides) was achieved by performing transfers of Langmuir monolayers, which provide formation of defect-free films with good reproducibility. Further, deposited films were functionalized by introduction of membrane proteins and enzymes. To get the insights into morphology and thickness, the obtained systems were analyzed by surface-sensitive techniques, such as atomic force microscopy, ellipsometry, and contact angle

measurements. Activity of inserted biomolecules was evaluated by electrical conductance measurements and activity assays.

In summary, this thesis provides valuable impact in the preparation of membranes in a controllable and reproducible way. Furthermore, it presents different strategies for introduction of biomolecules into such systems, in order to obtain tailored functionality and properties. This work impact fundamental understanding and development of functional membranes. Such artificial membranes and hybrid materials can be further adapted for potential applications.

2. Introduction

2.1. Biological membranes

A biological membrane is a complex structure, which is essential for all living organisms. Membranes separate the interior of the cells and cell organelles from their environment. They are also involved in a number of important processes, such as passive and active transport through the membrane, molecular recognition, enzymatic catalysis, cell signaling, and cell adhesion.¹

In 1972 Singer and Nicolson introduced the fluid mosaic model of the cell membrane.² According to this model a main structural element of the membrane is a self-assembled phospholipid bilayer (Figure 2.1-1). The phospholipids are organized in such a way that the hydrophilic head groups are oriented towards intracellular and extracellular spaces, while the fatty acid chains face each other in order to isolate them from the surrounding environment. The formation of the bilayer is driven by strong hydrophobic interactions between nonpolar fatty acid chains.³ In addition, the cell membrane consists also of proteins and oligosaccharides however the exact composition of the membrane depends critically on its functions.

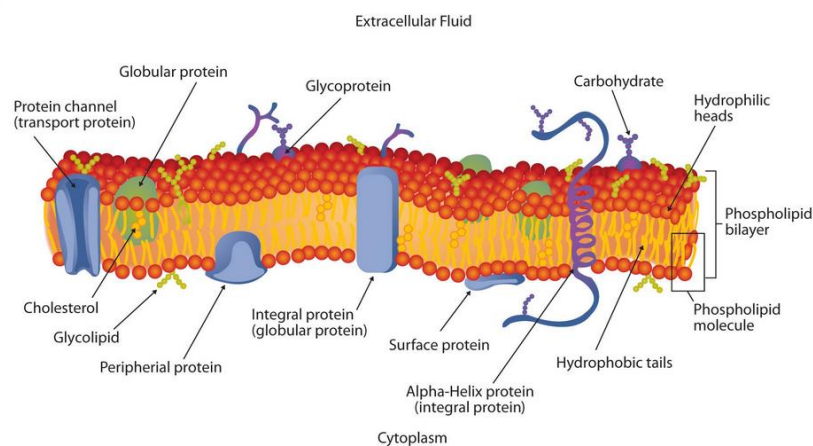


Figure 2.1-1. Fluid mosaic model of cell membrane.⁴

Membranes are the scope of many studies nowadays in order to understand the functions of membrane proteins and individual membrane-related processes.

Transmembrane proteins are important targets for drugs however because of the hydrophobicity of these proteins, the studies have to be performed in their natural environment, which is a membrane. Due to the high complexity, it has not yet been possible to reconstruct an artificial membrane with equal functionality to the biological membrane. In order to facilitate the investigation of the membrane-related processes, membrane mimics have been developed. Such artificial membranes can also find industrial applications, *e.g.*, in medicine as drug carriers, or in technology as biosensors.^{5,6}

2.2. Biomimetic membranes

2.2.1. Amphiphilic block copolymers and general aspects of self-assembly

The most common biomimetic membranes have been prepared from phospholipids due to the fact that they are components of the biological membranes, thus they are biocompatible, biodegradable, and non-toxic.⁷ On the other hand, the phospholipidic membranes suffer some limitations, *i.e.* high permeability, low stability of phospholipids, which sometimes undergo oxidation, and limited possibilities of chemical modifications.^{7,8} Amphiphilic block copolymers have been shown to overcome these limitations. Thanks to their higher molecular weights, the membranes formed by block copolymers are thicker and thus more stable, less fluid, and less permeable (Figure 2.2-1).^{9,10}

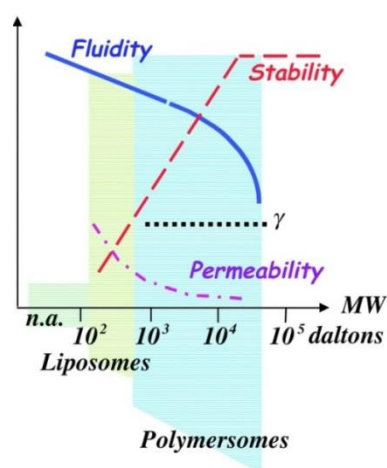


Figure 2.2-1. Schematic representation of membrane properties versus molecular weight of the amphiphile.¹⁰

Through polymer engineering, it is possible to design properties of the resulting polymer, and thus the thickness of the membrane, shape of the formed assemblies, and stimuli-responsiveness can be tuned.^{11,12} A number of block copolymers have been already reported to form membrane mimics.¹³ Typically, such artificial membranes are formed by amphiphilic diblock (AB) or triblock (ABA or ABC) copolymers,^{10,12} which possess the necessary biocompatibility for biological applications. For example, poly(2-methyl-2-oxazoline)-*block*-poly(dimethylsiloxane)-*block*-poly(2-methyl-2-oxazoline) (PMOXA-*b*-PDMS-*b*-PMOXA) triblock copolymer is a good candidate to mimic biological membranes.¹⁴⁻¹⁷ The hydrophobic PDMS block is suitable for development of biomaterials due to its biocompatibility, non-toxicity, and high flexibility.¹⁸ Furthermore, PMOXA is a bioinspired polymer, which has a structure similar to polypeptides.¹⁹ Thanks to the presence of the tertiary amine in the backbone chain, it is poorly recognizable by enzymes and thus it is highly stable in biological environments.²⁰

Formation of membranes is possible by self-assembly process in aqueous media. At certain concentration, which is called the critical micelle concentration (CMC), amphiphile molecules self-assemble into a large array of structures, *e.g.* micelles, vesicles, or worm-like structures, in order to minimize the free energy of the system and reach thermodynamic equilibrium.²¹⁻²³ This process is driven by the hydrophobic effect, in which the hydrophobic part of the amphiphile withdraws in order to reduce contact with the aqueous solution.¹¹ Several factors influence the self-assembly, such as i) geometry, chemical composition, molecular weight, and polydispersity index of the amphiphile, ii) preparation method, and iii) external factors (pH, solvent, temperature).²⁴ The shape of the resulting structures depends strongly on the ratio of the hydrophilic to the hydrophobic part of the amphiphile,²⁵ and it can be predicted from the molecular packing parameter (P), which is defined as:

$$P = \frac{v_o}{al_o} \quad (1)$$

Where v_o and l_o is the volume and length of the hydrophobic tail, and a is an optimal area of the hydrophilic head group.^{11,26} The dimensionless value of P characterize the morphology of the self-assemblies: spherical micelle ($0 < P \leq 1/3$), cylindrical micelle ($1/3 < P \leq 1/2$), or bilayer structure, such as vesicle ($1/2 < P \leq 1$).^{26,27}

2.2.2. 2D and 3D polymeric membranes

Various biomimetic membranes have been developed. When considering the shape, they can be divided into two general groups, *i.e.* planar membranes and spherical compartments. Due to different properties and architecture, each model has its advantages and limitations, and can find different applications.⁶ The group of planar membranes (2D) include: i) Langmuir monolayers at the air-water interface,²⁸ ii) freestanding membranes,²⁹ and iii) solid-supported membranes (Figure 2.2-2).³⁰

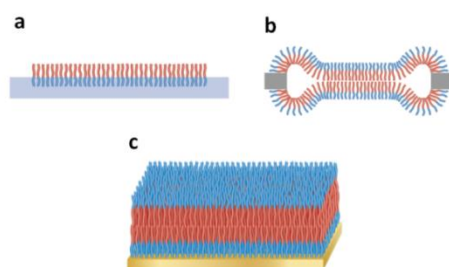


Figure 2.2-2. Models of planar membranes: (a) Langmuir monolayer, (b) freestanding membrane, and (c) solid-supported membrane.

Freestanding membranes have both sides of the membrane accessible. This is why they are appropriate for studying the protein insertion mechanism and functions of the proteins. Since a pristine membrane is known to be a perfect insulator, the insertion of the membrane protein can be monitored by change in the conductance of the system.^{31,32} The disadvantage of freestanding membranes is their low stability due to the limited lateral tension.³³ This may lead to membrane rupture and thus make them less attractive for technological applications. The research of freestanding membranes is then focused on the fundamental understanding of membrane interactions with proteins.³⁴

Langmuir monolayers and solid-supported membranes will be described in detail in sections 2.3 and 2.4, respectively.

Two representatives of the 3D spherical compartments are vesicles and micelles (Figure 2.2-3).^{21,35}

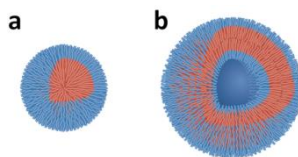


Figure 2.2-3. Models of spherical compartments: (a) micelle and (b) vesicle.

Vesicles are hollow spherical structures, which can be used as cavities for encapsulation and transport of compounds, such as enzymes, proteins, or drugs. They possess a lot of advantages, *e.g.* they protect encapsulated molecules from external stimuli, and transport the encapsulated molecules into cells.³⁶ Depending on the hydrophilic/hydrophobic ratio, vesicles formed by PDMS-*b*-PMOXA diblock copolymers could result in different membrane thicknesses and different dimensions.²⁴ For copolymers having the same hydrophilic/hydrophobic ratio, the molecular weight of the PDMS block was a decisive factor influencing self-assembly, *i.e.* when low M_w PDMS was used (1.3 kDa) formation of nanoparticles and micelles could be observed instead of vesicles.

The properties of the vesicles can be tuned by choosing appropriate composition and decoration of the vesicle surface with specific ligands. One way to make the wall of the vesicle permeable is insertion of membrane protein. Such a permeable vesicle with encapsulated enzyme, is called a nanoreactor and allows production of active compounds *in situ*.³⁷ Thanks to this strategy the active compounds can be produced in a controlled way and on demand.^{17,38} Number of membrane proteins have been successfully inserted into the membrane of polymeric vesicles, *e.g.* Complex I,¹⁵ OmpF,¹⁷ or gramicidin.³⁹ For instance, vesicles formed from PMOXA-*b*-PDMS-*b*-PMOXA with incorporated bacterial porin OmpF were used to encapsulate an enzyme penicillin acylase. Due to the presence of pores in the membranes the substrates (7-aminodesacetoxycephalosporanic acid, 7-ADCA, and phenylglycine methyl ester, PGME) could enter the nanoreactors and cephalexin was produced.¹⁷ Additionally, these nanoreactors have been covalently attached on a solid support resulting in self-defending surfaces, inhibiting the growth of bacteria (Figure 2.2-4).⁴⁰

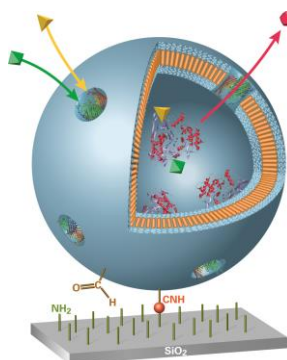


Figure 2.2-4. Scheme of enzymatically active, immobilized nanoreactors synthesizing antibiotics. Encapsulated enzyme is catalyzing the conversion of 7-ADCA and PGME into cephalixin.⁴⁰

Most polymer membranes are symmetric, being formed by the self-assembly of AB or ABA amphiphilic block copolymers however, in order to perform a directional membrane protein insertion/attachment, or to generate membranes with a different specificity at each surface, asymmetric triblock copolymers, ABC, represent ideal candidates. For example, it has been shown that PEO-*b*-PDMS-*b*-PMOXA triblock copolymer could form vesicles with different hydrophilic block directed toward the outside of the vesicle, depending on the length of PEO and PMOXA.⁴¹ The asymmetry of the polymer membrane was a key factor favoring the functionality of Aquaporin 0 with the desired orientation.⁴²

Micelles have a characteristic core-shell structure, in which the core is hydrophobic and the shell – hydrophilic. Even though, they do not exhibit membrane's structure, they find application as hydrophobic molecule carriers, *e.g.* for drug delivery.³⁵ In contrast to vesicles, poorly water soluble drugs can be accommodated in the hydrophobic core of the micelle, and then delivered and released at the specified area of the body.²² Encapsulation of the drug not only increases its solubility, but also provides protection and minimizes side effects. The release can take place by slow degradation of the micelle upon reaction to some stimuli (pH, temperature), or by conjugation with some antibody.⁴³ Thanks to the small size of these systems (< 100 nm) micelles can circulate in the organism for a long time without being recognized by proteins or phagocytic cells.⁴³

2.2.3. Hybrid materials

Hybrid materials composed of phospholipids and amphiphilic block copolymers are considered as another type of membrane mimic. Hybrid materials blend the robustness of the amphiphilic block copolymers with biocompatibility of the phospholipids.⁴⁴ These systems are particularly interesting for fundamental studies of interactions between specific components of the membranes. By modulating the composition of such mixtures, desired properties of the material can be obtained, and interactions between hybrid materials and biological membranes can be controlled.⁸ Such mixed systems can be developed further by introduction of the biomolecules and depending on the mixture composition the number and distribution of such biomolecules can be regulated. The most interesting approach in hybrid materials is formation of membrane mimics with lipid “raft-like” domains, which occur in biological membranes, and are known to participate in important processes, such as lateral protein organization, virus uptake, or membrane tension regulation.⁴⁵

Different morphologies of the hybrid materials can be obtained, depending on the components used and molar composition of the mixture.^{8,46,47} For example, Chemin et al. studied mixing of poly(ethylene glycol)-*grafted*-poly(ethylene oxide) (PEG-*g*-PEO) diblock copolymer with saturated 1,2-dihexadecanoyl-*sn*-glycero-3-phosphocholine (DPPC) and 1-palmitoyl-2-oleoyl-*sn*-glycero-3-phosphocholine (POPC) having one unsaturated hydrocarbon chain (Figure 2.2-5).⁴⁴ In mixtures of PEG-*g*-PEO with DPPC domains formation could be observed, when polymer content ranged from 50 to 80%. At polymer content higher than 80% homogeneous vesicles were formed. In mixtures where polymer (≥ 60 mol%) was mixed with POPC, lipid was homogeneously distributed within the vesicle however when lipid was a major component of the mixture, the hybrid vesicles tended to form separated polymersomes and liposomes within few hours.

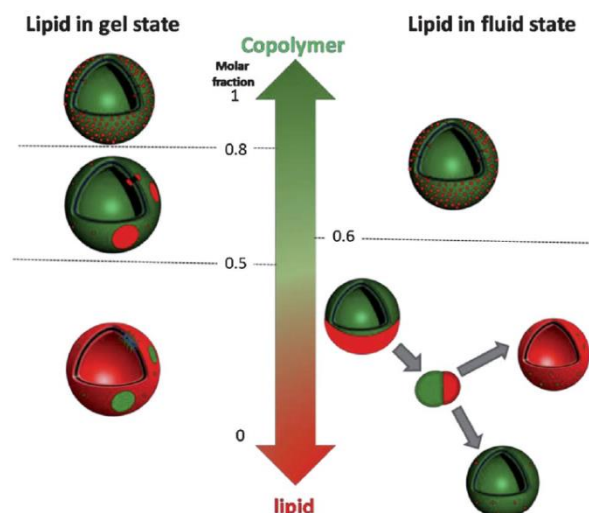


Figure 2.2-5. Schematic of hybrid vesicles, formed by PEG-*g*-PEO mixed with DPPC (lipid in gel state) or POPC (lipid in fluid state), according to the molar composition and fluidity of the lipid at room temperature.⁴⁴

It is of high importance to control not only domain formation but also insertion of the active compounds into such hybrid membranes, *e.g.* proteins, in order to obtain materials of desired biocompatibility, properties, and functions. By incorporation of the membrane protein into heterogeneous membrane, the location and concentration of the protein can be controlled, which enables modulation of the membrane permeability and biocompatibility.^{44,48,49} Schulz et al. have demonstrated, that hybrid materials composed of poly(ethylene oxide)-*block*-poly(butylene oxide) (PEO-*b*-PBO) and ganglioside-functionalized DPPC can be successfully used for molecular recognition of the cholera toxin B, which binds specifically to ganglioside.⁵⁰ The mixture composition played a crucial role when binding the protein to mixed vesicles. In this work, a hybrid material served as the model for studying receptor/ligand recognition, due to its biofunctionality and possibility to tune the organization of the components in the mixture.⁵⁰ The protein attachment was driven by interaction with a specific receptor, thus it was not spontaneous.

Thoma et al. were the first to investigate the interactions between a binary mixture of PMOXA-*b*-PDMS-*b*-PMOXA and DPPC with the outer membrane protein F (OmpF), and showed that OmpF distributed preferentially in the polymer-rich phase,⁵¹ which is the first step in development of controlled multicomponent materials. However no further systematic investigation was performed on this process.

2.3. Langmuir monolayers

2.3.1. Langmuir technique

The Langmuir technique, in its simplicity, gives great possibilities to investigate the behavior of water insoluble molecules at the air-water interface and enables investigation of interactions between amphiphilic molecules at the air-water interface. Langmuir monolayers are considered the simplest model of the biological membrane, since they represent only one membrane leaflet.

Benjamin Franklin was the first to report scientifically the phenomenon of oil monolayer formation at the water surface in 1774.⁵² However, the mechanism of monolayer formation and organization of molecules at the air-water interface has been developed by Irving Langmuir, who is considered to be the father of this technique.^{53,54}

The typical experiment concerning monolayer formation is performed with an apparatus called a Langmuir trough. This instrument consists of: i) hydrophobic Teflon trough, which is filled with an aqueous subphase, *e.g.* water, or buffer, ii) two movable, hydrophilic barriers, and iii) surface pressure sensor, *i.e.* Wilhelmy plate. To form a monolayer at the air-water interface the solution of amphiphile, prepared in a water-immiscible and volatile solvent (*e.g.* chloroform), is spread on the water surface, the solvent is allowed to evaporate, and then the movable barriers close, inducing the Langmuir monolayer formation. A recording of the monolayer compression is usually presented as a surface pressure-area isotherm (Figure 2.3-1). In the beginning of the compression, the surface pressure corresponding to 0 mN m⁻¹ means that no interactions between amphiphile molecules occur and that the molecules are in the gaseous state. Upon barrier compression, the trough's area decreases and molecules start to interact with each other forming, respectively, a monolayer at the liquid-expanded (LE), liquid-condensed (LC) and condensed (solid, S) states.²⁸ At the moment when molecules are fully packed and no more free space between molecules is available, the monolayer collapses and a multilayer is formed.⁵⁵ The isotherm provides information about formation, stability, and state of the monolayer, and about reorganization of the molecules during the compression.⁵⁶

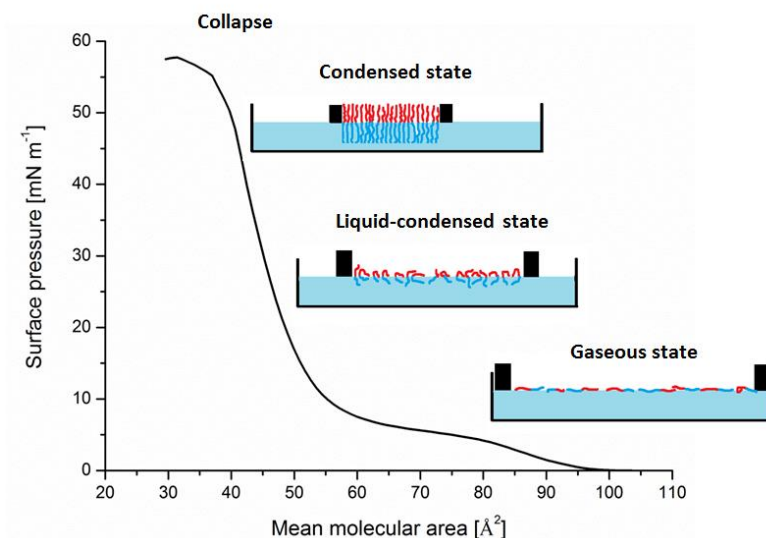


Figure 2.3-1. Surface pressure-area isotherm of DPPC and the monolayer states during the compression (blue color corresponds to hydrophilic part of the molecule, and red – to hydrophobic).

2.3.2. Properties of the monolayers at the air-water interface

A characteristic of the monolayer defines the shape of the isotherm and this depends on different factors, like experimental conditions (temperature, pH, and subphase), or size and structure of the molecule building the monolayer. It has been shown that monolayers formed by a compound bearing polar groups differ from each other depending on pH of the subphase. For example, fatty acids become ionized by increasing the pH, resulting in repulsive interactions between the molecules, which leads to expansion and stability decrease of monolayer.⁵⁷ Length of the chain and degree of saturation are other criteria that influence monolayer formation. With increasing carbon chain length, an increase in van der Waals interactions between the chains can be observed which results in a more packed and stable monolayer.⁵⁸ The presence of the double bond in the hydrocarbon chain of the amphiphile limits the flexibility of the chain and decreases adhesion between two molecules. It results in higher lift-off area and a lower condensation of the monolayer, comparing to saturated analogues, which is due to the bigger space occupied by the unsaturated molecule.⁵⁹ The isotherms of saturated DPPC and unsaturated 1,2-dioleoyl-*sn*-glycero-3-phosphocholine (DOPC) show clearly the influence of double bonds on the isotherm shape (Figure 2.3-2). DPPC has a lift-off area at mean molecular area of 97 \AA^2 ,

while that for DOPC is at 125 \AA^2 . Additionally, the lower condensation of DOPC monolayer is represented by a collapse point at a much higher mean molecular area as well as by lower surface pressure of the collapse point, which indicates lower stability of this monolayer.^{60,61}

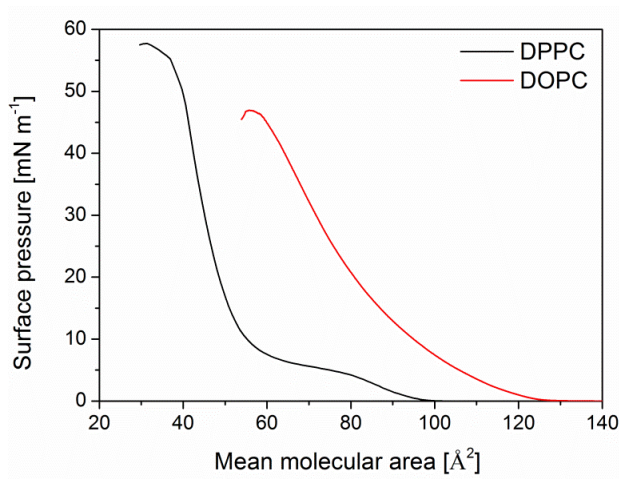


Figure 2.3-2. Comparison of surface pressure-area isotherms of DPPC (in black) and DOPC (in red).

The surface pressure-area isotherms provide information about phase transitions of the monolayer at the air-water interface,⁵⁶ which are expressed by the change of the isotherm's slope. The phase transition depends strongly on the amphiphile's character and does not have to take place instantaneously. For instance, the isotherm of DPPC represents a plateau at surface pressures ranging from 4 to 7 mN m^{-1} , corresponding to a change of the monolayer state from liquid-expanded to liquid condensed state.⁶² In both of these states the monolayer is uniform and continuous however in LE state most of the molecules are organized horizontally and in LC – vertically. Plateaus can be also observed during compression of high molecular weight amphiphilic block copolymers. The plateau formation is due to the rearrangement of the molecules during monolayer compression, like stretching of the hydrophobic and hydrophilic block and formation of the densely packed film.⁶³ It was shown that depending on the hydrophobic and hydrophilic blocks' lengths, the plateau can be more or less pronounced.^{64,65}

The state of the monolayer at the air-water interface depends on the condensation degree and can be established by calculations of compressibility modulus, which is defined as:

$$C_s^{-1} = -A \left(\frac{\partial \pi}{\partial A} \right)_T \quad (2)$$

Where A is the mean molecular area ($\text{\AA}^2/\text{molecule}$), π is the surface pressure (mN mol^{-1}), and T is the temperature ($^{\circ}\text{C}$).⁶⁶ Depending on the C_s^{-1} value following states of the monolayer can be distinguished: gaseous ($C_s^{-1} = 0 - 10 \text{ mN m}^{-1}$), liquid-expanded ($C_s^{-1} = 10 - 50 \text{ mN m}^{-1}$), liquid ($C_s^{-1} = 50 - 100 \text{ mN m}^{-1}$), liquid-condensed ($C_s^{-1} = 100 - 250 \text{ mN m}^{-1}$), and solid ($C_s^{-1} > 250 \text{ mN m}^{-1}$). Note, that not all molecules form monolayers at the solid state and it depends strictly on the molecule structure.

2.4. Solid-supported polymer membranes

2.4.1. Strategies for planar solid-supported membranes preparation

Development of solid-supported membranes is of high interest, since it enables investigation of biological membrane-related processes. Deposition of the membrane allows biofunctionalization of the inorganic solids for formation of ultrathin electric-resistant layers and design of biosensors.³⁰ The solid support provides increased stability of the membrane and in addition, the membrane can be characterized by surface sensitive-techniques, which is not possible in the case of other membrane models.⁶⁷

Two main approaches for preparation of the solid-supported films can be distinguished: *grafting from* and *grafting to* strategies (Figure 2.4-1). *Grafting from* strategy involves surface-initiated polymerization. This method provides good control over the brush thickness and homogeneity.⁶⁸ In *grafting to* strategy, the prefabricated polymer is deposited on the surface either by electrostatic interactions (physisorption) or formation of a covalent bond between the modified end-group and the surface (chemisorption).⁶⁹ The advantage of this method is its simplicity, *i.e.* it does not involve elaborate synthetic procedures.⁷⁰ On the other hand, this strategy suffers some limitations, like difficulty to obtain a densely packed and thick polymer film due to the steric repulsions between polymer chains.³⁴

In order to prepare ordered, membrane-like systems having discrete hydrophilic-hydrophobic-hydrophilic regions two other techniques, which can be attributed to the *grafting to* approach, have been applied, *i.e.* spreading of the vesicles on the surface, and transfer of the monolayers from the air-water interface.⁷¹ These two techniques as well as *grafting from* method will be described in more details in the following sections.

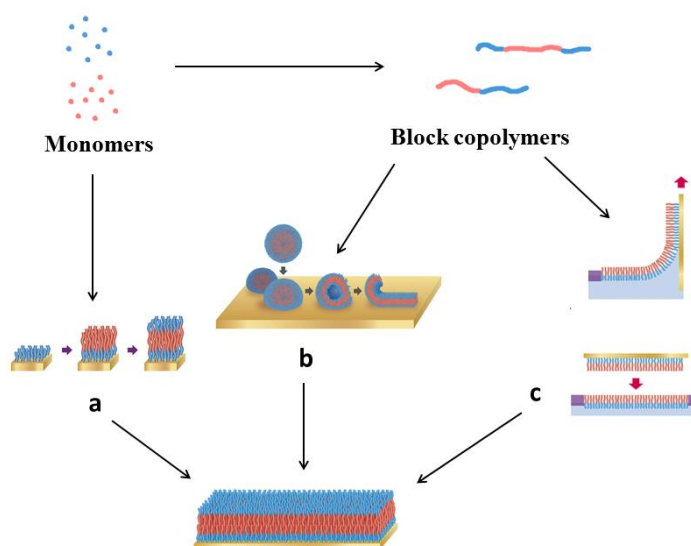


Figure 2.4-1. Strategies for preparation of solid-supported membranes: (a) surface-initiated polymerization (*grafting from* approach), (b) vesicles spreading (*grafting to* approach), and (c) Langmuir-Blodgett and Langmuir-Schaefer transfers (*grafting to* approach).³⁴

2.4.2. Membranes prepared by surface-initiated polymerization

Membranes grafted from the surface consist of amphiphilic triblock copolymers, where a middle block is hydrophobic and peripheral blocks are hydrophilic. Such polymer membranes can be prepared, for example, by surface-initiated atom transfer radical polymerization, which provides a good control over the brush thickness.^{69,72} Rakhmatullina et al. were the first to present the synthesis of a biomimetic membrane, composed of poly(2-hydroxyethyl methacrylate)-*block*-poly(*n*-butyl methacrylate)-*block*-poly(2-hydroxyethyl methacrylate) (PHEMA-*b*-PBMA-*b*-PHEMA) triblock copolymer, from a gold surface.⁷³ Attenuated total reflection Fourier transform infrared spectroscopy (ATR-FTIR) measurements proved the growth of the brush, which was confirmed by

thickness measurements by ellipsometry. It was shown that length of each block can be modulated by change of the reaction time. PHEMA-*b*-PBMA-*b*-PHEMA brush showed to be responsive to the solvents in which it was placed as established by atomic force microscopy (AFM) (Figure 2.4-2). In ethanol, which is a good solvent for both blocks, the polymer chains stretched and formed a homogeneous brush. Incubation in the hexane, having different polarity than ethanol, induced the reorganization of the polymer chains in this way, that hydrophobic PBMA block was exposed toward hexane, resulting in a more rough and rippled surface.

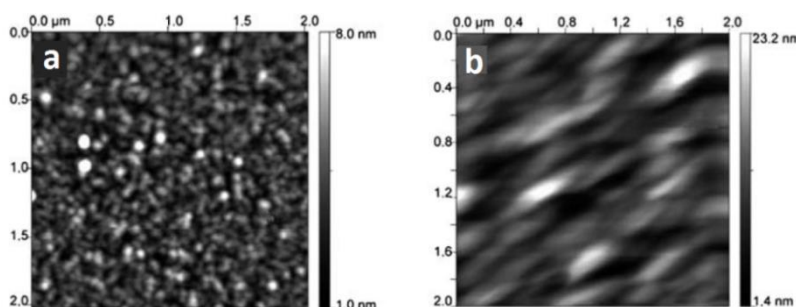


Figure 2.4-2. AFM analysis of triblock copolymer brushes treated with (a) ethanol, and (b) hexane.⁷³ Size of images is 2 x 2 μm^2 .

Even though this technique provides a good control over the brush density and thickness, and enables obtaining structures resembling biological membranes, the polymer chains are attached covalently to the surface. They have low lateral mobility, which reduces the possibility of protein insertion.⁷¹ In order to overcome this limitation, other techniques, such as vesicle spreading or transfer of monolayer from air-water interface, have been applied for biomimetic membrane preparation.

2.4.3. Membranes prepared by vesicle spreading

Vesicle spreading is a straightforward method to obtain solid-supported membranes and it is commonly used for preparation of solid-supported lipid membranes.⁷⁴⁻⁷⁷ However, only few reports concerning polymer vesicles spreading on solid supports can be found,^{78,79} due to the emergence of this research area. The advantage of this technique is the possibility of obtaining a membrane consisting of two layers (a bilayer) if spread

vesicles were formed by phospholipids or diblock copolymers. In addition, formation of the membrane can be monitored by techniques such as surface plasmon resonance spectroscopy (SPR),⁷⁸ or by quartz crystal microbalance with dissipation (QCM-D).⁸⁰

Different parameters are influencing membrane formation, *e.g.* vesicle size, temperature, osmotic pressure, and choice of solid support.⁷⁷ By finding appropriate conditions for spreading, homogeneous membranes can be formed. For example, it was shown that the charge of the phospholipid and its interactions with the slightly anionic silica support determines the deposition pathway (Figure 2.4-3).⁷⁶ Positively charged small unilamellar vesicles (SUVs) formed by N-[1-(2,3-dioleoyloxy)]-N,N,N-trimethylammonium propane (DOTAP) spread directly on the substrate forming bilayer discs, which after continuous exposure to liposomes coalesced. Negatively charged vesicles, formed by 50% of 1,2-dioleoyl-*sn*-glycero-3-phosphocholine (DOPC) and 50% of 1,2-dioleoyl-*sn*-glycero-3-phospho-L-serine (DOPS), attached to the substrate, but did not rupture. Slightly negatively charged vesicles (20% of DOPS and 80% of DOPC) first attached to the surface and then collapsed to form an uniform membrane.

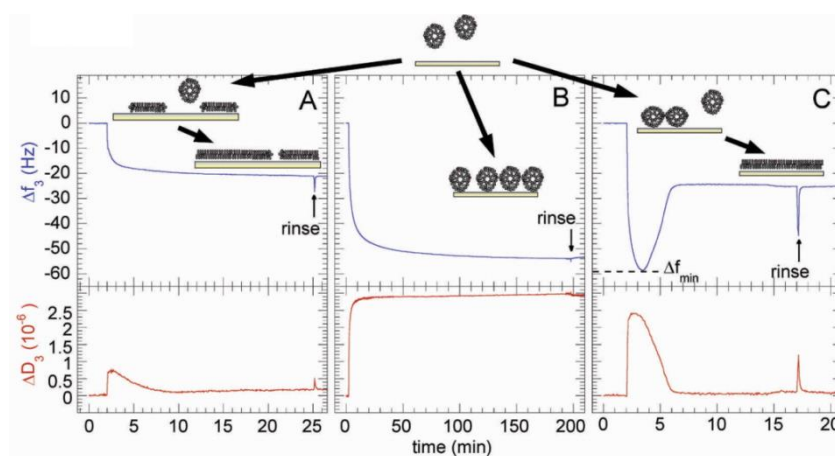


Figure 2.4-3. QCM-D data presenting deposition of SUVs on the silica substrate. The SUVs were formed by: (a) positively charged phospholipid, DOTAP, (b) 50% zwitterionic DOPC and 50% negatively charged DOPS, and (c) 80% DOPC and 20% DOPS.⁸¹

Rakhmatullina et al. were the first to investigate the interactions of poly(2,2-dimethylaminoethyl methacrylate)-*block*-poly(*n*-butyl methacrylate)-*block*-poly(2,2-dimethylaminoethyl methacrylate) (PDMAEMA-*b*-PBMA-*b*-PDMAEMA) triblock copolymers with three different surfaces, *i.e.* highly ordered pyrolytic graphite (HOPG),

silicon oxide, and mica.⁷⁹ Mica is a strongly hydrophilic and negatively charged substrate,⁸² while silicon oxide is weakly anionic.⁸³ HOPG is known to be hydrophobic and chemically inert.⁸⁴ Since the PDMAEMA block is a polycation, the surface of the vesicles formed from PDMAEMA-*b*-PBMA-*b*-PDMAEMA triblock copolymer is positively charged and thus different interactions with each substrate were observed (Figure 2.4-4).

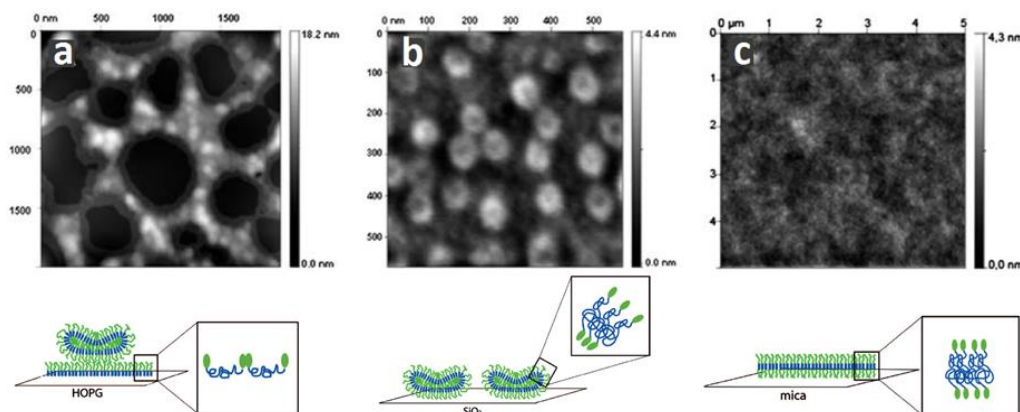


Figure 2.4-4. Organization of PDMAEMA-*b*-PBMA-*b*-PDMAEMA triblock copolymer on the: (a) HOPG substrate, (b) silicon oxide substrate, and (c) freshly cleaved mica.⁷⁹

On a HOPG substrate, the polymer attached to the substrate through the hydrophobic PBMA block and formed an inhomogeneous film. On the top of this film some collapsed vesicles could be found. Since the silicon oxide substrate is weakly anionic, intact vesicles attached to the substrate and after drying they collapsed and formed bigger aggregates. Only when spreading on freshly cleaved mica, formation of a stable and homogeneous membrane could be observed, which was due to the strong electrostatic interactions between negatively charged mica and positively charged vesicles. Different polymer organization could be obtained depending on substrate properties, and due to strong electrostatic interactions, solid-supported polymer membranes could be obtained. However, when considering biological applications this particular system would not be suitable, due to the toxicity of cationic PDMAEMA block. This is why Dorn et al. studied spreading of vesicles formed by the poly(butadiene)-*block*-poly(ethylene oxide) (PB-*b*-PEO) diblock copolymer.⁷⁸ The vesicle spreading was accompanied by investigation of covalent interactions between lipic acid-functionalized PB-*b*-PEO and gold substrate.

Since the vesicles were formed by diblock copolymers after spreading on the surface authors expected to obtain a solid-supported bilayer. Only the bottom layer was attached covalently to the gold substrate, whereas a second layer was attached by hydrophobic interactions. Such a system is more similar to the biological membrane and makes the membrane more fluid, than the one formed by a triblock copolymer. The vesicle spreading was performed in the solution containing 1.4 M NaCl and at a temperature of 45 °C, which resulted in a membrane of high homogeneity (Figure 2.4-5). Quick rinsing with salt solution, drying, and consecutive rehydration, increased the homogeneity of the bilayer however some additional polymer aggregates attached to the bilayer surface could be still observed. The SPR and force/distance (AFM) measurements showed the thickness of the bilayer to be approximately 14 nm, which was in good agreement with previously reported data.⁸⁵

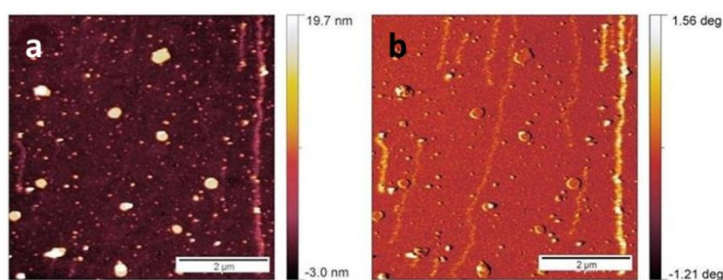


Figure 2.4-5. AFM (a) height and (b) phase images of polymer bilayer formed by vesicle spreading in 1.4 M NaCl and at 45 °C.⁷⁸ Scale bars: 2 μm.

2.4.4. Membranes prepared by monolayer transfer from the air-water interface

Transfers of the monolayers from the air-water interface form homogeneous and defect-free membranes. The advantage of this method is a high control over the surface pressure of the transferred monolayer (thus density of the monolayer) and no substrate size restrictions. The Langmuir-Blodgett (LB) technique enables deposition of more than one layer on a solid support. Depending on the deposition strategy, different multilayer preparation types can be distinguished: X-, Y-, and Z- type (Figure 2.4-6). Successive emersion and immersion of the substrate, corresponding to Y-type deposition, results in the formation of a head-to-head and tail-to-tail multilayer structure.⁵⁶ Multilayers can also

be formed by multiple immersions (X-type) or emersions (Z-type) of the substrate. However, very often the interactions between two monolayers are not strong enough to induce desorption of the monolayer from the water surface, precluding the method of monolayer transfer.⁸⁶ To overcome this problem, Langmuir-Schaefer (LS) deposition technique can be applied.

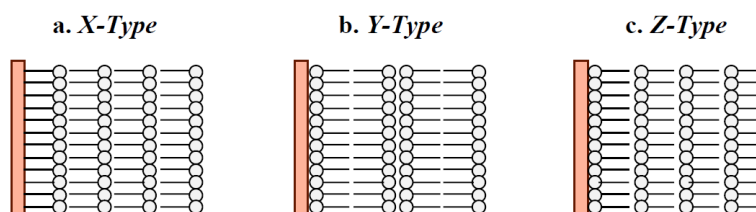


Figure 2.4-6. Strategies for multilayer deposition on a hydrophilic substrate by LB technique.⁵⁶

Formation of the membranes involves two transfers, *i.e.* LB and LS transfers (Figure 2.4-7). In LB transfers the substrate is dipped out from the water allowing attachment of the Langmuir film to the substrate with the hydrophobic part of the molecule.⁸⁷ LS transfers allow building of the second upper layer of the membrane by dipping a horizontally placed substrate, with the deposited first layer, into the subphase. Combination of LB and LS techniques allow construction of asymmetric multilayers, as membrane's mimics.⁸⁸

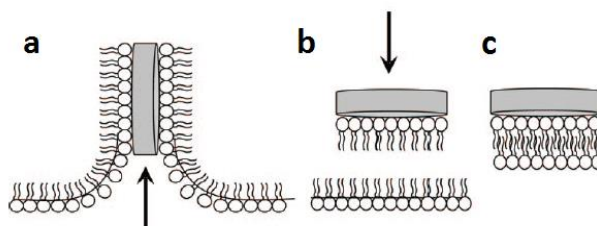


Figure 2.4-7. (a) Langmuir-Blodgett (LB) and (b) Langmuir-Schaefer (LS) deposition of the monolayer and (c) resulting solid-supported membrane.⁸⁸

In order to perform a successful transfer the monolayer at the air-water interface has to be homogeneous, which can be established by Brewster angle microscopy (BAM), and stable in time. This is why before performing deposition on the substrate the compound should be carefully investigated on the Langmuir trough. It should be also noted that

transfer might disrupt the structure of the monolayer, so it is not applicable for all kinds of monolayers.⁸⁹ Transfer ratio is a parameter describing the quality of the deposition and it is defined as the ratio of decrease in Langmuir monolayer surface area to the total surface area of the substrate.⁹⁰ Transfer ratio (TR) near unity indicates the successful deposition of the monolayer, however in some cases it might happen, that during transfer the molecular packing density within the monolayer changes and then $TR = 1$ does not correspond to the defect-free film. This is why this parameter can give an idea about transfer quality, but it cannot be taken as decisive.⁹⁰

Beleguinou et al. were the first to prepare a solid-supported polymer membrane composed from PB-*b*-PEO diblock by applying LB and LS transfer techniques. The first layer of the membrane was attached covalently to the gold surface by formation of Au-sulfur linkage between the substrate and a lipoic acid-functionalized polymer.⁸⁵ The second layer prepared by LS transfer was attached by hydrophobic interactions between PB blocks of both layers. The SPR and AFM analysis revealed formation of stable, uniform, and fluid membranes with a thickness of 11 nm. The polymer bilayers were stable in air for approximately 2 h, which is advantageous when comparing with solid-supported lipid membranes which are known to break down immediately after drying.⁹¹⁻⁹³ After 12 h of exposure to air the PB-*b*-PEO bilayers disassembled and rearranged to form the aggregates (Figure 2.4-8).

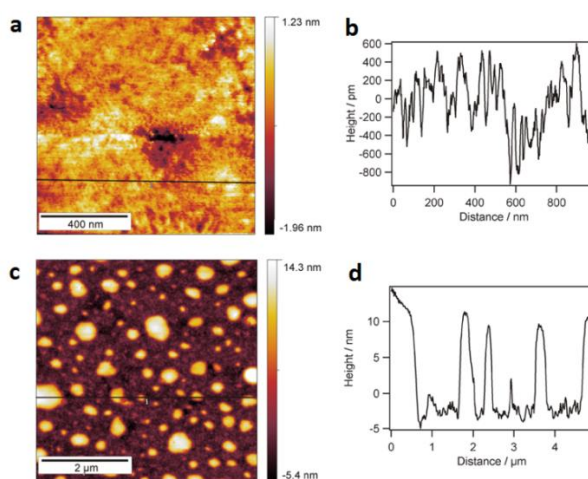


Figure 2.4-8. AFM height images of solid-supported PB-*b*-PEO membranes: after (a) 1.4 h of drying, and (b) the corresponding height profile, (c) after 12 h of drying, and (d) the corresponding height profile.⁸⁵

2.4.5. Functionalization of solid-supported membranes

The main purpose for preparation of solid-supported membranes is to mimic the biological membranes and to obtain functional surfaces. This is why a step further after preparation of the artificial membrane is an introduction of biomolecules into such membranes, as the active compounds. Three general strategies for membrane functionalization can be distinguished: i) adsorption/immobilization on the surface, ii) insertion into the membrane, or iii) biotin-streptavidin and metal-His-tag protein couplings.^{6,94} In order to perform successful membrane functionalization it has to be performed in organic solvent-free environment and in physiological conditions.⁹⁵ The membrane should also possess specific composition and properties, such as thickness, density, and fluidity, which will promote biomolecules attachment.³⁴

Immobilization of the biomolecules is a straightforward method to develop active surfaces for applications in sensing,⁹⁶ food packaging,⁹⁷ and catalysis.⁹⁸ For example, immobilization of enzymes on surfaces enhances enzyme's solubility and stability, facilitates separation of the enzyme from the product, and allows continuous repeated use.⁹⁹⁻¹⁰¹ Various methods have been proposed for enzyme's immobilization: i) physical adsorption, ii) covalent binding to modified surfaces, iii) cross-linking, and iv) entrapment in matrices, such as polymer networks, channels or capsules.^{6,102,103} In order to obtain high enzyme loading, immobilization is frequently performed on porous materials *e.g.*, mesoporous silicates,¹⁰⁴ nanoporous gold,¹⁰⁵ or nanozeolites.¹⁰⁶ However porous materials suffer diffusional limitations because of the large molecular weight substrates involved in the enzymatic reaction. Whilst non-porous materials should overcome this limitation, their drawbacks are low enzyme loading, and the risk of protein denaturation on contact with a hard support.¹⁰⁷ Thus to avoid protein denaturation, the solid support has to be covered with soft layers, as for example lipids or polymers.⁹² There are numerous examples of successful enzyme immobilization on surfaces covered with lipid layers *via* physical adsorption. Examples include immobilization of rat osseous plate alkaline phosphatase on phospholipid films deposited on gold LB transfers,¹⁰⁸ and immobilization of tyrosinase by ionic interactions between the enzyme and a solid support.¹⁰² As stability in time and robustness are key factors for potential applications of active surfaces, an elegant approach is to use polymer instead of lipid membranes.

Insertion of the protein follows a complex scenario and number of requirements has to be fulfilled. For example, a membrane has to be stable, highly homogeneous while fluid enough to host a protein.¹⁰⁹ The biggest challenge one meets in the functionalization of membranes, is insertion of the transmembrane protein, in such a way that the protein keeps its native structure and function. If the transmembrane protein is inserted into the membrane, which is directly deposited on the substrate, there is a risk of protein denaturation by contact with the bare and hard substrate.^{67,92} This problem has been overcome by introducing, a few nm thick, polymer “cushion” in between the solid substrate and the artificial membrane (Figure 2.4-9). The appropriate “cushion” should be thermodynamically and mechanically stable, and need to interact in the repulsive way with the membrane.⁶⁷ Several types of polymers have been applied to form a membrane support, such as: cellulose, dextran, chitosan, or polyelectrolytes.^{92,110} Another strategy is usage of lipopolymers tethers, which are soft polymer chains bearing a macromolecular head groups, which can be incorporated into the membrane.¹¹¹ Furthermore, they have been frequently used for insertion of the proteins, *e.g.* incorporation of ATPase,¹¹² outer membrane proteins (OmpF and OmpA),¹¹³ or α -hemolysin (α -He).¹¹⁴ The most commonly used technique for preparation of a solid-supported lipid membrane with inserted proteins is adsorption and fusion of proteoliposomes.¹¹⁵

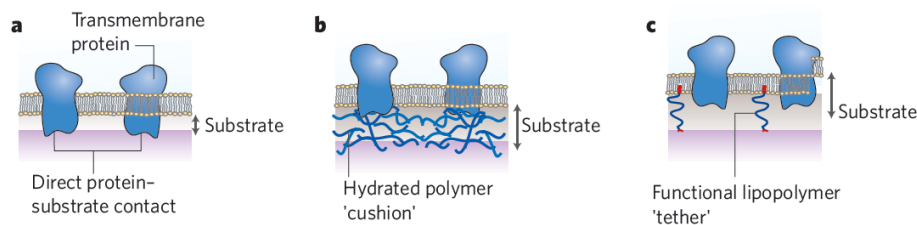


Figure 2.4-9. Solid-supported lipid membrane with inserted transmembrane protein. Membrane deposited (a) directly on the substrate, (b) on polymer “cushion”, and (c) lipopolymer-tethered membrane.⁶⁷

Insertion of the protein into the solid-supported polymer membranes has not yet been studied extensively, even though they are good candidates to host a membrane protein. Due to the increased thickness of the polymeric membrane (3 – 40 nm) comparing to lipid membranes thickness (3 – 4 nm),¹¹⁶ the interactions between a solid substrate and incorporated membrane proteins can be reduced, preventing the protein from

denaturation.³⁴ Dorn et al. were the first to study the interactions between solid-supported polymer membrane, composed from PB-*b*-PEO diblock copolymer, and a polypeptide, namely polymyxin B by performing electrochemical impedance spectroscopy measurements.⁷⁸ The authors showed that the peptide was attaching to the membrane only temporarily and then slowly diffused into the solution. A step further was insertion of α -He into a solid-supported PB-*b*-PEO membrane upon applied electrical current, which destabilized the membrane.¹¹⁷ The protein was inserted permanently and it preserved its functions, as shown by flow of the ions through the membrane until Donnan equilibrium was reached. This method suffers some limitations: i) protein insertion has to be performed in a special chamber and with usage of a setup for electrical current generation, ii) the size of membrane is limited to the dimensions of the chamber in which the electrical current is applied, iii) the membrane has to be prepared on gold substrate, and iv) applied current may be too high which may lead to denaturation of the protein, or disruption of the membrane.

Besides these two examples, no other attempts of protein incorporation into the solid-supported polymer membranes have been made, which evidences that it is still an emerging area of research.

3. Results and Discussion

3.1. Surface engineering by insertion of membrane proteins into solid-supported polymer membranes

The scope of this project was the development of a new strategy for insertion of a membrane protein into solid-supported polymer membranes. The goal was to introduce a straightforward approach, which would allow for protein insertion into large area membranes, by using a more gentle method of destabilization of the protein than electrical current.

The solid-supported membranes were prepared from PDMS-*b*-PMOXA diblock copolymers by LB and LS transfer techniques. In order to increase the stability of the membrane the first layer was attached covalently to the amino modified substrates (silica wafer, glass, and gold), by formation of weak imine bond. The second layer was attached by non-covalent, hydrophobic interactions between the PDMS blocks of both layers (Figure 3.1.-1). A cyclic nucleotide-modulated potassium channel from *Mesorhizobium loti* (MloK1) was selected as the model membrane protein,^{118,119} due to the structure similarity to eukaryotic cyclic nucleotide-modulated ion channels, which are well known for signal transduction in eukaryotes.¹²⁰⁻¹²² Insertion of the membrane protein was performed by using Bio-Beads, which are capable to adsorb detergent molecules from aqueous solutions, and can thus destabilize the protein in a gentle way.¹²³

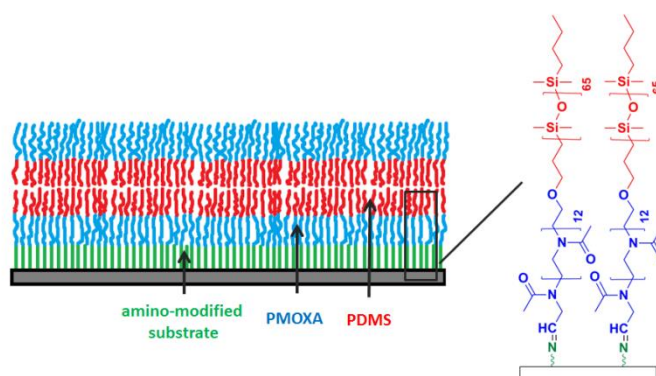


Figure 3.1-1. Schematic representation of solid-supported polymer membrane of PDMS₆₅-*b*-PMOXA₁₂ diblock copolymer.

3.1.1. Polymer modification and characterization

The PDMS-*b*-PMOXA diblock copolymer was synthesized by cationic ring opening polymerization.¹⁴ The polymerization was terminated with potassium hydroxide, which resulted in a hydroxyl-terminated polymer. The obtained copolymer was composed of 65 PDMS units and 12 PMOXA units, and the molar mass of the polymer was 5735 g mol⁻¹ as calculated from ¹H NMR data. Gel permeable chromatography (GPC) characterization showed the PDI of the obtained copolymer to be 1.67.

In order to attach the first layer of the membrane to the surface, the hydroxyl end-group of PDMS-*b*-PMOXA was selectively oxidized to the aldehyde, by a Dess-Martin oxidation.¹²⁴ Both copolymers, *i.e.* with hydroxyl and aldehyde groups have been characterized by ¹H NMR and ATR-FTIR in order to prove that the oxidation did not influence the polymer structure. In the ¹H-NMR spectra of hydroxyl terminated and oxidized polymer (Figure 3.1-2), the signal at $\delta = 0$ ppm corresponds to the Si-CH₃ group (6H, a) in the PDMS block, the signal at $\delta = 1.96 - 2.08$ ppm is assigned to the CH₃-CON group (3H, b) in the PMOXA block, and the signal at $\delta = 3.39$ ppm corresponds to N-CH₂-CH₂-CHO (4 H, c). The detailed assignment of ¹H-NMR peaks can be found in section 6. Both ¹H-NMR spectra represent the same shift of peaks, which indicate that no structural reorganization of the polymer occurs during oxidation. This was confirmed by ATR-FTIR measurements (Figure 3.1-3), in which the peak at 2960 cm⁻¹ is associated with the C-H bond from alkyl groups, the peak at 1642 cm⁻¹ corresponds to amide group, the bands at 1257 cm⁻¹ and 1010 cm⁻¹ are due to the Si-O-Si stretching, and the peak at 790 cm⁻¹ is assigned to Si-CH₃ group.

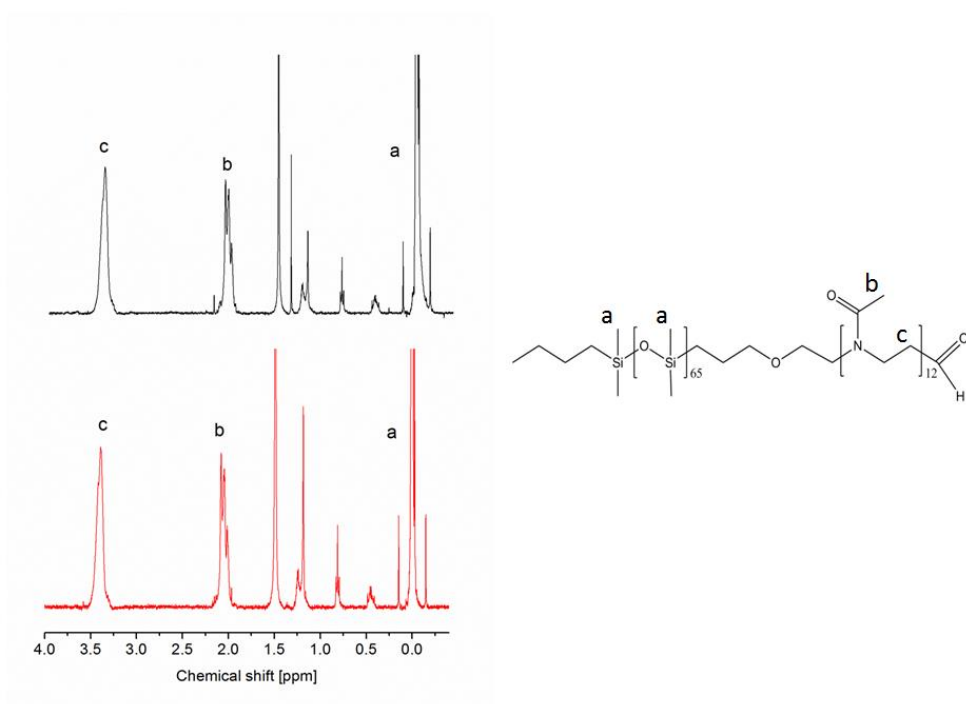


Figure 3.1-2. Representative ^1H -NMR spectra of hydroxyl terminated (in black), and oxidized PDMS₆₅-*b*-PMOXA₁₂ diblock copolymer (in red), and copolymer structure.

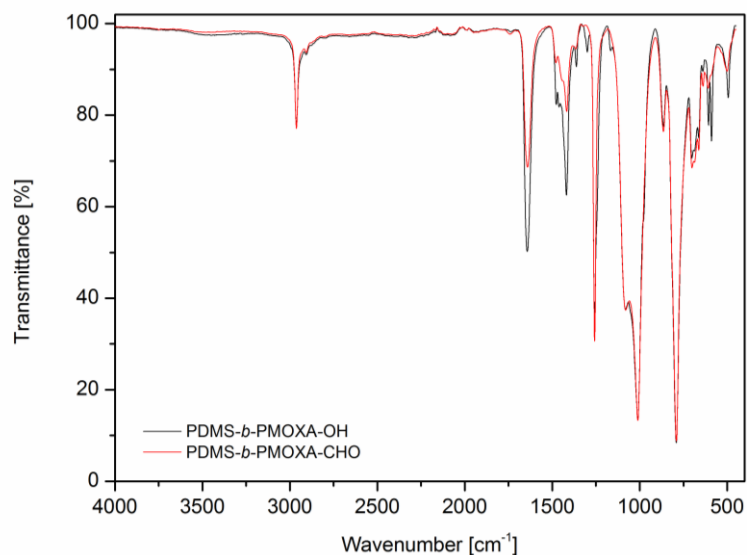


Figure 3.1-3. Representative ATR-FTIR spectra of hydroxyl terminated (in black), and oxidized PDMS₆₅-*b*-PMOXA₁₂ diblock copolymer (in red).

Since the PDMS-*b*-PMOXA diblock copolymer is a macromolecule ^1H -NMR and ATR-FTIR techniques turned out to not be sensitive enough to detect oxidation of the

polymer end-group. This is why the presence of the aldehyde group in the polymer was confirmed by performing two analytical tests, *i.e.* Brady's test and Tollens' test (details are given in the experimental part). In the Brady's test the reaction between 2,4-dinitrophenylhydrazine and aldehyde resulted in a yellow precipitate (Figure 3.1-4 a), whilst in the Tollens' test, a black precipitate of silver was observed when performing the experiment in the presence of aldehyde-terminated copolymer (Figure 3.1-4 b). In both tests, the hydroxyl-terminated copolymer was used as the control and in both cases no precipitates were observed.

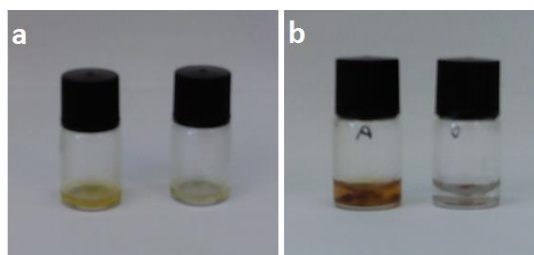


Figure 3.1-4. Pictures of aldehyde terminated (left side) and hydroxyl terminated (right side) copolymer after (a) the Brady's test and (b) the Tollens' test.

3.1.2. Labeling of the protein with fluorescent dye

The potassium channel, MloK1, which is a transmembrane protein, was labeled with the fluorescent dye DyLight 488. This dye is activated with an *N*-hydroxysuccinimide (NHS) ester group, which reacts with primary amines ($-NH_2$), resulting in the formation of a stable amide bond (Figure 3.1-5). MloK1 was dissolved in Tris, a primary amine buffer, which is not compatible for labeling due to competing for reaction with dye. For this purpose the first step to obtain a labeled protein was a change of buffer to Bicine (2-(bis(2-hydroxyethyl)amino)acetic acid). The reaction was performed in dimethyl formamide (DMF) over 1 h, and after this time the unbound dye was removed by dialysis (details are given in the experimental part).

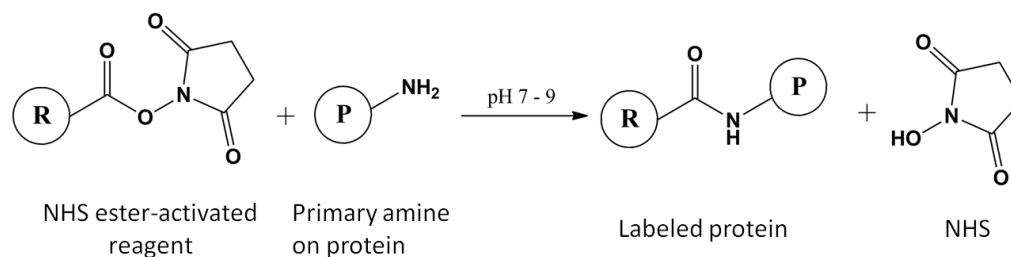


Figure 3.1-5. Scheme of the reaction between the NHS ester group of dye and primary amine of the protein.

The successful labeling of the protein was proven by ultraviolet-visible spectrophotometry (UV/Vis) and sodium dodecyl sulfate polyacrylamide gel electrophoresis (SDS-PAGE). The UV/Vis spectrum of labeled MloK1 showed the appearance of an absorption peak at 495 nm, which is characteristic for DyLight 488 (Figure 3.1-6). The SDS-PAGE of the pure non-labeled MloK1 presents bands which are due to monomeric ($M_w = 37$ kDa), dimeric ($M_w = 74$ kDa), and tetrameric ($M_w = 210$ kDa) forms of the protein (Figure 3.1-7).¹¹⁸ The strongest band corresponding to monomeric MloK1 is doubled, because it corresponds to two populations: with and without disulfide bonds. The bands corresponding to the labeled MloK1 appear at slightly higher molecular weights indicating successful modification with the fluorescent dye. The bands corresponding to the monomeric MloK1 do not appear exactly at the M_w of 37 kDa, according to the ladder. This phenomenon is common for membrane proteins and can be explained by small differences in the amount of bound SDS resulting in anomalous mobility during electrophoresis.^{125,126}

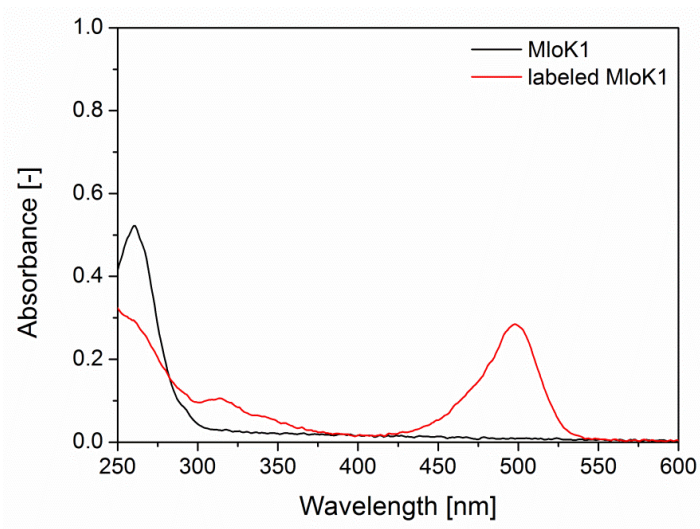


Figure 3.1-6. UV-Vis spectra of pure (black) and labeled (red) MloK1.

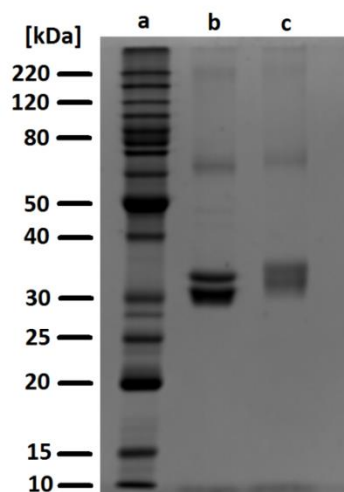


Figure 3.1-7. SDS-PAGE of (a) protein marker, (b) purified full-length MloK1, and (c) MloK1 labeled with a fluorescent dye.

In order to show that labeling did not influence the secondary structure of the MloK1, circular dichroism (CD) measurements were performed. CD profiles of both pure and labeled proteins revealed dual minima at 208 and 222 nm, which are characteristic for α -helices, indicating that MloK1 kept its secondary structure (Figure 3.1-8).¹²⁶

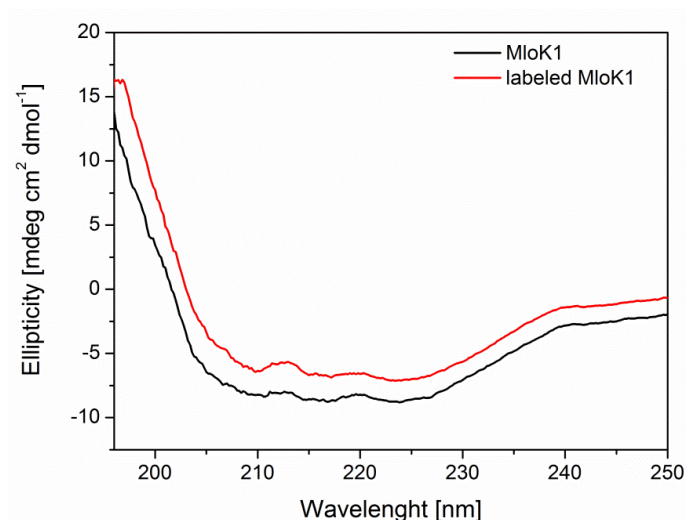


Figure 3.1-8. CD spectra of purified MloK1 (black) and MloK1 labeled with a fluorescent dye (red).

Finally, the purity of the labeled protein was examined by fluorescence correlation spectroscopy (FCS) and confocal laser scanning microscopy (CLSM). FCS provided information about number of fluorescent fractions in the probed solution of labeled MloK1. The measurements showed that the solution was composed up to 86% of components having relaxation time of 327.6 μs , and of 17% of component with relaxation time of 30 μs . Longer relaxation time corresponds to component of higher molecular weight. It can thus be assigned to labeled MloK1, whilst the lighter component of shorter relaxation time corresponds to the free dye, which was not removed during dialysis. CLSM control measurements, which is described in details further, in paragraph 3.1.6, confirmed that no dye aggregates were formed and attached to the surface.

3.1.3. Polymer at the air water interface

In order to get information about polymer organization and behavior at the air-water interface we investigated monolayers formed by PDMS₆₅-*b*-PMOXA₁₂ diblock copolymer on the Langmuir trough. A chloroform solution of the polymer was spread dropwise on the water surface, and after evaporation of the solvent, the compression was performed. The surface pressure-area isotherm of this polymer has a lift-off area at 1082 \AA^2 and a collapse point at 60 \AA^2 , which corresponds to surface pressure of 53 mN m^{-1} (Figure 3.1-9). The isotherm has two characteristic plateaus corresponding to the

rearrangements of the polymer chains during the compression. The first plateau at surface pressure of 12 mN m^{-1} is due to desorption of the hydrophobic block from water, while the second one at 17 mN m^{-1} stands for further stretching of the polymer chain and formation of a uniform film.^{63,65} These rearrangements are well pronounced in the graph presenting the compressibility modulus at mean molecular area of 400 Å^2 .

The maximal C_s^{-1} , close to the collapse point, has a value of 44 mN m^{-1} , indicating liquid-expanded state of the monolayer.

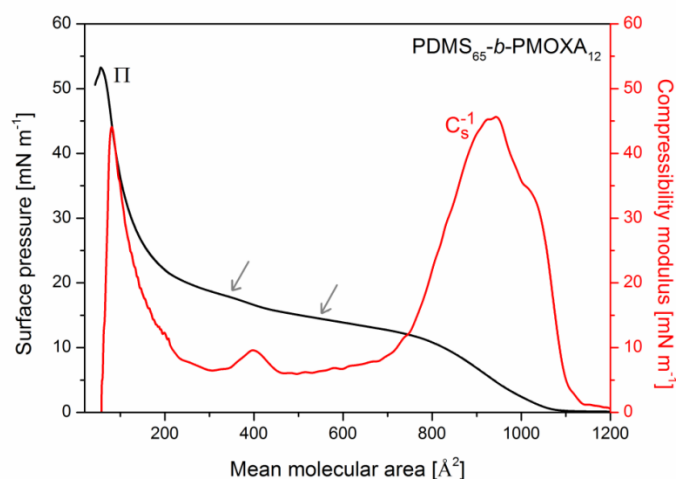


Figure 3.1-9. Surface pressure (Π , black line) and compressibility modulus (C_s^{-1} , red line) versus mean molecular area of PDMS₆₅-*b*-PMOXA₁₂ diblock copolymer. Gray arrows indicate two plateaus.

The film compression was additionally monitored by BAM. These measurements revealed that during the whole compression, the film stayed homogeneous (Figure 3.1-10). The only features visible on the BAM images are small white spots, which correspond to surface micelles formed by hydrophobic chains and which have been observed also for other amphiphilic block copolymers at the air-water interface.¹²⁷⁻¹²⁹

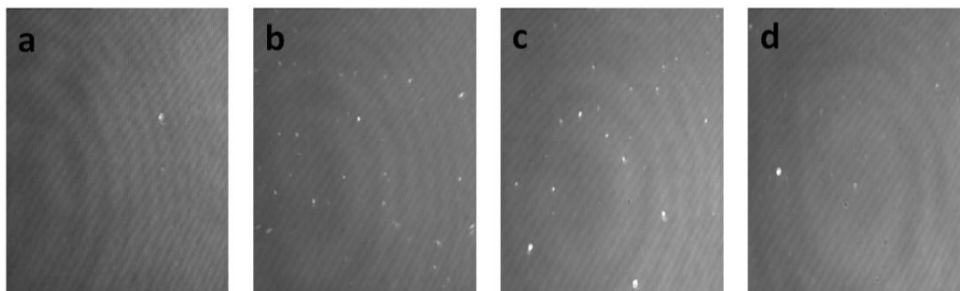


Figure 3.1-10. BAM images of a PDMS₆₅-*b*-PMOXA₁₂ diblock copolymer monolayer at the air-water interface at surface pressures of: (a) 10, (b) 20, (c) 30, and (d) 40 mN m⁻¹. Size of images: 200 x 250 μm².

In order to perform successful transfer of the monolayer to a solid support, the monolayer has to be stable at the air-water interface. For this purpose the polymer was compressed to 37 mN m⁻¹ and then the surface pressure of the monolayer was monitored over one hour (Figure 3.1-11). After this time the surface pressure did not change significantly, which indicated that the polymer chains do not desorb from the air-water interface to the aqueous subphase, forming stable films. The stability of the polymer monolayer was also investigated after addition of the small volume of detergent on the monolayer at the air-water interface. These measurements showed that presence of the detergent does not influence neither formation nor stability of the polymer monolayer.

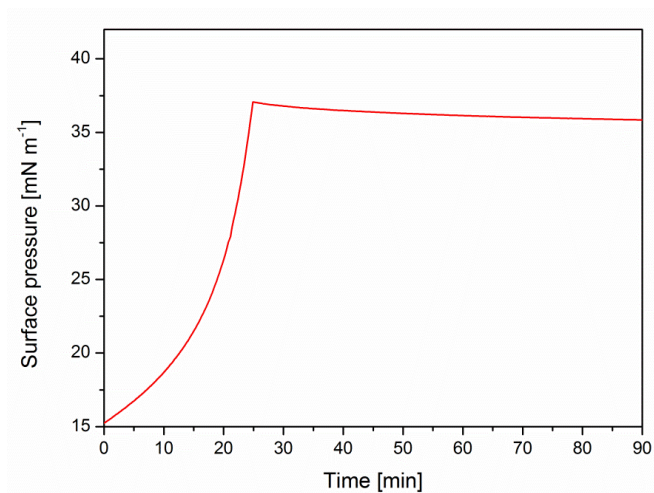


Figure 3.1-11. Stability of the PDMS₆₅-*b*-PMOXA₁₂ diblock copolymer monolayer at the air-water interface.

In summary, measurements performed on the Langmuir trough reveal that PDMS₆₅-*b*-PMOXA₁₂ diblock copolymer at the air-water interface forms homogeneous and stable monolayers in the liquid-expanded state, which makes it a good candidate to further explore solid-supported membranes.

3.1.4. Functionalization of the solid support with amino groups

Three different substrates, *i.e.* silica, glass, and gold, have been used for the preparation of polymer membranes, which enabled use of various characterization techniques. Silica and glass are frequently used as models for the investigation of protein adsorption on modified surfaces.^{83,130} Glass substrates were used for CLSM measurements, for which transparent surfaces are essential. On the other hand, gold substrates were used for electrical conductance measurements.

All the substrates were modified with linkers whose amino end-group could form an imine bond with the aldehyde end-group of the copolymer. In this way the stability of the membrane could be increased, but since the imine bond is weak, not all polymer chains attach permanently to the substrate and the fluidity of the membrane could thus be preserved. In addition, the linker layer acts as a spacer between the substrate and the membrane, which prevents strong interactions between the membrane protein and the hard substrate.

Silica and glass substrates were modified with 3-aminopropyltriethoxysilane (APTES). Such a strategy has been applied before for immobilization of the polymer vesicles composed of PEO-*b*-PLA diblock copolymers functionalized with aldehyde end-group.¹³¹ APTES is known to easily form multilayers thus functionalization was performed in water- and oxygen-free conditions with a short reaction time.^{132,133} The thickness of the resulting monolayer established by ellipsometry was approximately (0.9 ± 0.1) nm, in agreement with the theoretical value of 0.8 nm.¹³² Contact angle of the substrate increased from 35° for bare silica to 66° for a silanized surface. AFM measurements revealed the silanized silica substrate to be smooth with an average roughness (R_a) of 0.2 nm (Figure 3.1-12).

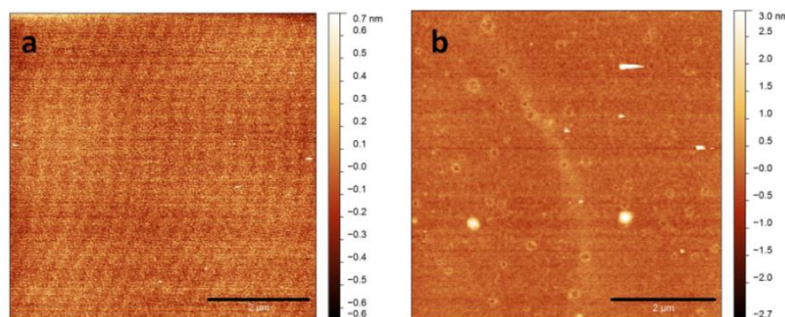


Figure 3.1-12. AFM images of: (a) bare silica slide, and (b) APTES modified silica slide. Scale bars: 2 μm .

Silanized substrates were also investigated by ATR-FTIR. A bare silica slide was measured as the reference. The appearance of peaks characteristic for APTES in the spectrum indicates successful functionalization (Figure 3.1-13). The observed peaks from the functional groups of APTES are: Si-O at 615 cm^{-1} , 740 cm^{-1} , and 1106 cm^{-1} , and C-H from the alkyl groups at 2675 cm^{-1} .

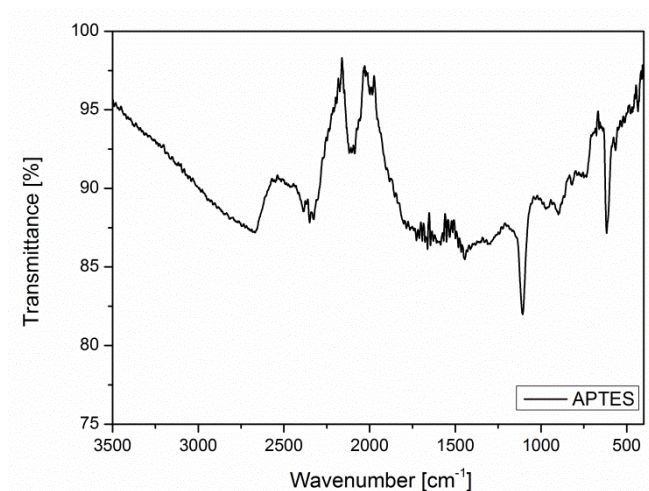


Figure 3.1-13. ATR-FTIR spectrum of silanized silica substrate.

Gold substrates were modified with 11-amino-1-undecanethiol hydrochloride (AUT), which bears amino and thiol end-groups and is known to form self-assembled monolayers on gold substrates.¹³⁴ After functionalization, the contact angle decreased from 103° for bare gold to 76° for the AUT modified substrate. Ellipsometry measurements indicated that the AUT layer had a thickness of $(3.3 \pm 0.2)\text{ nm}$, and AFM showed the film to be homogeneous (Figure 3.1-14). ATR-FTIR confirmed successful surface modification. A

blank gold substrate was used as the background and the spectrum of AUT-modified substrate showed: a peak at 1046 cm^{-1} corresponding to the C-N group, and peaks at 2897 cm^{-1} and 2985 cm^{-1} corresponding to the C-H stretching modes (3.1-15).

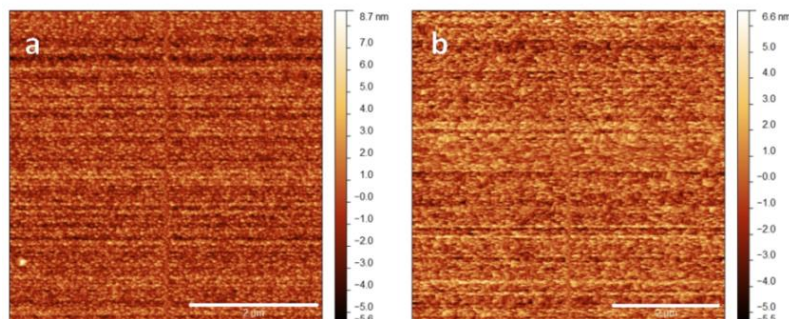


Figure 3.1-14. AFM images of: (a) bare gold substrate, and (b) AUT modified gold substrate. Scale bars: $2\text{ }\mu\text{m}$.

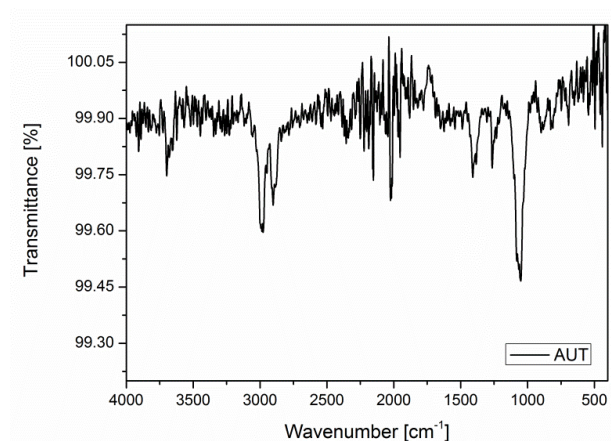


Figure 3.1-15. ATR-FTIR spectrum of AUT modified gold substrate.

Such amino-functionalized slides were directly used for preparation of the polymer membranes, by Langmuir-Blodgett and Langmuir-Schaefer transfer techniques.

3.1.5. Preparation of solid-supported membranes

Solid-supported membranes were prepared by transfer of the polymer monolayers from the air-water interface, which provides defect-free deposition of highly ordered

films. The transfers were performed at a surface pressure of 37 mN m^{-1} , since at this surface pressure the isotherm reveals a steep slope, indicating formation of a densely packed film. At a surface pressure of 37 mN m^{-1} the polymer monolayer is in the liquid-expanded state, as established by the compressibility modulus ($C_s^{-1} = 45 \text{ mN m}^{-1}$). Additionally, this surface pressure corresponds well to the surface pressure of the natural membranes, which ranges between 30 and 35 mN m^{-1} .¹³⁵

The first layer was attached covalently to the amino modified substrates by performing a Langmuir-Blodgett transfer. Freshly transferred films on silica were characterized by contact angle, ellipsometry and AFM. After the transfer, contact angle increased from 66° (for APTES-modified silica) to 80° , which indicates that the hydrophobic PDMS block was directed upwards. The thickness of the monolayer was $(6.5 \pm 0.5) \text{ nm}$, as established by ellipsometry. The morphology of the monolayer was studied by AFM (Figure 3.1-16).

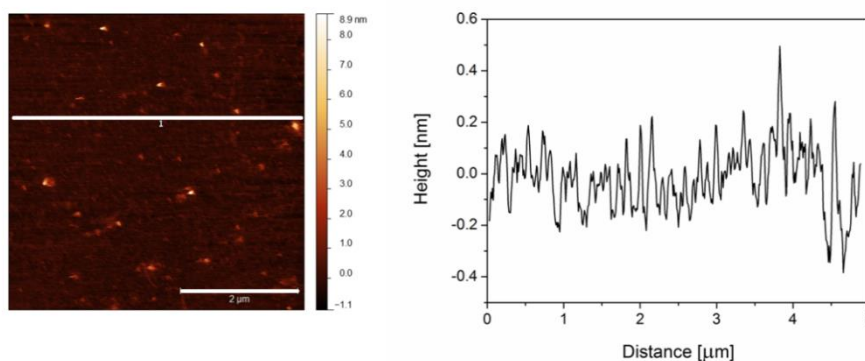


Figure 3.1-16. AFM image of a polymer monolayer and the corresponding height profile. Scale bar: $2 \mu\text{m}$.

The AFM image revealed that the monolayer is homogeneous and smooth with a roughness of approximately 0.2 nm . Bright structures visible on the surface correspond to some adsorbed impurities as well as to the fine aggregates of the hydrophobic unreacted PDMS. Since the AFM measurements were performed in liquid the PDMS blocks tended to rearrange in order to reduce contact with the water. However, the covalent attachment of the polymer to the substrate limited their freedom, which resulted in formation of aggregates. Scratching a membrane area of $1 \mu\text{m}^2$ with a hard cantilever produced a trough with a depth of 2 nm (Figure 3.1-17). Due to the fact that most of the polymer

chains were attached covalently it was not possible to remove them by scratching with a cantilever. The trough came to exist due to the removal of loosely bound polymer chains.⁸⁵

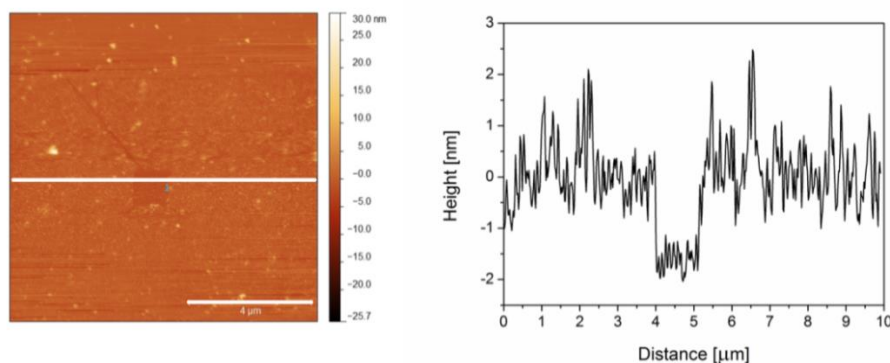


Figure 3.1-17. AFM image of the scratched monolayer and the corresponding height profile. Scale bar: 4 μm .

The second layer of the membrane was attached to the first layer by non-covalent, hydrophobic interactions and it was deposited by Langmuir-Schaefer transfer. The average thickness of the bilayer, measured by ellipsometry, was (11.2 ± 0.5) nm. The thickness of the resulting membrane was slightly lower than a doubled thickness of the monolayer, due to the interdigitating of the PDMS blocks of both layers.¹³⁶ The contact angle of the bilayer decreased from 80° (for monolayer) to 62° , which indicates the presence of the hydrophilic PMOXA block on the top of the membrane and confirms a hydrophilic-hydrophobic-hydrophilic character of the membrane. AFM measurements revealed the bilayer to be smooth and homogeneous with a R_a of 0.6 nm (Figure 3.1-18).

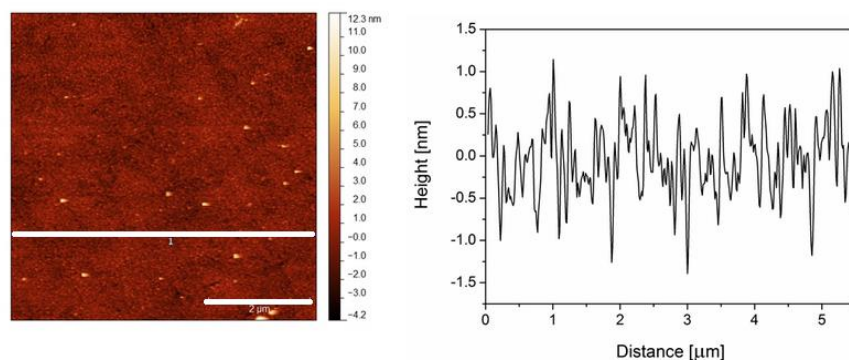


Figure 3.1-18. AFM image of polymer bilayer and the corresponding height profile. Scale bar: 2 μm .

Covalent attachment of the polymer membrane to the amino modified substrates was examined by ATR-FTIR spectroscopy. The freshly prepared membranes, prepared on both, silica and gold substrates, were measured by ATR-FTIR. Bare silicon or gold slides were used as references. Then the bilayers were thoroughly rinsed with ethanol, which is a good solvent for the PDMS-*b*-PMOXA diblock copolymer, and measured again. The peaks characteristic for the polymer had lower intensity after rinsing, due to removal of the upper polymer layer, which confirms covalent attachment of the first layer to the substrate (Figure 3.1-19). The peaks at 2958 cm^{-1} (on the spectrum of the polymer membrane prepared on SiO_2 substrate), and at 2963 cm^{-1} (on the spectrum of the polymer membrane prepared on Au substrate), are associated with the C-H bond from alkyl groups, those at 1634 cm^{-1} (SiO_2 substrate) and 1645 cm^{-1} (Au substrate) are from the amide group, the peaks between 1265 cm^{-1} and 1050 cm^{-1} correspond to Si-O-Si stretching, and the peaks at 820 cm^{-1} are assigned to Si-CH₃ group.

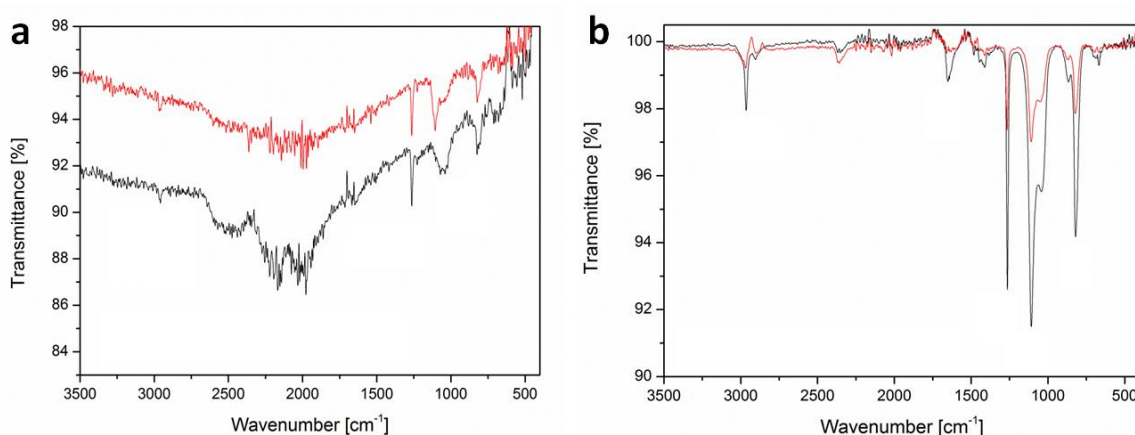


Figure 3.1-19. ATR-IR spectra of polymer bilayer on (a) silica and (b) gold substrates before (black line) and after (red line) rinsing with ethanol.

3.1.6. Incorporation of membrane protein into polymer membrane

A cyclic nucleotide-modulated potassium channel from *Mesorhizobium loti* (MloK1) was selected as the model membrane protein, due to the structure similarity to eukaryotic cyclic nucleotide-modulated ion channels, which are well known for signal transduction in eukaryotes.¹²⁰⁻¹²² MloK1 consists of six transmembrane α -helices and an N-terminal cytoplasmic cyclic nucleotide binding domain (CNBD). MloK1 forms a tetrameric complex with a molecular mass of approximately 210 kDa, a height of 10 nm, and a

width of 8.5 nm.¹¹⁸ The tetrameric full-length channel is composed of: i) a transmembrane part containing the central pore and putative voltage sensing domains, and ii) the cytosolic part comprising four CNBDs. When the latter bind 3',5'-cyclic adenosine monophosphate (cAMP) or cyclic guanosine monophosphate (cGMP), they induce conformational changes that activate the channel.¹³⁷

MloK1 is insoluble in water because of its hydrophobic transmembrane region. This is why in aqueous solution it is stabilized by a detergent (*n*-decyl- β -*D*-maltopyranoside, DM). Incorporation of the detergent-solubilized protein into a membrane requires the removal of the detergent and thus destabilization of the protein which is a factor driving insertion. The detergent was removed from solution by adding Bio-Beads, which are polystyrene porous beads with pore diameter of approximately 90 Å.¹³⁸ This method allows efficient but gentle detergent removal, without affecting neither the protein nor membrane.^{139,140} After destabilization, the protein is forced to incorporate in the polymer membrane, in order to preserve its structure due to the suitable hydrophobic environment of the polymer membrane (Figure 3.1-20).

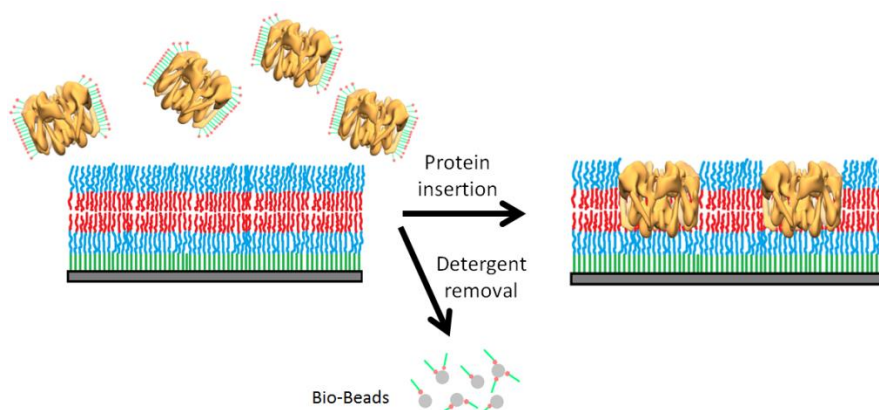


Figure 3.1-20. Schematic representation of the strategy for insertion of the membrane protein into the solid-supported polymer membrane using Bio-Beads.

Insertion of the MloK1 into the polymer membrane was observed by CLSM. For this purpose the polymer membrane was prepared on a transparent, amino modified glass substrate, and the protein was labeled with a fluorescent dye (DyLight 488). After incubation of the MloK1 in the vial with the polymer membrane and Bio-Beads, attachment/insertion of the protein to the membrane could be observed (Figure 3.1-21 a). Addition of the detergent-solubilized protein to the solution, in which the solid-supported

membrane was present, but in absence of Bio-Beads, was not sufficient for protein insertion (Figure 3.1-21b). Two control samples were also measured: i) polymer membrane after incubation with the dye in the presence of Bio-Beads, and ii) silanized substrate (no polymer membrane) after incubation with the protein in the presence of Bio-Beads. The first control proved that the dye which was used for protein labeling did not form any aggregates and that fluorescent features visible on the figure 3.1-21a are indeed corresponding to the labeled protein (Figure 3.1-21c). Additionally, no protein attachment took place on the silanized substrate, which demonstrates that the labeled protein does not just deposit on the surface, but inserts into the polymer bilayer (Figure 3.1-21d).

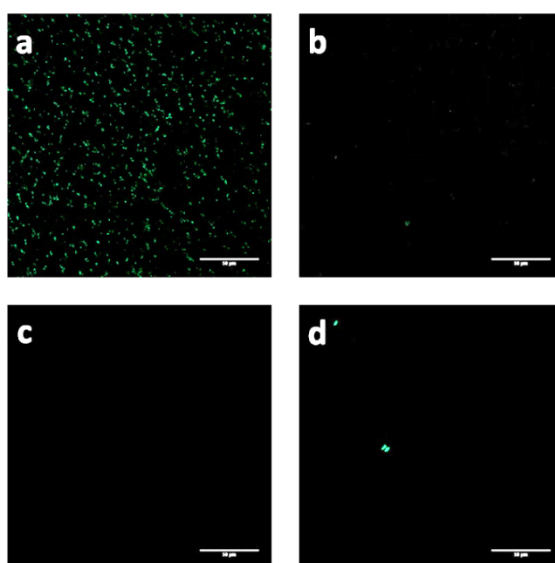


Figure 3.1-21. CLSM micrographs of: (a) polymer membrane after incubation with MloK1 and Bio-Beads, (b) polymer membrane after incubation with MloK1 but without Bio-Beads, (c) polymer membrane after incubation with dye and Bio-Beads, and (d) silanized substrate after incubation with MloK1 and Bio-Beads. Scale bars: 50 μ m.

CLSM micrographs confirmed that MloK1 adsorbs to the substrate only when the polymer membrane and Bio-Beads are present in the system. In order to show that protein is inserted into the polymer membrane and that it preserves its functions, electrical conductance measurements were performed. Due to the fact that an intact membrane is known to be a perfect insulator, which results in high resistance, any disruption of the membrane, *e.g.* by protein insertion, can be observed as an increase in the electrical conductance.³¹ A current across the membrane, deposited on a gold slide, was measured

as a function of time for a constant applied voltage of 40 mV (Figure 3.1-22). The conductance was calculated as $G = I/V$, where I is an electrical current, and V a voltage. Due to the fact that each defect, *e.g.* inhomogeneity of the membrane, and surface contamination, influences the final result, conductance measurements have high inherent errors.

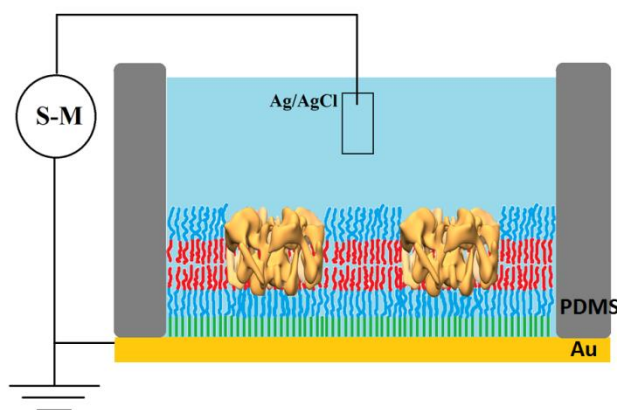


Figure 3.1-22. Schematic representation of the setup used for measurements of electrical conductance through the polymer membrane (S-M – source-meter, PDMS stamp).

Electrical conductance of the pristine membrane was shown to be very low, of (25 ± 9) nS, which corresponds to a resistance (I/G) value of $40 \text{ M}\Omega \text{ cm}^{-2}$ (Figure 3.1-23). In order to investigate the influence of Bio-Beads on membrane stability, electrical measurements of the polymer membrane after three hours of incubation with Bio-Beads in Tris buffer were performed. Conductance increased to (33 ± 4) nS, which is a value close to the conductance of the bilayer, and indicates that Bio-Beads do not affect the membrane structure. A bilayer incubated for three hours with the protein, but without Bio-Beads, exhibited a conductance at the same level as that of the intact membrane (35 ± 6 nS), which indicates that the protein was not inserted into the polymer bilayer. Conductance increased to (71 ± 23) nS, only when the protein was incubated with the polymer membrane and Bio-Beads, which indicates a successful insertion of the protein into the membrane.^{114,141} The same measurements were performed for a solid-supported lipid membrane prepared with DPPC. The lipid membrane presented a conductance of (313 ± 14) nS, while after insertion of MloK1 it increased to (423 ± 17) nS. As expected, the lipid membranes are characterized by a lower resistance ($3.2 \text{ M}\Omega \text{ cm}^{-2}$) than the

polymer membrane, because of the smaller molecule size, and thus lower membrane thickness.³² The change of conductance after protein insertion was higher for lipid membranes than for polymer membranes, which corresponds to a higher number of inserted MloK1.¹¹⁷

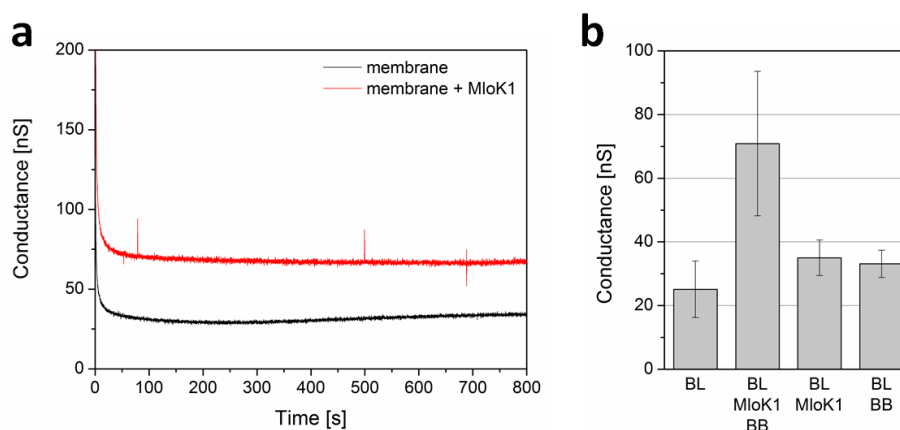


Figure 3.1-23. (a) Raw data presenting a time course for conductance of solid-supported polymer bilayer (black line) and solid-supported polymer bilayer with incorporated MloK1 (red line). (b) Conductance measured at a constant applied voltage of 40 mV (BL – polymer membrane, BB – Bio-Beads).

The activity of the potassium channel was established by electrical conductance measurements performed in the presence and absence of cAMP, which is known to modulate its functionality.^{142,143} Presence of this ligand in the solution did not influence the conductance of the solid-supported polymer membrane (Figure 3.1-24). The high conductance of the polymer membrane with incorporated MloK1 in the presence of cAMP (71 ± 23 nS), corresponds to an open channel of the protein. In contrast, when the polymer membrane with incorporated MloK1 was measured in cAMP-free buffer, the conductance was (40 ± 8) nS. The decrease of the conductance of the MloK1-containing polymer membrane in the absence of cAMP indicates closure of the protein channel.

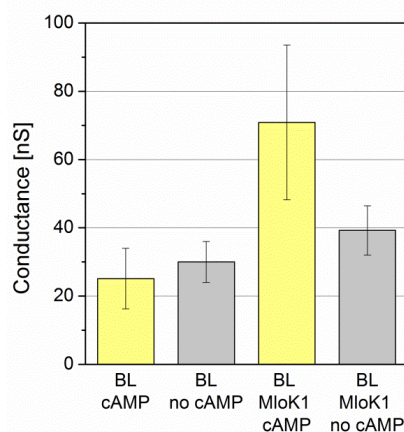


Figure 3.1-24. Electric conductance measurements showing activity of the inserted protein. Measurements performed in presence of cAMP (in yellow), and absence of cAMP (in gray).

3.1.7. Summary

In this section the development of functional solid-supported polymer membranes has been introduced.

Membranes based on the PDMS₆₅-*b*-PMOXA₁₂ diblock copolymer were prepared by LB and LS transfer techniques, which resulted in highly ordered, defect-free polymer films. The stability of the membrane was improved by covalent attachment of the first layer to an amino-modified substrate with weak imine bonds. An amino linker was introduced as a spacer between the solid surface and membrane to preserve membrane's fluidity and to prevent the protein from denaturation. The polymer bilayer was smooth, homogeneous, and stable, as established by AFM, ellipsometry, and ATR-FTIR measurements.

It was shown that use of Bio-Beads is an appropriate method for insertion of the transmembrane protein into solid-supported polymer membrane composed of PDMS₆₅-*b*-PMOXA₁₂. The Bio-Beads destabilize the protein and act as a driving force for its incorporation. CLSM micrographs showed the affinity of the protein to the polymer membrane. Additionally, electrical conductance measurements confirmed successful reconstitution of MloK1 into the membrane by showing potassium channel's activity in presence and absence of the ligand. This method allows straightforward preparation of functionalized membranes on substrates of unrestricted sizes, which is advantageous

when considering technological applications. The biomimetic properties and functionalities of solid-supported polymer membranes can be further modulated by decoration with other membrane proteins.

3.2. Hybrid polymer-lipid materials as platforms for directed membrane protein insertion

The scope of this project was the preparation of hybrid materials, in which membrane protein distribution within a film is controllable, as a result of different morphological properties of the membrane (Figure 3.2-1). Mixtures were prepared by using three PDMS-*b*-PMOXA diblock copolymers, differing in the length of the hydrophobic block (16, 37, and 65 PDMS units), and lipids (DPPC, DOPC, 1,2-dipalmitoyl-*sn*-glycero-3-phosphoethanolamine (DPPE), and 1-palmitoyl-2-oleoyl-*sn*-glycero-3-phosphoethanolamine (POPE)), with a different saturation degree and a head group. By characterizing the membranes formed by binary mixtures at different components' ratios it was possible to establish the conditions, in which the hybrid membranes formed distinct domains of lipid- and polymer-rich phases. First, BAM and CLSM were used to establish the formation and morphology of the mixed monolayers generated by the Langmuir technique and transferred to glass substrates. Then the distribution of MloK1¹¹⁹ within the membrane was assessed. MloK1 was selected as a model membrane protein since it has been already successfully inserted into solid-supported membrane assembled by PDMS-*b*-PMOXA diblock copolymer.¹⁰⁹

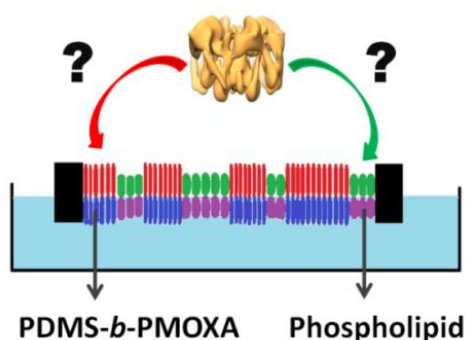


Figure 3.2-1. Schematic representation of the concept of the project.

3.2.1. Surface pressure – area isotherms of pure amphiphiles

In order to better understand the mixing properties of lipids with amphiphilic block copolymers, first the behavior of pure components at the air-water interface was investigated in respect to monolayer formation, state, and homogeneity of the monolayer. The structures of used lipids are presented in the figure 3.2-2. The most important parameters describing monolayers of pure lipids and polymers were collected in Table 3.2-1.

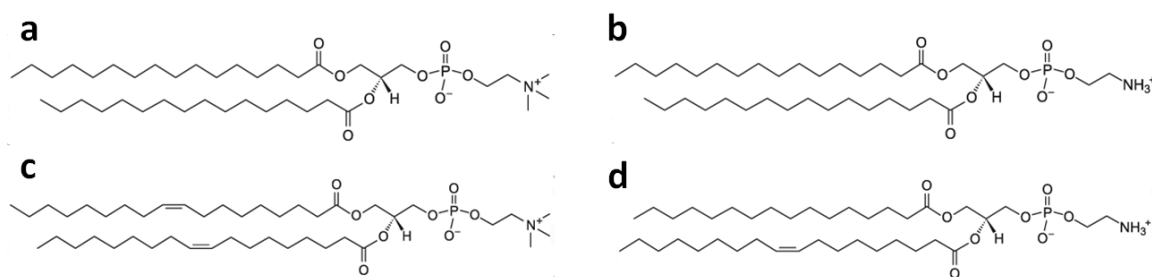


Figure 3.2-2. Structures of saturated (a) DPPC and (b) DPPE, and unsaturated (c) DOPC and (d) POPE.

Table 3.2-1. Molecular and monolayer properties of the investigated lipids and polymers.

Parameter	DPPC	DOPC	DPPE	POPE	$A_{65}B_{12}^{(1)}$	$A_{37}B_9^{(1)}$	$A_{16}B_9^{(1)}$
M_w [g mol ⁻¹]	734	786	692	718	5735	3704	2151
d [nm] ⁽²⁾	2.1	2.0	2.5	1.6	6.5	4.5	1.8
$Mma_{\text{lift-off}}$ [Å ²] ⁽³⁾	97	125	51	92	1082	800	400
Mma_{col} [Å ²]	37	57	36	33	60	53	55
Π_{col} [mN m ⁻¹] ⁽⁴⁾	55	47	50	51	53	45	43
C_s^{-1} [mN m ⁻¹]	184	95	514	48	45	42	34
Monolayer state ⁽⁵⁾	LC	L	S	LE	LE	LE	LE

⁽¹⁾ “A” corresponds to PDMS, and “B” to PMOXA blocks of the diblock copolymer; ⁽²⁾ thickness established from ellipsometry with error of ± 0.05 nm; ⁽³⁾ mean molecular area; ⁽⁴⁾ Π_{col} – surface pressure of collapse point; ⁽⁵⁾ L – liquid, LE – liquid-expanded, LC – liquid condensed, S – solid.

Compression of the DPPE monolayer was completed within a short mean molecular area range. The lift-off area of the DPPE isotherm was at a mean molecular area of 51 \AA^2 , while the collapse point was at 36 \AA^2 (Figure 3.2-3 a), which resulted in a steep slope of the isotherm and is indicative of a solid state of the monolayer.¹⁴⁴ The monolayer state was confirmed by compressibility modulus calculations. The C_s^{-1} value of 514 mN m^{-1} corresponds indeed to a solid state of the monolayer.

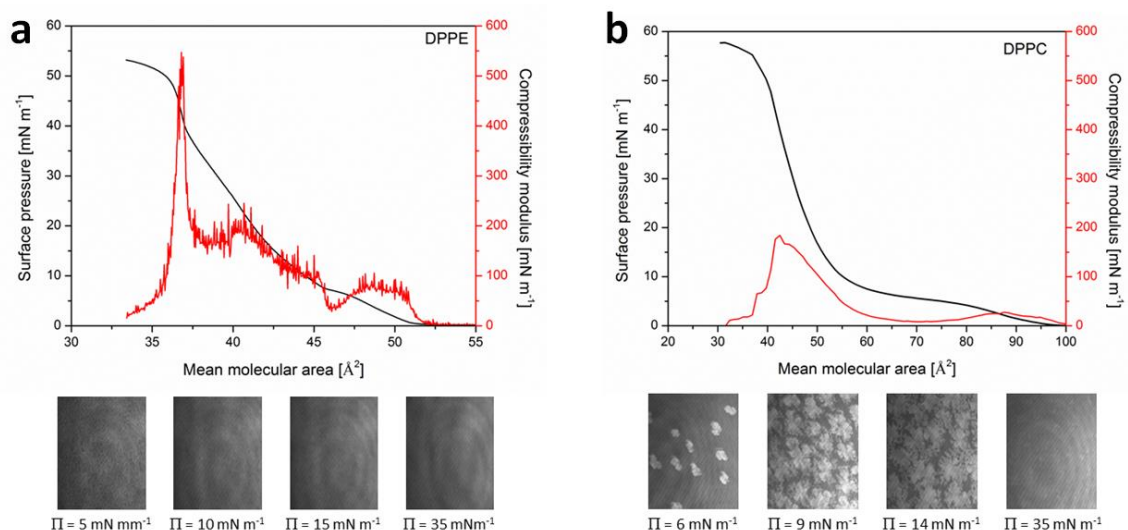


Figure 3.2-3. Surface pressure-area isotherms (in black) and compressibility modulus (in red) of (a) DPPE and (b) DPPC. BAM images at different stages of compression, respectively.

The Langmuir isotherm of DPPC possessed a characteristic plateau which was due to the transition from the liquid-expanded (LE) to liquid-condensed state (LC).¹⁴⁵ The transition can be well observed by BAM, as formation of flower-shaped structures, which become more expanded with increasing surface pressure (Figure 3.2-3 b). The formation of these structures is due to the fact that not all DPPC molecules change their conformation at the same time, thus these molecules which are in vertical position form domains. Obviously the higher the surface pressure, the more molecules are organized vertically, this is why the domains expand. At high surface pressure, the film became homogeneous due to the organization of lipid, and the compressibility modulus of the DPPC monolayer reached the value of 184 mN m^{-1} which corresponds to a LC state.

The isotherms of unsaturated lipids had a lift-off area at higher values than their saturated equivalents, due to the fact that the double bond in the hydrocarbon chain limits the flexibility of the chain and decreases the adhesion between two molecules.^{56,58} During

the compression, POPE exhibited a transition at a surface pressure of 36 mN m⁻¹,¹⁴⁶ which was well pronounced in the compressibility modulus graph (Figure 3.2-4 a). The C_s^{-1} value indicates that at this point the monolayer changed a physical state from LC ($C_s^{-1} = 120$ mN m⁻¹) to LE ($C_s^{-1} = 48$ mN m⁻¹). DOPC monolayer was at a liquid state at $C_s^{-1} = 95$ mN m⁻¹. Comparing to DPPC, the collapse point of DOPC occurs at a higher mean molecular area (57 Å² for DOPC and 37 Å² for DPPC) and at lower surface pressure ($\pi_{\text{col}} = 47$ mN m⁻¹ for DOPC and 55 mN m⁻¹ for DPPC) (Figure 3.2-4 b), which indicates that it was more expanded and had lower stability.⁶⁰

In summary, all lipids formed homogeneous and reproducible monolayers. Figure 3.2-5 shows clearly, that saturated lipids formed more condensed and thus more rigid monolayers than their unsaturated equivalents.

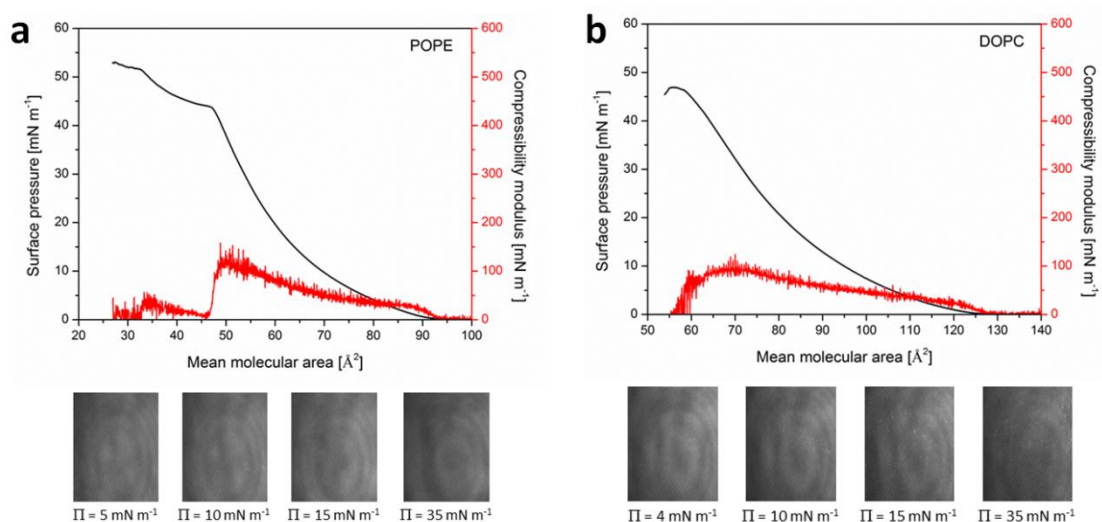


Figure 3.2-4. Surface pressure-area isotherms (in black) and compressibility modulus (in red) of (a) POPE and (b) DOPC. BAM images at different stages of compression, respectively.

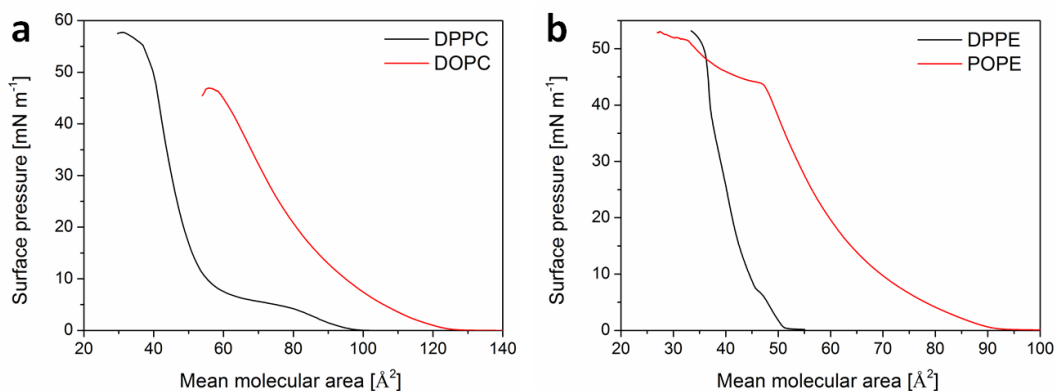


Figure 3.2-5. Comparison of isotherms of saturated and unsaturated lipids: (a) DPPC and DOPC, and (b) DPPE and POPE.

For formation of hybrid materials three block copolymers have been used: PDMS₆₅-*b*-PMOXA₁₂, PDMS₃₇-*b*-PMOXA₉ and PDMS₁₆-*b*-PMOXA₉. The isotherms of the two shorter copolymers at the air-water interface were similar to the isotherms of the longest polymer (described in 3.1.4) however their lift-off areas were at lower values due to the smaller size of the copolymer, and therefore smaller area that one molecule occupies (Figure 3.2-6, Table 3.2-1). The plateaus became shorter for PDMS₃₇-*b*-PMOXA₉ and in the isotherm of the shortest polymer (PDMS₁₆-*b*-PMOXA₉) only one plateau was present, suggesting that two rearrangement states, pronounced for larger polymers, overlap each other (Figure 3.2-7), because of the limited organization possibilities.⁶³ Both shorter polymers formed monolayers at the LE state, represented by slightly lower compressibility modulus values than for the longest polymer ($C_s^{-1} = 42 \text{ mN m}^{-1}$ for PDMS₃₇-*b*-PMOXA₉, and 36 mN m^{-1} for PDMS₁₆-*b*-PMOXA₉).

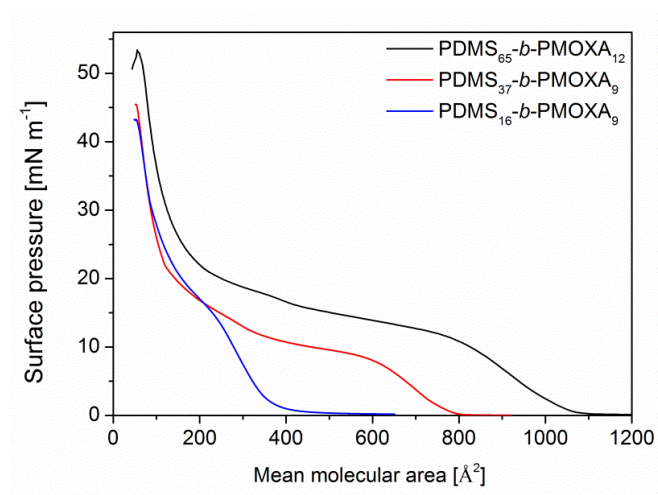


Figure 3.2-6. Surface pressure-area isotherm of PDMS₆₅-*b*-PMOXA₁₂ (black), PDMS₃₇-*b*-PMOXA₉ (red), and PDMS₁₆-*b*-PMOXA₉ (blue).

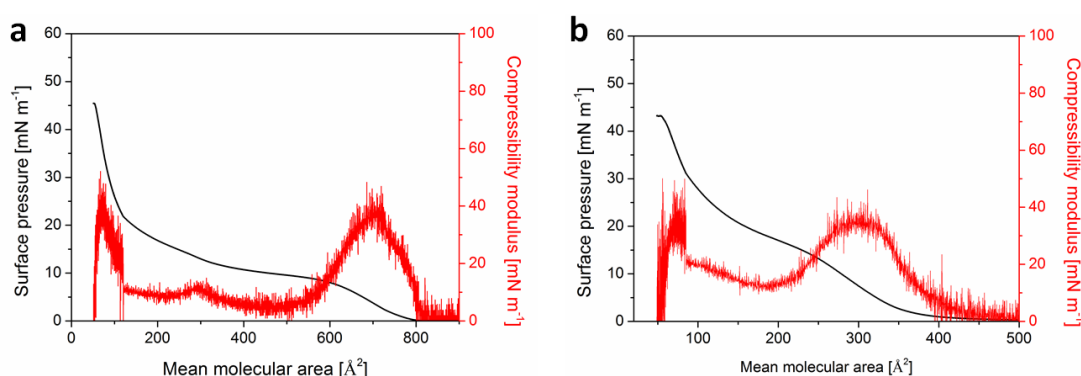


Figure 3.2-7. Surface pressure-area isotherm and compressibility modulus of: (a) PDMS₃₇-*b*-PMOXA₉ and (b) PDMS₁₆-*b*-PMOXA₉.

All three polymers formed homogeneous monolayers throughout the whole compression as established by BAM measurements (Figure 3.2-8). The only features that could be observed were small bright aggregates, which have been observed before for other polymer films formed at the air-water interface, and which correspond to surface micelles formed by hydrophobic chains.¹²⁷⁻¹²⁹ The formation of these micelles is not fully understood, but the purity of the copolymer can have an influence on the size of the micelles. For example, in PDMS-*b*-PMOXA diblock copolymers some unreacted residues of PDMS can be found, which at the air-water interface will form micelles. In addition,

formation the bright aggregates can be also influenced by the impurities present in the aqueous subphase.

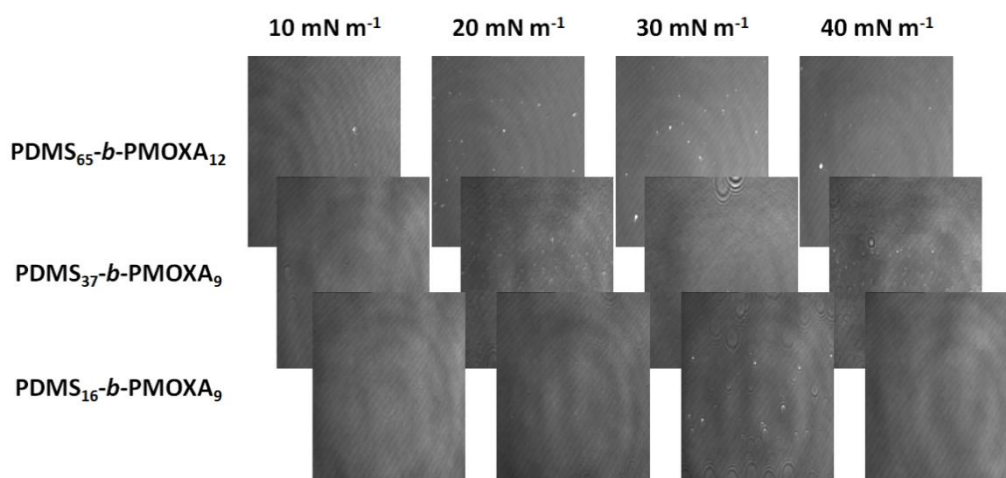


Figure 3.2-8. BAM images of PDMS-*b*-PMOXA diblock copolymer with different PDMS block lengths, and at various surface pressures, respectively.

3.2.2. Surface pressure-area isotherms of mixed monolayers

The mixing properties of all three diblock copolymers (PDMS₆₅-*b*-PMOXA₁₂, PDMS₃₇-*b*-PMOXA₉, and PDMS₁₆-*b*-PMOXA₉) with DPPC, DOPC, DPPE, and POPE, were investigated by performing Langmuir monolayer compressions in the whole range of the components' molar ratios, *i.e.* molar fraction of polymer ($x_{polymer}$) equal to 0.25, 0.50, and 0.75. With decreasing amount of polymer in the mixture, the mean molecular area of the monolayers decreases stepwise (Figure 3.2-9, 3.2-10, and 3.2-11). The plateau span becomes smaller. It is visible even at low molar fraction of polymer, suggesting segregation of the components. The separation of the mixture's components is due to molecular factors, such as: i) the size difference between the polymer and lipid, and ii) a different state of the mixture's components (LE for polymer, LC for DPPC, and S for DPPE), and iii) chemical incompatibility.⁶³ The shortest polymer, with 16 PDMS units, due to the size similarity, was interacting more with the lipid, for this reason the plateau of the isotherms could be barely seen (Figure 3.2-12). Upon addition of lipid, the binary monolayers became more rigid, as seen by the compressibility modulus calculations (Table 3.2-2 and 3.2-3).

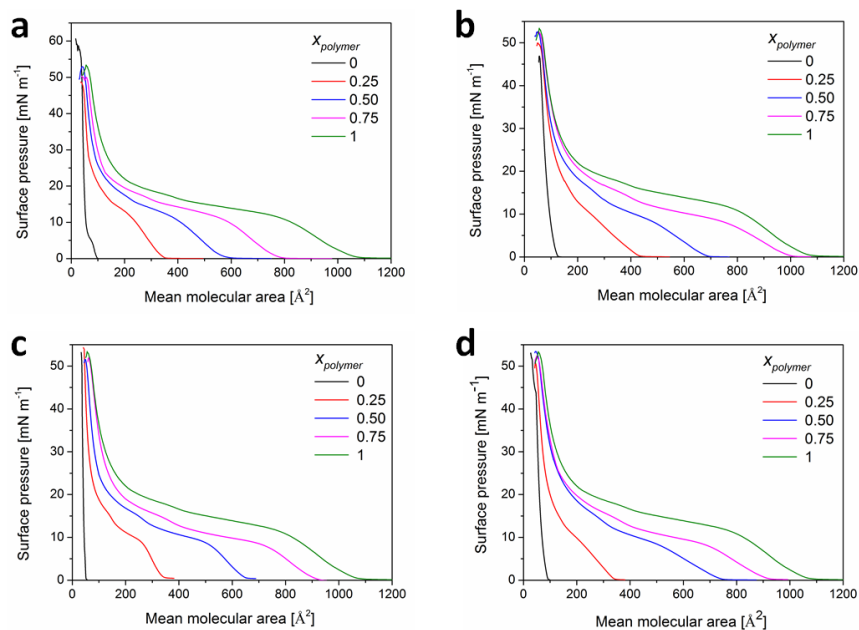


Figure 3.2-9. Surface pressure-area isotherms of PDMS₆₅-*b*-PMOXA₁₂ mixed with: (a) DPPC, (b) DOPC, (c) DPPE, and (d) POPE.

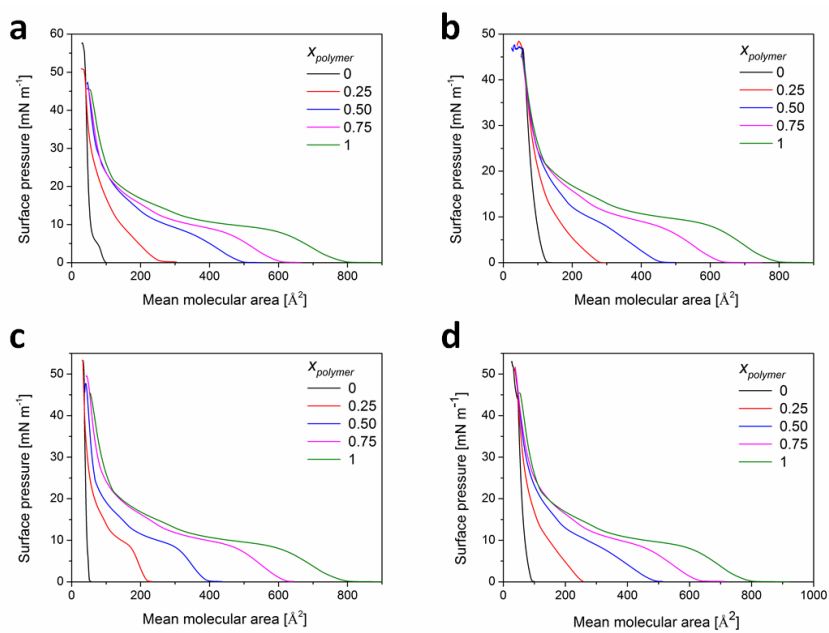


Figure 3.2-10. Surface pressure-area isotherms of PDMS₃₇-*b*-PMOXA₉ mixed with: (a) DPPC, (b) DOPC, (c) DPPE, and (d) POPE.

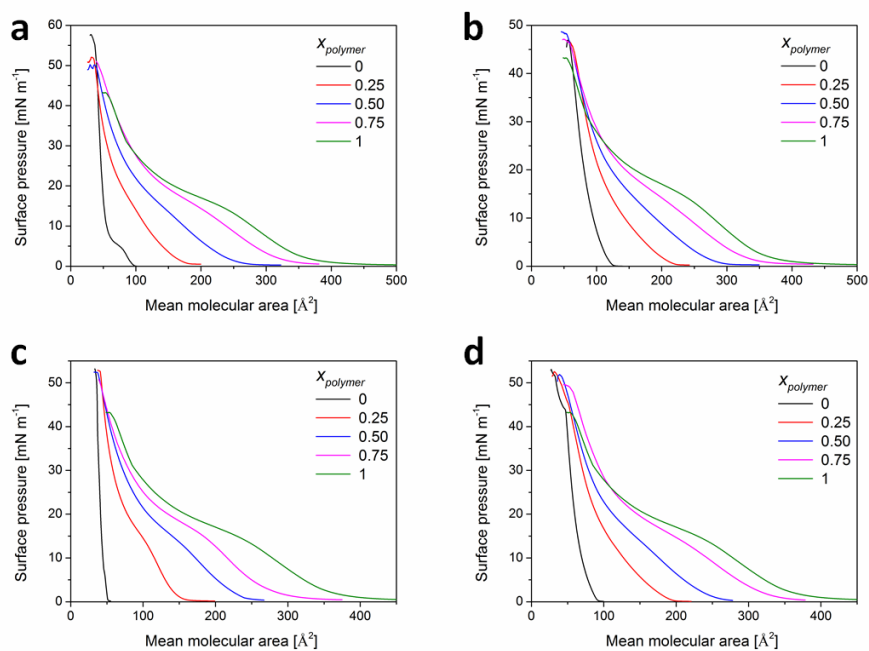


Figure 3.2-11. Surface pressure-area isotherms of PDMS₁₆-*b*-PMOXA₉ mixed with: (a) DPPC, (b) DOPC, (c) DPPE, and (d) POPE.

Table 3.2-2. Compressibility moduli of PDMS-*b*-PMOXA (AB) mixed with DPPC and DOPC.

x_{AB}	Compressibility modulus [mN m^{-1}]					
	A ₆₅ B ₁₂ -DPPC	A ₃₇ B ₉ -DPPC	A ₁₆ B ₉ -DPPC	A ₆₅ B ₁₂ -DOPC	A ₃₇ B ₉ -DOPC	A ₁₆ B ₉ -DOPC
0	184	184	184	102	102	102
0.25	69	71	55	55	58	65
0.50	51	51	36	46	50	44
0.75	51	40	28	40	44	40
1	44	37	36	44	37	36

Table 3.2-3. Compressibility moduli of PDMS-*b*-PMOXA (AB) mixed with DPPE and POPE.

x_{AB}	Compressibility modulus [mN m ⁻¹]					
	A ₆₅ B ₁₂ - DPPE	A ₃₇ B ₉ - DPPE	A ₁₆ B ₉ - DPPE	A ₆₅ B ₁₂ - POPE	A ₃₇ B ₉ - POPE	A ₁₆ B ₉ - POPE
0	514	514	514	51	51	51
0.25	106	100	85	65	52	23
0.50	57	67	40	46	41	42
0.75	49	48	31	41	34	41
1	44	37	36	44	37	36

3.2.3. Formation of domains at low surface pressures

PDMS₆₅-*b*-PMOXA₁₂ and PDMS₃₇-*b*-PMOXA₉ showed a similar tendency, *i.e.* in the presence of saturated lipids they formed domains, alike mixtures of PMOXA-*b*-PDMS-*b*-PMOXA triblock copolymer and DPPC, which have been previously studied.¹²⁸ Noted, that, neither BAM nor CLSM measurements did not provide resolution high enough to observe phase separation at the nanoscale and here we concentrate on investigations of the mixing properties at the micro-scale.

At low surface pressures, during compression of PDMS₆₅-*b*-PMOXA₁₂ mixed with DPPC or DPPE ($x_{polymer}$ = 0.25 and 0.5) and PDMS₆₅-*b*-PMOXA₁₂ or PDMS₃₇-*b*-PMOXA₉ mixed with DOPC ($x_{polymer}$ = 0.5), formation of bright spherical domains was observed (Figure 3.2-12 a-c). These domains were assumed to consist of lipid with a certain amount of embedded polymer, since: i) the domains are bright, thus thicker than continuous phase, ii) they appear only at lower molar fractions of polymer, and iii) at $x_{polymer}$ = 0.25 the domains occupy most of the analyzed area. In order to confirm this assumption the polymer-lipid film labeled with a fluorescent dye (sulforhodamine B, SRB) polymer, was transferred at surface pressure of 10 mN m⁻¹ and investigated by CLSM (Figure 3.2-12 d). CLSM micrographs revealed that a continuous phase was composed of polymer (red color on the micrograph), while the domains being much darker than the polymer-rich phase are composed mainly of DPPC. The lipid-rich

domains on CLSM micrograph are however not definitely black, indicating that some labeled polymer is also present there.¹⁴⁷

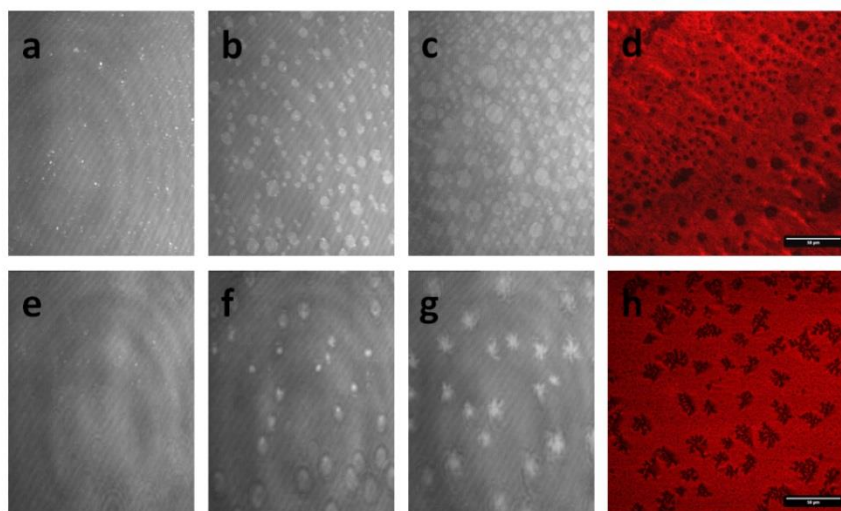


Figure 3.2-12. BAM images of monolayers from PDMS₆₅-*b*-PMOXA₁₂-DPPC: (a) 0.75 – 0.25, (b) 0.5 – 0.5, (c) 0.25 – 0.75 (at 10 mN m⁻¹), and PDMS₁₆-*b*-PMOXA₉-DPPC: (e) 0.75 – 0.25, (f) 0.5 – 0.5, (g) 0.25 – 0.75 (at 16 mN m⁻¹). CLSM micrographs of: (d) PDMS₆₅-*b*-PMOXA₁₂-DPPC (0.25 – 0.75, at 10 mN m⁻¹), and (h) PDMS₁₆-*b*-PMOXA₉-DPPC (0.25 – 0.75, at 16 mN m⁻¹), scale bars are 50 μm.

In the mixtures of the shortest polymer (PDMS₁₆-*b*-PMOXA₉) and DPPC or DPPE the domains appeared at higher surface pressures than it was in case of PDMS₆₅-*b*-PMOXA₁₂ (at 14 mN m⁻¹), in addition they were more pronounced, smaller, and their shape was star-like (Figure 3.2-12 f, g) however they also consisted of lipid-rich phase, as established by CLSM (Figure 3.2-12 h). The different shape and surface pressure (in comparison with PDMS₆₅-*b*-PMOXA₁₂-DPPC mixtures), at which domains formed, was due to the lower thickness of the PDMS₁₆-*b*-PMOXA₉ monolayer, which is very close to the thickness of DPPC ($d = 1.8$ nm for polymer, and 2.1 nm for DPPC). PDMS₁₆-*b*-PMOXA₉ does not have a decisive influence on the film formation, therefore the domains which appeared in this case were similar, as those observed during pure DPPC compression, occurring at the LE-LC transition of the lipid.

The question which has to be answered is: why are these domains thicker than the continuous polymer-rich phase? The domains appear at surface pressure of 3 mN m⁻¹. At so low surface pressure both DPPC and PDMS₆₅-*b*-PMOXA₁₂ components are not well

organized yet (Figure 3.2-13). Lipid and copolymer phase separate due to the size difference, and the lipid starts to expel the polymer chains from the lipid-rich phase. However, at this surface pressure, the polymer is in the so-called mushroom conformation, in which both hydrophobic and hydrophilic chains are shrunken,⁶³ this is why the lipid chains, which are organized vertically to the air-water interface, are thicker than polymer at this stage.^{62,148} With increasing surface pressure the domains disappear, because the polymer chains become more stretched.

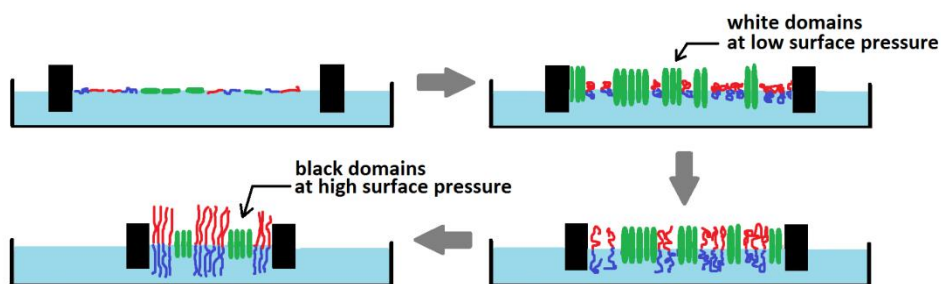


Figure 3.2-13. Scheme presenting the formation of a domain in mixed polymer-lipid monolayer, at low and high surface pressures. Molecules in green correspond to lipid and red-blue to amphiphilic block copolymer.

3.2.4. Formation of domains at high surface pressures

Upon compression of the binary monolayers the bright domains disappeared and at higher surface pressures ($> 30 \text{ mN m}^{-1}$), for certain mixtures composition, black domains appeared (Figures 3.2-14 and 3.2-15). These domains corresponded to a lipid-rich phase, as established by CLSM measurements (Figure 3.2-16). At higher surface pressures the monolayer is well organized which means that the polymer chains are fully stretched, forming a thicker phase than lipids. This phenomenon could be well observed for PDMS₆₅-*b*-PMOXA₁₂ and PDMS₃₇-*b*-PMOXA₉ diblock copolymers (Figure 3.2-13). The small, white aggregates visible on most of the BAM images correspond to hydrophobic, PDMS block surface micelles.^{128,129}

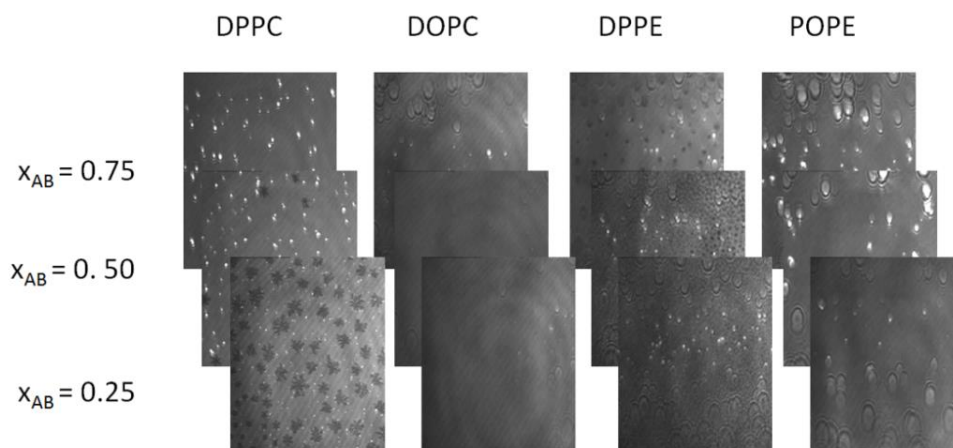


Figure 3.2-14. BAM images of PDMS₆₅-*b*-PMOXA₁₂ mixed with lipids at different molar ratios, respectively. Images were taken at a surface pressure of 35 mN m⁻¹.

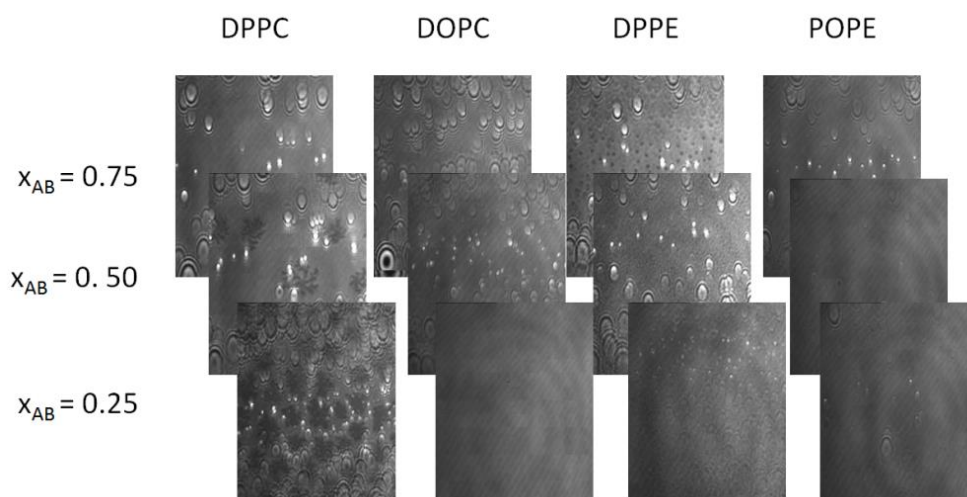


Figure 3.2-15. BAM images of PDMS₃₇-*b*-PMOXA₉ mixed with lipids at different molar ratios, respectively. Images were taken at a surface pressure of 35 mN m⁻¹.

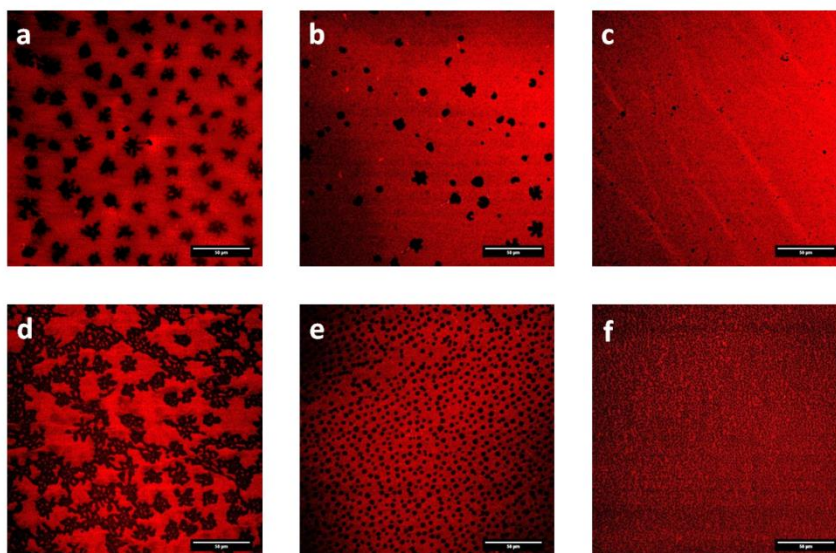


Figure 3.2-16. CLSM micrographs of: (a) PDMS₆₅-*b*-PMOXA₁₂ (x_{AB} = 0.25)-DPPC, (b) PDMS₆₅-*b*-PMOXA₁₂ (x_{AB} = 0.75)-DPPE, (c) PDMS₆₅-*b*-PMOXA₁₂ (x_{AB} = 0.25)-DOPC, (d) PDMS₃₇-*b*-PMOXA₉ (x_{AB} = 0.25)-DPPC, (e) PDMS₃₇-*b*-PMOXA₉ (x_{AB} = 0.5)-DPPE, and (f) PDMS₃₇-*b*-PMOXA₉ (x_{AB} = 0.25)-DPPE. All of the films were transferred at the surface pressure of 35 mN m⁻¹. Scale bars are 50 μm.

Mixtures composed of PDMS₆₅-*b*-PMOXA₁₂ or PDMS₃₇-*b*-PMOXA₉ and DPPC ($x_{polymer}$ = 0.25 and 0.5), formed domains of flower-like shape and depending on the molar ratio and polymer used, the amount and shape of the domains varied. For example, in the mixtures of DPPC with middle-length polymer, having 37 PDMS units, the domains were more extended and the phase separation seemed not to be as definitive as with PDMS₆₅-*b*-PMOXA₁₂-DPPC mixtures (Figure 3.2-15 and 3.2-16 d), which was due to the lower thickness of the monolayer and thus higher amount of interactions between lipid- and polymer-rich phases. In mixtures with DPPE, domains were smaller and of more regular, spherical shape, and they could be observed also at low lipid content (x_{DPPE} = 0.25) in contrary to mixtures with DPPC. The difference in the size and shape of domains was due to the fact that head group of PE is smaller than PC, which allows for closer packing of the molecules.¹⁴⁹ Additionally, PE is known to form intermolecular hydrogen bonds is thus more difficult to hydrate.¹⁵⁰ At the surface pressure of 35 mN m⁻¹, at which domains were investigated, DPPE is in a liquid expanded state (C_s^{-1} = 173 mN m⁻¹, Table 3.2-1) and for this reason it adopts fast spherical shape domains, in order to reduce contact with the LE polymer-rich phase.

PDMS₁₆-*b*-PMOXA₉ did not form any domains at high surface pressures due to the size similarity with lipids and therefore better mixing properties (Figure 3.2-17).

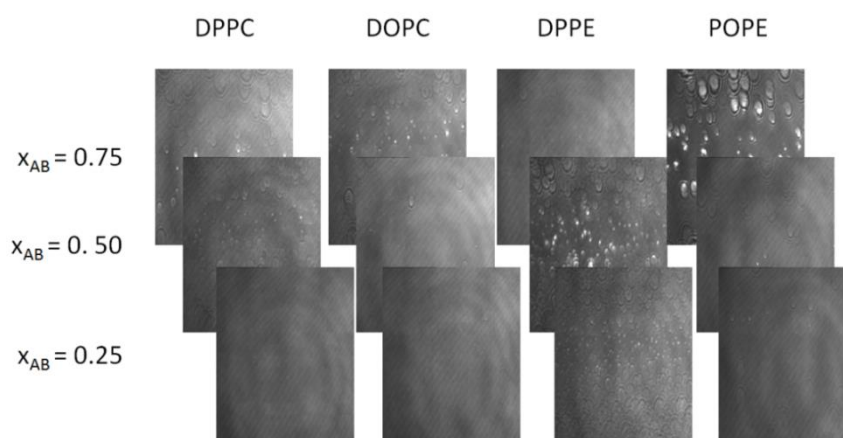


Figure 3.2-17. BAM images of PDMS₁₆-*b*-PMOXA₉ mixed with lipids at different molar ratios, respectively. Images were taken at a surface pressure of 35 mN m⁻¹.

In the monolayer composed of PDMS₆₅-*b*-PMOXA₁₂ ($x_{AB} = 0.25$) and DOPC very small domains were observed by CLSM (Figure 3.2-16 c). Otherwise, all PDMS-*b*-PMOXA–DOPC and PDMS-*b*-PMOXA–POPE mixtures formed uniform films for all polymers and at all molar ratios. Since all components of these mixtures are in the L or LE state, the phase separation is not as pronounced as for other mixtures, containing more rigid lipids, and no domains in micro-scale can be observed.^{8,150}

3.2.5. Distribution of the protein in the polymer-lipid mixed film

Prior to transferring the mixed monolayers with inserted protein, the influence of the protein on monolayer formation was investigated. The protein was injected onto the pre-formed mixed monolayer of PDMS₆₅-*b*-PMOXA₁₂ ($x_{AB} = 0.25$) and DPPC at surface pressure of 20 mN m⁻¹. After stabilization the monolayer was compressed further (Figure 3.2-18).



Figure 3.2-18. Procedure of protein insertion: 1) spreading of polymer solution and monolayer compression to 20 mN m^{-1} , 2) addition of protein, 3) monolayer compression to 35 mN m^{-1} , and 4) transfer to solid support.

Introduction of MloK1 to the monolayer did not change the shape of the isotherm however it could be observed that the collapse point was shifted to the higher surface pressure (Figure 3.2-19). The mixed monolayer had a collapse point at 47 mN m^{-1} , whereas upon protein insertion it collapses at 52 mN m^{-1} . Additionally, a change in the compressibility moduli was observed, which indicated an increase in the monolayer fluidity ($C_s^{-1} = 69 \text{ mN m}^{-1}$ for pure monolayer and 62 mN m^{-1} for monolayer with inserted protein, Figure 3.2-19).

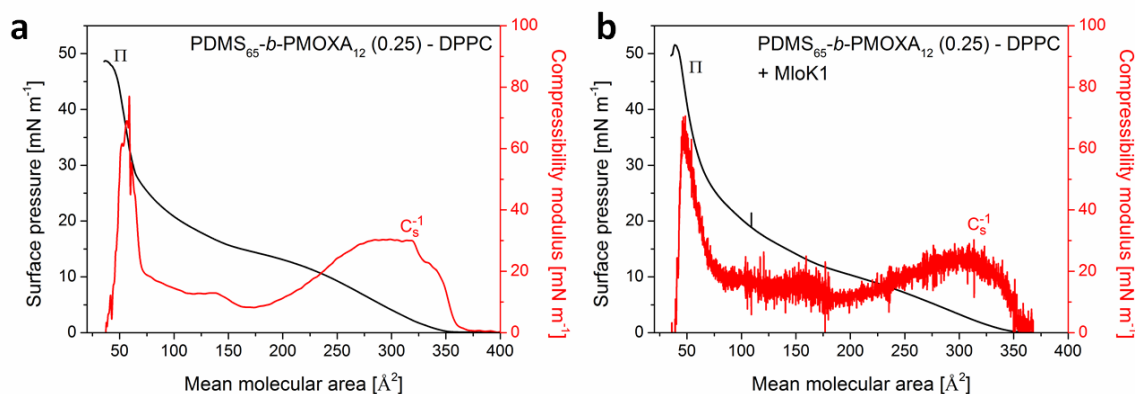


Figure 3.2-19. Surface pressure-area isotherms of PDMS₆₅-*b*-PMOXA₁₂ ($x_{AB} = 0.25$) and DPPC: (a) without and (b) with inserted protein.

Increase in the fluidity of the mixture of PDMS₆₅-*b*-PMOXA₁₂ ($x_{polymer} = 0.25$) and DPPC could be observed as a slight change of the domains shape, as established by BAM (Figure 3.2-20). After protein insertion, the DPPC-rich domains at 35 mN m^{-1} became bigger and more expanded, compared to the same mixture without protein, in which the

domains were smaller and more spherical. Interestingly, this expanded shape of domains was similar to the domains observed in the mixture containing 30% of the polymer (PDMS₆₅-*b*-PMOXA₁₂ and DPPC, without protein) at the same surface pressure. With increasing molar fraction of polymer, the lipid-rich domains are formed at higher surface pressures, *e.g.* in mixture containing 25% of polymer (no protein) the expanded domains started to form at a surface pressure of approximately 27 mN m⁻¹ and at 35 mN m⁻¹ they were well organized forming smaller and more spherical domains (Figure 3.2-20). For mixtures with 30% polymer fraction, at 27 mN m⁻¹ only few small domains could be observed, while at 35 mN m⁻¹, the expanded domains were formed, and spherical well organized domains appeared only at a surface pressure of 40 mN m⁻¹.

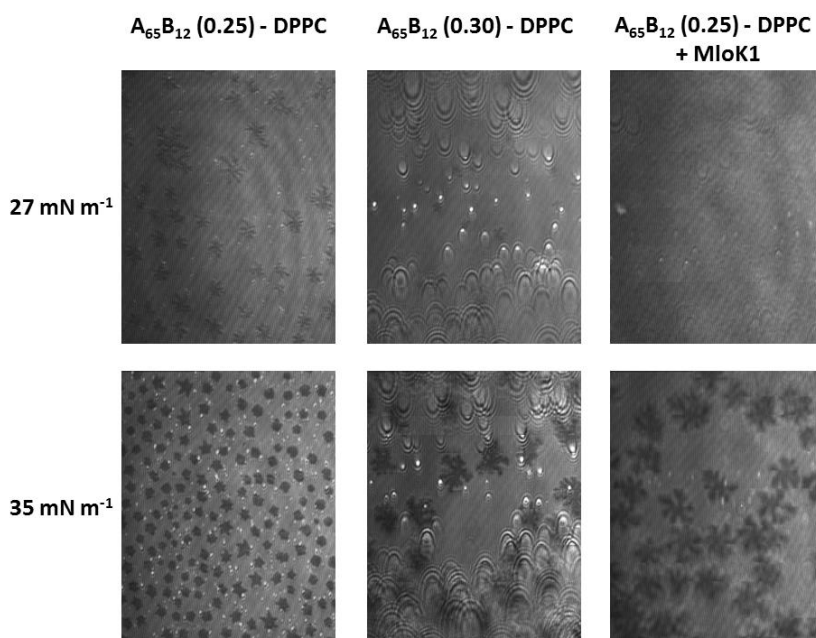


Figure 3.2-20. BAM images of PDMS₆₅-*b*-PMOXA₁₂ (A₆₅B₁₂) and DPPC mixtures, with and without inserted protein, at certain component ratios (given in the brackets). Images were taken at 27 and 35 mN m⁻¹. Size of the images is 200 x 250 μm².

The change of the monolayer behavior after protein insertion can be attributed to the fact that protein inserts into polymer-rich phase, increasing in this way the fraction of the polymer, so the mixture starts to behave as there was 30% of polymer, and not 25%. This assumption was supported by a decrease of the compressibility moduli values, which was also observed for the mixtures with higher polymer molar fraction, *e.g.* mixture with 30% of PDMS₆₅-*b*-PMOXA₁₂ had a C_s^{-1} close to 60 mN m⁻¹. However, such pronounced

changes in the domain formation process were observed only for mixtures composed of 25% of PDMS-*b*-PMOXA and 75% of DPPC. In the mixtures with DPPE, spherical domains were formed immediately and did not change their shape upon monolayer compression or protein insertion. It is due to the high stiffness of the DPPE monolayers (LC state) and formation of hydrogen bonds between the PE head-groups.

In order to investigate the distribution of the protein, both protein and the polymer were labeled with fluorescent dyes (DyLight 488 and SRB, respectively). The labeled membrane protein was inserted into the mixtures containing PDMS₆₅-*b*-PMOXA₁₂ and PDMS₃₇-*b*-PMOXA₉ diblock copolymers and then transferred to a glass slide and observed by CLSM. In the mixtures containing DPPC (x_{DPPC} = 0.75 and 0.5) and DPPE (x_{DPPE} = 0.25 and 0.5), the protein was solely distributed in the polymer-rich phase, while the lipid-rich domains remained black indicating no protein accommodation (Figure 3.2-21 a-c, f). This result is in good agreement with previous report, which describe the mixing of PMOXA-*b*-PDMS-*b*-PMOXA triblock copolymer with DPPC. OmpF was preferentially distributing in polymer-rich phase.⁵¹ The slight change of the DPPC-rich domains was also observed by CLSM, in good agreement with BAM images. For the mixtures with DOPC formation of small lipid domains could be observed, as described before. Interestingly, in this case the proteins were accommodated exactly in these spherical domains (Figure 3.2-21 d). In the uniform PDMS₆₅-*b*-PMOXA₁₂ and POPE mixtures protein was distributes throughout the whole film (Figure 3.2-21 e).

The physical state of the components of mixtures has a crucial influence on protein distribution within the binary monolayer. DPPC and DPPE form the stiffest monolayers in the liquid condensed states. For this reason, the protein accommodates preferentially in the polymer-rich phase, which is in a liquid expanded state in mixtures containing these lipids. In this state the polymer is more flexible, has more conformational possibilities, and possesses a PDMS block of high hydrophobicity, which is able to host membrane proteins. However, if the lipid is more liquid, as for example in mixtures with DOPC, the protein inserts into the lipid-rich domains. Mixtures of PDMS₆₅-*b*-PMOXA₁₂-POPE provide a uniform distribution of the protein in the whole monolayer, due to the similar fluidity of the mixture components.

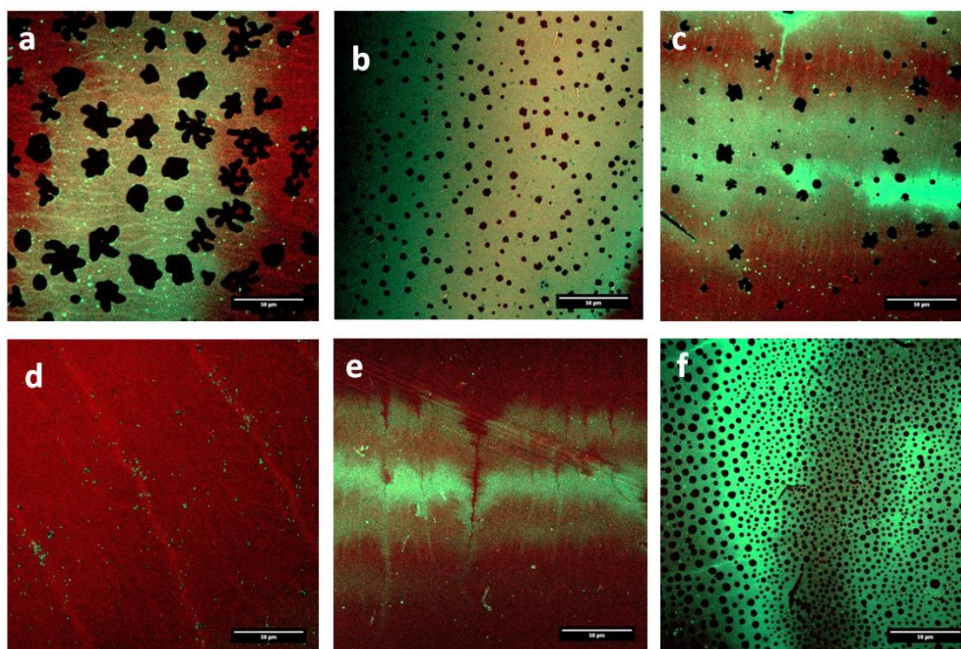


Figure 3.2-21. CLSM micrographs presenting protein distribution in films consisting of mixtures of PDMS₆₅-*b*-PMOXA₁₂ and: (a) DPPC ($x_{DPPC} = 0.75$), (b) DPPC ($x_{DPPC} = 0.5$), (c) DPPE ($x_{DPPE} = 0.25$), (d) DOPC ($x_{DPPC} = 0.25$), and (e) POPE ($x_{DPPC} = 0.25$). (f) PDMS₃₇-*b*-PMOXA₉ mixed with DPPE ($x_{DPPE} = 0.5$). Films were transferred at the surface pressure of 35 mN m⁻¹. Scale bars correspond to 50 μm.

3.2.6. Summary

In this work hybrid materials, based on amphiphilic block copolymers and lipids, have been introduced. It has been shown that depending on the components' character, size, and molar fraction, different morphologies of the material can be obtained. The most phase separation between two components could be observed when the longest polymer (PDMS₆₅-*b*-PMOXA₁₂) and saturated lipids (DPPC and DPPE) were used. The micro-sized domains were formed due to the size difference between polymers and lipids as well as the different states of the mixture's components. The state of the pure amphiphiles could be established by investigation of monolayers formation at the air-water interface and calculation of compressibility moduli. DPPC and DPPE showed to form rigid films in LC and S state, respectively, whilst copolymers and two unsaturated lipids (DOPC and POPE) were more fluid, in LE and L states.

A physical state of the mixture components had a crucial influence on the protein distribution within the binary monolayer. In mixtures containing rigid DPPC or DPPE, the protein was preferentially accommodating in the polymer-rich phase, which was in the LE state. In this state, the polymer is more flexible, has more conformational freedom, and in addition, it possesses a PDMS block of high hydrophobicity, which is able to host membrane proteins. However if the lipid was in the liquid state, as for example in mixtures with DOPC, the protein inserted into the lipid-rich domains. The mixtures of PDMS-*b*-PMOXA-POPE provided uniform distribution of the protein in the whole monolayer due to good mixing of the monolayer's components.

Hybrids build of copolymers and lipids constitute a new group of functional materials which can find applications in medicine, biosensing, and surface coating. By combination of all mixture's components, special properties of the material can be developed, such as increased stability and lower permeability of the material (thanks to the presence of the polymer) and higher biocompatibility (thanks to the lipid). It was shown that it is possible to obtain materials of different morphologies by choosing appropriate mixture's components and ratios. In addition, the distribution of the membrane protein could be controlled.

3.3. Asymmetric triblock copolymer-based active surfaces

The scope of this project was a development of an active surface by immobilization of laccase to solid-supported asymmetric film formed by poly(ethylene glycol)-*block*-poly(γ -methyl- ϵ -caprolactone)-*block*-poly[(2-dimethylamino) ethyl methacrylate] (PEG-*b*-PMCL-*b*-PDMAEMA, ABC) triblock copolymers (Figure 3.3-1). This asymmetric polymer has appealing properties to serve as a cushion for the enzyme, since PEG is a hydrophilic biocompatible block, PMCL is a flexible hydrophobic block, and PDMAEMA is a second hydrophilic block with tertiary amine active groups.¹⁵¹ The polymer films were prepared by LB transfers, in order to provide well-organized and highly reproducible monolayers. Laccase which is a copper-containing oxidase was chosen as a model enzyme. This enzyme can be found in many fungi, plants, and microorganisms¹⁵² and it is known to catalyze the oxidation of a number of organic and inorganic compounds, such as phenols.¹⁵³ Additionally, it is involved in the degradation

of lignin,¹⁵⁴ thus it might find applications in industry, as a detoxification, biodegradation, and catalytic agent.

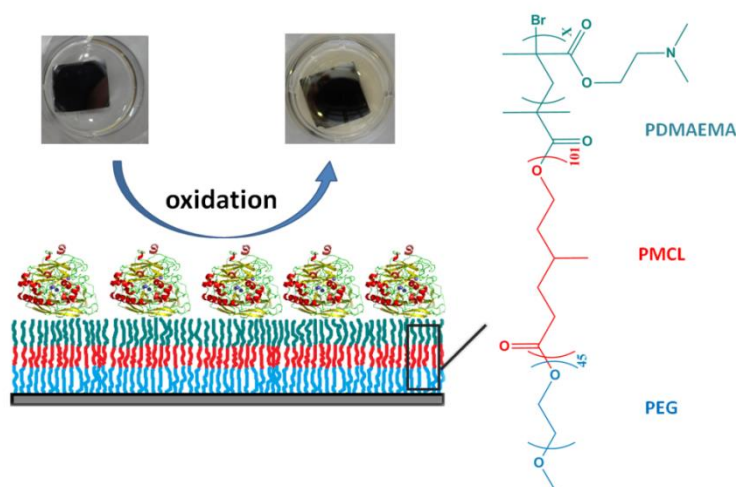


Figure 3.3-1. Scheme of asymmetric membrane composed of triblock copolymer, with immobilized, active enzyme.

Preparation of active surfaces required understanding of how PEG₄₅-*b*-PMCL₁₀₁-*b*-PDMAEMA_x triblock copolymers organize under compression at the air-water interface, and what are the structural properties, which determine film formation and availability for enzyme adsorption. This was established by measurements on Langmuir trough and characterization of films transferred to solid supports. The stability and reactivity of the “active surface” of an enzyme immobilized on the copolymer film was investigated by monitoring the oxidation of a phenolic electron mediator, 2,6-dimethoxyphenol (DMP), which undergoes reaction only in the presence of active laccase.

3.3.1. Characterization of the PEG-*b*-PMCL-*b*-PDMAEMA triblock copolymer

Synthesis of PEG₄₅-*b*-PMCL₁₀₁-*b*-PDMAEMA_x triblock copolymer has been performed and described before.¹⁵¹ In brief, ring-opening polymerization (ROP) of γ -methyl- ϵ -caprolactone (MCL) was performed using PEG as a macroinitiator. The modified PEG-*b*-PMCL diblock copolymer containing an atom transfer radical polymerization (ATRP)-initiating group was then used for synthesis of the third, PDMAEMA block. The synthesized polymers varied with the length of the PDMAEMA

block and possessed respectively: 3, 12, 17, and 27 PDMAEMA units, as calculated from $^1\text{H-NMR}$ spectra. GPC analysis showed the PDI of the synthesized polymers to be approximately 1.4.

The structure of the $\text{PEG}_{45}\text{-}b\text{-PMCL}_{101}\text{-}b\text{-PDMAEMA}_x$ triblock copolymers has been confirmed by $^1\text{H-NMR}$ (Figure 3.3-2). The signal at $\delta = 1.33 - 1.67$ ppm corresponds to the $-\text{CH}_2-$ and $-\text{CH}-$ groups (5H, c, d, e) of the PMCL block, the signal at $\delta = 2.51$ ppm is assigned to the $-\text{CH}_2-$ group (2H, f) in the PDMAEMA block, and the signal at $\delta = 3.57$ ppm corresponds to the $-\text{CH}_2-$ groups (4H, a, b) of the PEG block. The detailed peaks assignment can be found in the section 6.

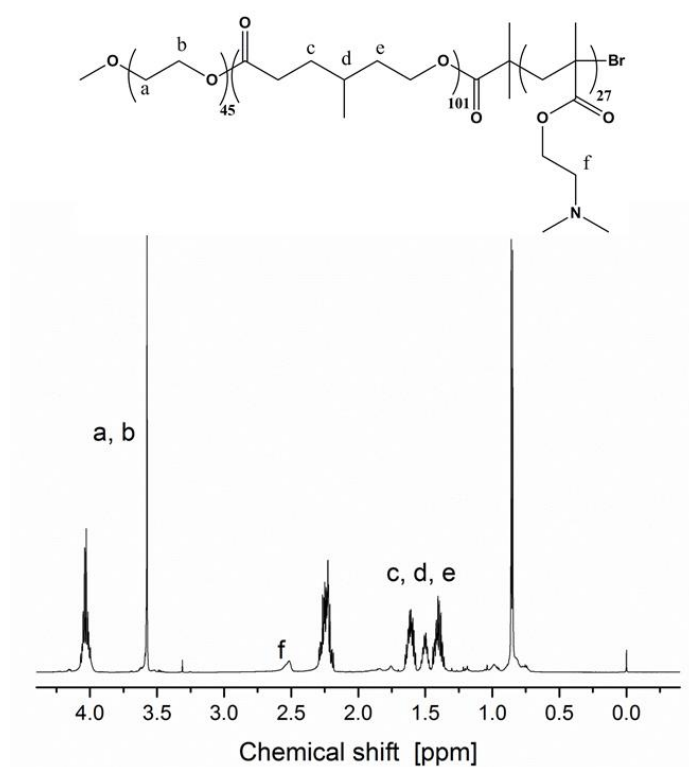


Figure 3.3-2. Representative $^1\text{H-NMR}$ spectrum and structure of $\text{PEG}_{45}\text{-}b\text{-PMCL}_{101}\text{-}b\text{-PDMAEMA}_{27}$ triblock copolymer.

ATR-FTIR measurements showed peaks characteristic for $\text{PEG}_{45}\text{-}b\text{-PMCL}_{101}\text{-}b\text{-PDMAEMA}_x$ triblock copolymer (Figure 3.3-3). The peaks at 2957 and 2860 cm^{-1} are associated with the C-H bond from alkyl groups, the peak at 1725 cm^{-1} corresponds to C=O group, the band at 1453 cm^{-1} is due to the C-H stretching, the group of peaks ranging from 1244 to 1100 cm^{-1} corresponds to the C-H and C-N stretching, and the peak at 527 cm^{-1} is assigned to the C-Br group.

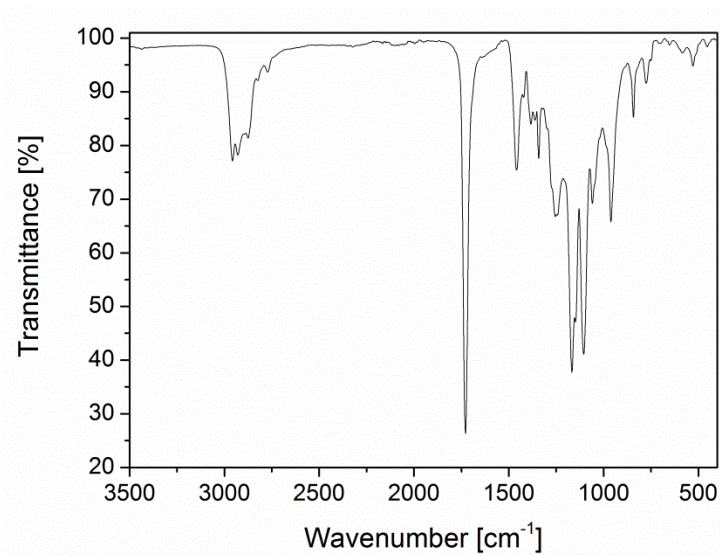


Figure 3.3-3. Representative ATR-FTIR spectrum of PEG₄₅-*b*-PMCL₁₀₁-*b*-PDMAEMA₂₇ triblock copolymer.

3.3.2. PEG-*b*-PMCL-*b*-PDMAEMA triblock copolymer at the air-water interface

Four copolymers varying in the length of the hydrophilic PDMAEMA block were first investigated on the Langmuir trough. Compression of the polymer spread at the air-water interface resulted in the formation of the monolayer. Surface pressure-area isotherms of all the polymers had similar shapes, with the characteristic plateaus at the surface pressures ranging from 13 to 16 mN m⁻¹ (Figure 3.3-4 a). These plateau areas correspond to the rearrangements of the polymer chains, which became more stretched,⁶³ as described in paragraphs 2.3.2 and 3.1.3. Depending on the molecular weight, monolayers collapsed at different mean molecular areas and surface pressures, *i.e.* whereas A₄₅-B₁₀₁-C₃ achieved the collapse surface pressure up to the mean molecular area of 200 Å², A₄₅-B₁₀₁-C₂₇ had a collapse at mean molecular area of about 350 Å² (Figure 3.3-4 b). Simultaneously, the surface pressure of the collapse point decreased with increasing number of PDMAEMA units. This behavior is explained by the higher area occupied by triblock copolymers having larger number of PDMAEMA units, which required more space for molecular arrangement during film formation.

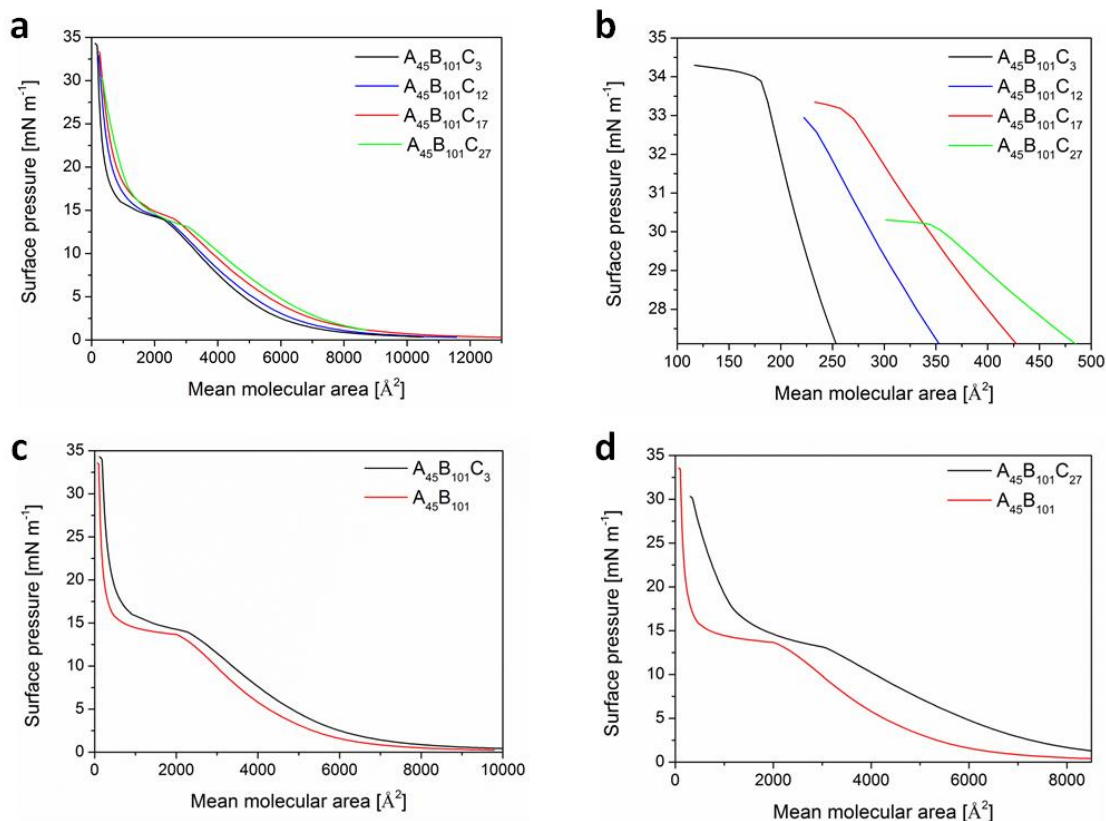


Figure 3.3-4. Surface pressure-area isotherms of the AB and ABC block copolymers; (a) $A_{45}B_{101}C_3$ (black), $A_{45}B_{101}C_{12}$ (blue), $A_{45}B_{101}C_{17}$ (red) and $A_{45}B_{101}C_{27}$ (green), and (b) zoom in to the collapse area; (c) $A_{45}B_{101}$ (red) and $A_{45}B_{101}C_3$ (black); (d) $A_{45}B_{101}$ (red) and $A_{45}B_{101}C_{27}$ (black).

In order to check the influence of the PDMAEMA block on Langmuir monolayer formation, isotherms of $A_{45}B_{101}C_3$ and $A_{45}B_{101}C_{27}$ were compared with isotherm of $A_{45}B_{101}$ diblock copolymer. As expected, there was almost no difference in the shape of the isotherms of $A_{45}B_{101}C_3$ and $A_{45}B_{101}$, because of the short hydrophilic C block of the triblock copolymer (Figure 3.3-4 c). Due to the absence of the C block, $A_{45}B_{101}$ copolymer was characterized by both lower surface pressure for film rearrangement during the compression (plateau zone), and slightly lower mean molecular area of the collapse point, in comparison to the triblock copolymer monolayer. Influence of the PDMAEMA block on the monolayer formation is well pronounced when comparing isotherm of $A_{45}B_{101}$ diblock copolymer with $A_{45}B_{101}C_{27}$ triblock copolymer (Figure 3.3-4d). Isotherm of $A_{45}B_{101}C_{27}$ is significantly shifted to higher values of mean molecular area, which is due to the larger size of the molecule.

The stability of monolayers at the air-water interface was assessed by measuring the surface pressure of the monolayer compressed to a surface pressure of 30 mN m^{-1} over 30 minutes. At this high surface pressure, the well-packed monolayer is already formed and the slow decrease of the surface pressure in time indicates that monolayers formed by $A_{45}\text{-}B_{101}\text{-}C_x$ are stable enough to be transferred to a solid substrate (Figure 3.3-5).

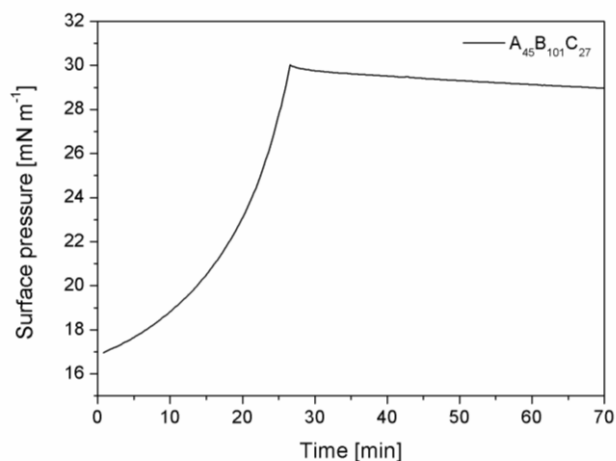


Figure 3.3-5. Stability of the $A_{45}\text{-}B_{101}\text{-}C_{27}$ triblock copolymer monolayer at the air-water interface.

The elasticity of ABC films was evaluated by recording three reversible compression-expansion cycles (Figure 3.3-6). As no relevant hysteresis was observed, ABC block copolymers did not dissolve in water, and their monolayers were elastic.

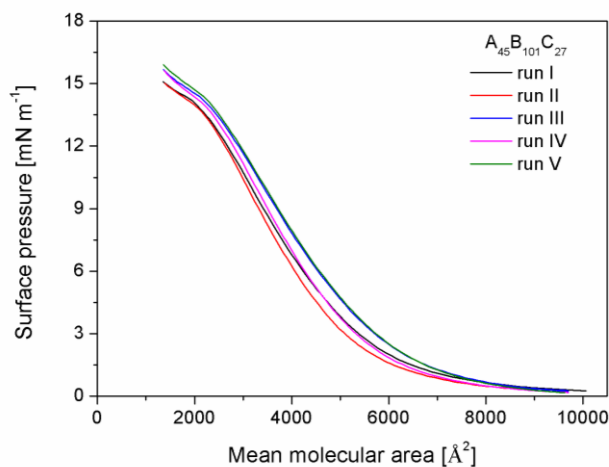


Figure 3.3-6. Compression-expansion cycles of $\text{PEG}_{45}\text{-PMCL}_{101}\text{-PDMAEMA}_{27}$ monolayer.

Modifications of polymer arrangements during compression of Langmuir monolayer, followed as surface pressure-area isotherms, were confirmed by the differences in BAM images (Figure 3.3-7), which showed different phase transitions. At the beginning of the compression, at low surface pressures, the ABC block copolymers have a large space at their disposal and no interactions between polymer chains occur, indicating that the film is in the gaseous state.⁵⁶ Then the copolymer chains organize, adopting a conformation in which all the blocks are coiled. At surface pressure corresponding to the plateau (16 mN m⁻¹) BAM images of A₄₅-B₁₀₁-C_x copolymers show formation of a rough monolayer at this stage of compression. With increasing surface pressure, the copolymers adopt a more ordered conformation with all blocks stretched, and finally a highly packed monolayer corresponding to the collapse point is formed. At high surface pressures (30 mN m⁻¹) the monolayer is again homogeneous without any significant features, such as aggregates (Figure 3.3-7).

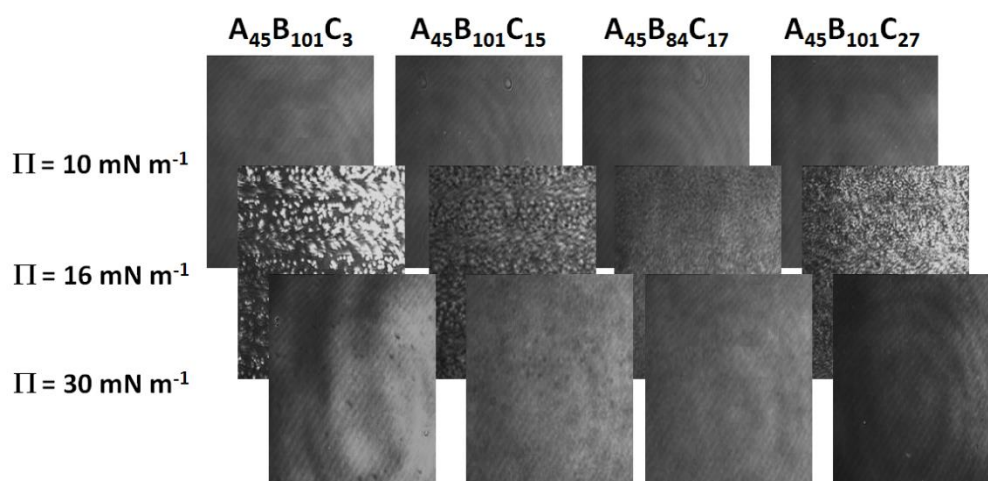


Figure 3.3-7. BAM images recorded during compression of A₄₅-B₁₀₁-C_x block copolymers at the air-water interface, at surfaces pressures (expressed in mN m⁻¹): 10, 16 and 30, respectively. Size of the images is 200 x 250 μm^2 .

Since the PDMAEMA block is pH sensitive, the influence of pH on monolayer formation was investigated. In this respect, Langmuir monolayers of PEG₄₅-PMCL₁₀₁-PDMAEMA₂₇ triblock copolymers were prepared on two different subphases: water and PBS buffer adjusted to pH 5, 6, and 7 (Figure 3.3-8). Surface pressure-area isotherms recorded for all subphase configurations do not show any significant deviations. However

the homogeneity of the monolayer was disrupted by changing the subphase from water to PBS, as observed with BAM (Figure 3.3-9). Whilst the monolayers prepared on water subphase were uniform at each pH, the introduction of ions coming from PBS to the subphase caused formation of aggregates upon compression of the monolayer.

The combination of Langmuir isotherms and BAM images clearly indicate that ABC block copolymers formed well-organized, closely-packed, defect free, elastic and stable films at the air-water interface at pH 7. For this purpose all the transfers to the solid supports were performed for monolayers prepared on water at pH 7, providing in this way homogeneity of the formed system.

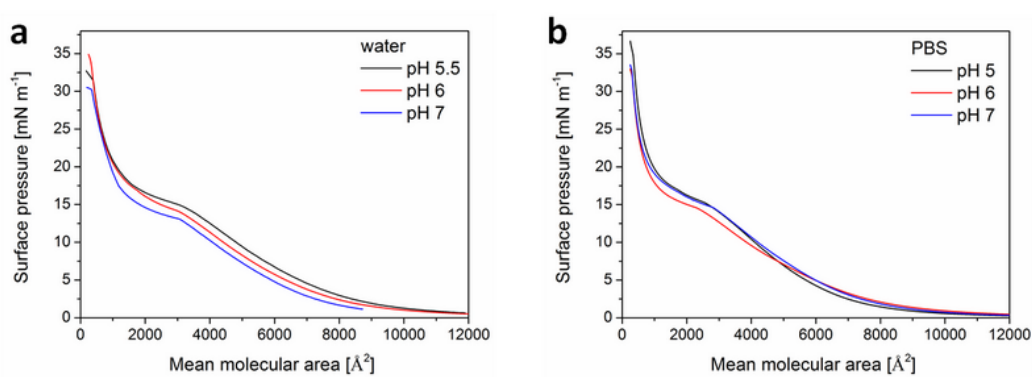


Figure 3.3-8. Surface pressure-area isotherms of PEG₄₅-PMCL₁₀₁-PDMAEMA₂₇ triblock copolymer recorded on (a) water and (b) PBS buffer adjusted to pH 5, 6, and 7.

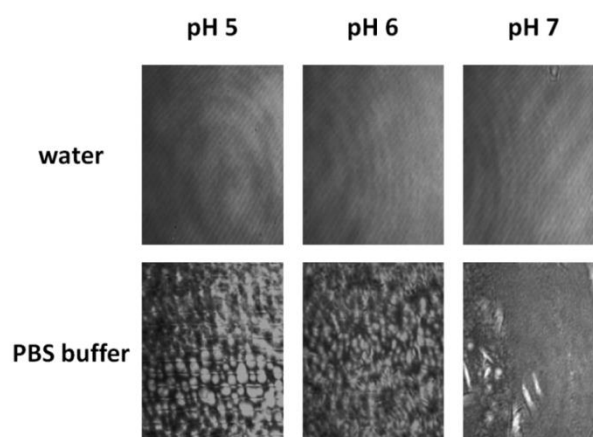


Figure 3.3-9. BAM images of monolayer formed from PEG₄₅-PMCL₁₀₁-PDMAEMA₂₇ on water and PBS buffer at different pH, respectively. Images were taken at surface pressure of 30 mN m⁻¹. Size of images is 200 x 250 μm².

3.3.3. Solid-supported monolayers formed from PEG₄₅-*b*-PMCL₁₀₁-*b*-PDMAEMA_x

A₄₅-B₁₀₁-C_x films were transferred from the air-water interface to silica plates at surface pressure values below the collapse pressure, to obtain a densely packed polymer monolayer with stretched chains. For all transfers, the transfer ratio was about 1, indicating a successful and defect-free deposition, with a yield close to 100%.⁹⁰ In order to understand the availability of the polymer film for enzyme adsorption, various surface properties of the film were studied: i) thickness (by ellipsometry), ii) surface energy (by contact angle), and iii) topography and roughness (by AFM) (Table 3.3-1).

It was assumed that at the air-water interface the ABC block copolymer adopts an orientation in which PEG, as hydrophilic block A, with constant length (45 units) is oriented towards water, whilst PDMAEMA, as the hydrophilic block C with variable lengths, is oriented towards the air phase. Such organization of polymer chains was expected, since PEG is more hydrophilic (a PEG film has a contact angle of approximately 30°)¹⁵⁵ than PDMAEMA (the contact angle of this polymer is approximately 50°).¹⁵⁶ Additionally, PEG can directly link to the silica slides through hydrogen bonding with silanol groups available at the silica surface, thus PEG acts as an anchor block during adsorption, whereas PDMAEMA is expected to be externally oriented. The purpose of all the following measurements was to confirm such organization of this asymmetric triblock copolymer.

Table 3.3-1. Properties of the A₄₅-B₁₀₁-C_x monolayers.

ABC block copolymer	Π [mN m ⁻¹] ⁽¹⁾	d [nm] ⁽²⁾	Contact angle [°] ⁽²⁾	R_a [nm]	
				pH 3	pH 7
A ₄₅ -B ₁₀₁ -C ₃	30	8.6 ± 0.1	61 ± 2	0.3	0.3
A ₄₅ -B ₁₀₁ -C ₁₂	30	8.0 ± 0.2	78 ± 1	0.3	0.6
A ₄₅ -B ₁₀₁ -C ₁₇	30	7.6 ± 0.1	67 ± 2	0.2	0.3
A ₄₅ -B ₁₀₁ -C ₂₇	30	7.7 ± 0.2	65 ± 1	0.6	1.0

⁽¹⁾ surface pressure at which the transfer was done; ⁽²⁾ average values calculated from measurements taken on two different plates, and on five different zones, with the related standard deviations.

Transfers of all four polymers were performed at a surface pressure of 30 mN m⁻¹. The length of the PDMAEMA block influenced monolayer arrangements and thickness (Table 3.3-1). The thickest film (8.6 nm) was obtained for A₄₅-B₁₀₁-C₃, whereas the film formed from copolymer having 27 units of PDMAEMA was 1 nm thinner (7.7 nm). The PDMAEMA block is a pH responsive block with a pK_a of 7.4. At the acidic pH of 2-3 it is strongly ionized and hydrophilic, however it was shown, that with increasing pH it becomes more and more hydrophobic.^{157,158} The thickness measurements were performed for films prepared at a neutral pH of 7, which is a boundary at which the polymer becomes more hydrophobic. Lower thickness of the polymers with longer PDMAEMA block can be caused by rearrangements of this peripheral block. The longer the PDMAEMA block the more hydrophobic it is and the more interactions with the PMCL block occur, resulting in formation of more coiled and compact structures, and as a consequence, thinner films.

Rearrangements of the ABC films upon pH change were confirmed by AFM measurements performed after immersion of the solid-supported monolayer in water at different pH values (3, 7, and 10). AFM images offer both qualitative and quantitative information regarding the morphology and roughness of the polymer films (Figure 3.3-10 and Table 3.3-1). The roughness of the ABC triblock copolymer films increased with increasing buffer pH from acidic to neutral values, which is in agreement with previously reported results for diblock copolymer films of poly(2-vinylpyridine)-*block*-poly(dimethylaminoethyl methacrylate) (PVP-*b*-PDMAEMA). All films formed by ABC block copolymers had high roughness (≤ 1.0 nm) at pH 10 and it was not possible to record images with AFM.

For both acidic and neutral pH values, low roughness characterized the films of A₄₅-B₁₀₁-C₃ copolymer ($R_a = 0.2$ nm at both pHs), whereas higher values were obtained for A₄₅-B₁₀₁-C₂₇, because of the influence of the C block on the orientation of the copolymer chains within the film. At pH 3 this copolymer formed a film with a roughness of 0.6 nm. After change of pH to value of 7, an increase of R_a to 1 nm was observed. Higher roughness of this copolymer can be due to the longer PDMAEMA blocks, which become more hydrophobic upon change of the pH and rearrange in order to reduce the contact area with water, which can be observed through formation of “holes” in the film.

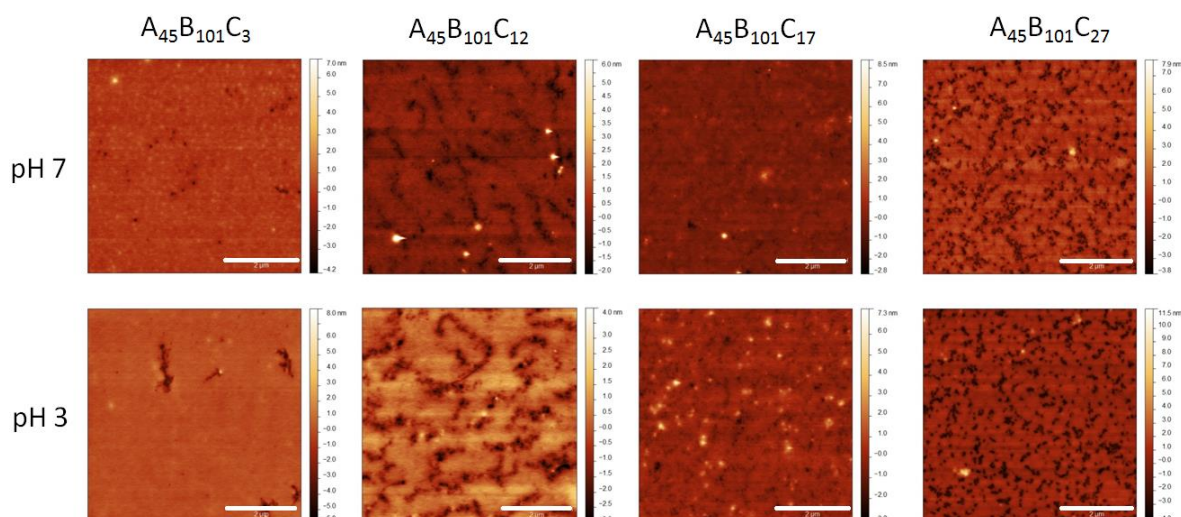


Figure 3.3-10. AFM images of: (a) $A_{45}B_{101}C_3$, (b) $A_{45}B_{101}C_{12}$, (c) $A_{45}B_{101}C_{17}$, and (d) $A_{45}B_{101}C_{27}$ transferred to silica slides and incubated in pH 3 or pH 7. Images were recorded in tapping mode in air. Scale bars are 2 μm .

AFM images of 7 months old copolymer films did not show any appreciable differences in topography when compared to freshly prepared samples, indicating that the films have long-term stability in air (Figure 3.3-11).

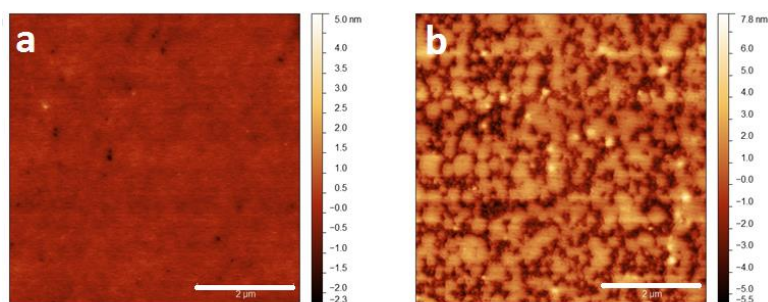


Figure 3.3-11. AFM images of: (a) $A_{45}B_{101}C_3$, and (b) $A_{45}B_{101}C_{27}$ measured after 7 months. Images were recorded in tapping mode in air. Scale bars are 2 μm .

The wettability of the polymer films was established by contact angle measurements. As the length of PEG and PMCL block is constant for all triblock copolymers studied in this project, the changes in the length of PDMAEMA block is expected to induce differences in contact angle values. The contact angle values for all $A_{45}B_{101}C_x$ monolayers ranged from 61° to 78° (Table 3.3-1), which indicates that the films

transferred onto silica slides generated a rather hydrophilic surface however no regularity has been observed, *i.e.* the highest contact angle of 78° was recorded for polymer having 12 PDMAEMA units, thus these changes cannot be clearly assigned to the change of the PDMAEMA block length.

3.3.4. Bilayers formed from PEG₄₅-PMCL₁₀₁-PDMAEMA₂₇

The number of polymer film layers deposited onto the solid surface was expected to influence the properties of the resulting polymer membrane. As A₄₅-B₁₀₁-C₂₇ block copolymer formed films with the highest monolayer roughness thus with higher surface area available for biomolecules adsorption, it was selected for successive deposition/transfer of two layers. As described in paragraph 2.4.4, different strategies for bilayer deposition have been developed, *i.e.* X-, Y-, and Z-type. However these strategies correspond to the situation, when the transferred monolayer is formed by phospholipids or amphiphilic diblock copolymers. In the case of amphiphilic triblock copolymers, which possess two peripheral hydrophilic blocks, it cannot be clearly predicted how the monolayer's deposition will proceed. For this purpose the bilayers composed of A₄₅-B₁₀₁-C₂₇ were prepared according to four deposition approaches, called: up-up, down-down, up-down, and down-up, where “up” corresponds to emersion and “down” to immersion of the slide.

Only the up-up strategy resulted in the formation of a bilayer with thickness of approximately 9.0 nm, as established by ellipsometry measurements (Table 3.3-2). This thickness corresponds to nearly the double of the thickness of the A₄₅-B₁₀₁-C₂₇ monolayer (5.3 nm). Up-down and down-up strategies gave a thickness 4.0 and 5.1 nm, respectively, which can be associated with successful deposition of only one polymer layer, while after a down-down approach, no material was transferred to the silica slide. The detected layer of 0.3 nm can be due to residues adsorbed from water however AFM measurements showed the roughness of this sample to be approximately 0.1 nm, which corresponds well to the roughness of the bare silica. The roughness of other samples ranged from 0.5 to 0.7 nm which is at the same level of roughness than that of the monolayer (0.8 nm).

AFM measurements showed that the up-up bilayer has fewer holes throughout the whole area, while up-down and down-up bilayers have the same topography as the

monolayer formed from A₄₅-B₁₀₁-C₂₇ (Figure 3.3-10 and 3.3-12). As expected, the sample prepared by down-down deposition resulted in a smooth surface with some little number of residues attached.

Table 3.3-2. Properties of the bilayers formed by A₄₅-B₁₀₁-C₂₇.

Deposition type	d [nm]	R _a [nm]
up-up	9.0 ± 0.4	0.5
down-down	0.3 ± 0.1	0.1
up-down	4.0 ± 0.3	0.7
down-up	5.1 ± 0.4	0.5

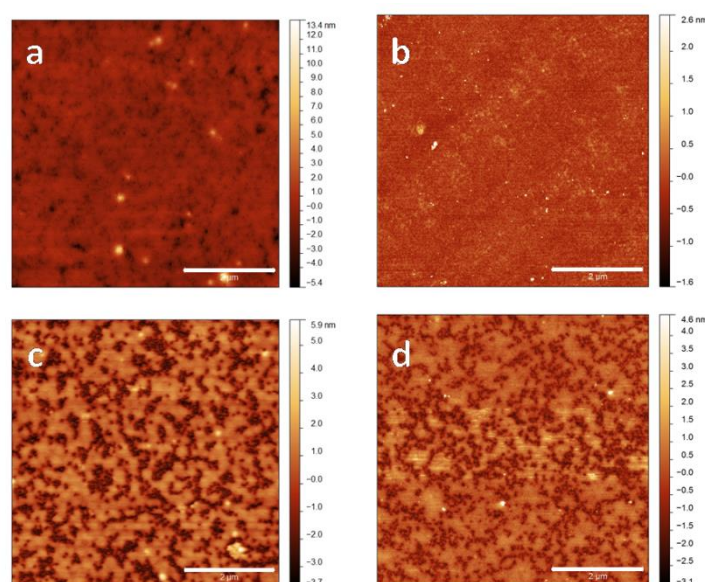


Figure 3.3-12. AFM images of bilayers of A₄₅-B₁₀₁-C₂₇ prepared by: (a) up-up, (b) down-down, (c) up-down, and (d) down-up deposition strategies.

Characterization of silica slides after double deposition of the A₄₅-B₁₀₁-C₂₇ triblock copolymer showed that in “down” deposition the interactions between the slide and the monolayer are weaker than interactions of the polymer with the subphase, and not strong enough to induce deposition of the monolayer on the solid support. Only the up-up strategy resulted in the formation of a bilayer and for this purpose it was used further for investigations of enzyme adsorption.

3.3.5. Adsorption of enzyme on PEG₄₅-PMCL₁₀₁-PDMAEMA_x films

The ability of ABC block copolymer films to adsorb laccase was investigated by QCM-D measurements. The change in frequency value (Δf) was used to calculate the mass which adsorbed to the sensor covered by polymer film, by using the Sauerbrey equation ($\Delta m = -C \Delta f$), where C is a proportionality constant, depending on the quartz properties ($C = 18 \text{ ng cm}^{-2} \text{ Hz}^{-1}$).¹⁵⁹ The transferred monolayers formed by the A₄₅-B₁₀₁-C_x triblock copolymers adsorbed laccase (Figure 3.3-13), and depending on molecular weight of the polymer, the amount of adsorbed enzyme ranged from 63 to 450 ng cm^{-2} (Table 3.3-3). These values are in agreement with previous reports, which indicated that gold surfaces covered with a zirconated layer of 11-mercaptopundecanol adsorbed 520 ng cm^{-2} of laccase,¹⁶⁰ and a self-assembled monolayer formed by a mixture of glutaraldehyde and cysteamine adsorbed 280 ng cm^{-2} of laccase.¹⁶¹ The immobilization of laccase was durable for at least 24 hours at room temperature as measured for a PEG₄₅-*b*-PMCL₁₀₁-*b*-PDMAEMA₂₇ film (Figure 3.3-14).

Based on the molecular weight of the laccase unit of 68 kDa,¹⁰⁵ the surface coverage was calculated as the $\Delta m/Mw$ ratio (Table 3.3-3). The maximum number of laccase molecules that can theoretically be attached in a completely packed mode on the silica slide surface (of about 1 cm^2) was calculated by taking into account the laccase size (6.5 nm x 5.5 nm x 4.5 nm).¹⁶² The mostly packed orientation of the enzyme on the surface was considered, with an occupation area of $5.5 \times 4.5 = 24.75 \text{ nm}^2$. The immobilization yield was determined by reporting the experimental number of immobilized enzymes to the maximum number of laccase that can possibly be attached (4.0×10^{12} molecules per cm^2) (Table 3.3-3). The immobilization yield exceeding 100% for A₄₅-B₁₀₁-C₂₇ monolayer is due to the fact that laccase was both adsorbed on the polymer surface, and inserted between the chains of the polymer film.

Table 3.3-3. Enzyme adsorption on ABC triblock copolymer films.

ABC block copolymer	Δm [ng cm ⁻²]	Surface coverage [nmol cm ⁻²]	Number of enzymes [10 ¹² · cm ⁻²]	Immobilization yield [%] ⁽¹⁾
A ₄₅ -B ₁₀₁ -C ₃	63	0.001	0.6	15
A ₄₅ -B ₁₀₁ -C ₁₂	324	0.005	3.0	74
A ₄₅ -B ₁₀₁ -C ₁₇	270	0.004	2.4	60
A ₄₅ -B ₁₀₁ -C ₂₇	450	0.007	4.2	104
A ₄₅ -B ₁₀₁ -C ₂₇ bilayer up-up	380	0.006	3.6	89

(1) calculated for $4.5 \times 5.5 = 24.75 \text{ nm}^2$ occupied by one laccase molecule.

(2)

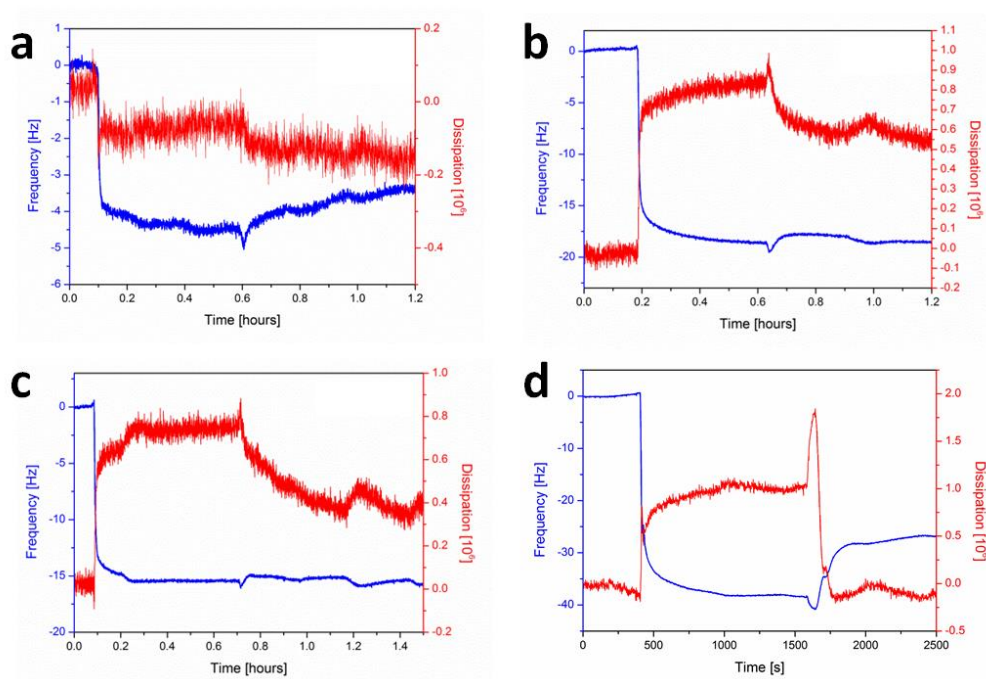


Figure 3.3-13. QCM-D data for laccase adsorption on: (a) A₄₅-B₁₀₁-C₃, (b) A₄₅-B₁₀₁-C₁₂, (c) A₄₅-B₁₀₁-C₁₇, and (d) A₄₅-B₁₀₁-C₂₇.

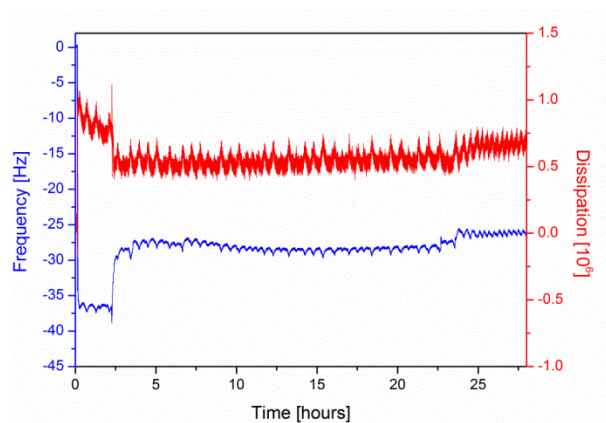


Figure 3.3-14. QCM-D data showing long-term stability of PEG₄₅-*b*-PMCL₁₀₁-*b*-PDMAEMA₂₇ film with adsorbed laccase.

The bilayer, formed by A₄₅-B₁₀₁-C₂₇ through up-up strategy, adsorbed high amount of 380 ng cm⁻² (yield of 89%), similarly as the analogous monolayer (Figure 3.3-15). The lower amount of enzyme attached to the bilayer is probably due to lower roughness of the surface, as explained further.

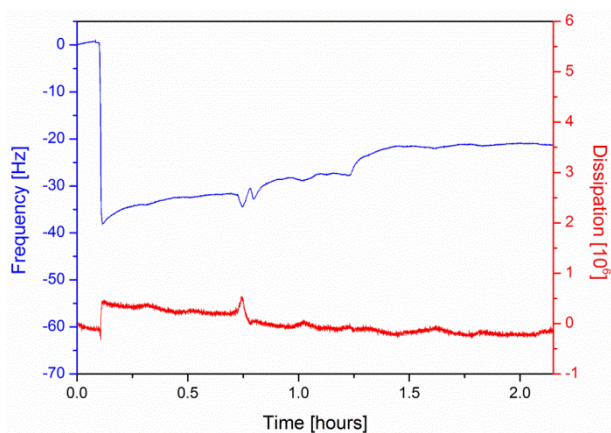


Figure 3.3-15. QCM-D data for laccase adsorption on A₄₅-B₁₀₁-C₂₇ bilayer, prepared by the up-up strategy.

Adsorption of the enzyme on the polymer film was influenced by various factors, such as surface roughness and charge, with electrostatic attraction as the driving force for adsorption. As the PDMAEMA (C) block is positively charged at pH values < 8, due to protonation of the amino groups,¹⁵⁷ and laccase possesses a negative charge at pH > 3.5,¹⁰⁵ they interact through electrostatic attraction. The adsorption of laccase was

performed at pH 4.25 which is optimal due to the electrostatic character of both polymer and enzyme. The limited enzyme adsorption properties of A₄₅-B₁₀₁-C₃ were due to the low roughness of the monolayer formed on the silica slide. The highest enzyme adsorption was observed for A₄₅-B₁₀₁-C₂₇ polymer films, having the highest roughness, which was providing a larger surface for enzyme attachment. The presence of small gaps (depth of about 3 nm, as measured by AFM) in the films could favor the enzyme adsorption, since they partly expose the hydrophobic block of the polymer. This slight increase in hydrophobicity enhanced the interactions between the enzyme and the polymer film, and therefore improved laccase adsorption, in agreement with the results of Deere et al. who showed that hydrophobic interactions decreased protein desorption from the surface.¹⁶³ The effect of roughness on enzyme adsorption is clearly seen for copolymer films with similar compositions. A₄₅-B₁₀₁-C₁₂ adsorbed more laccase (324 ng cm⁻²) than A₄₅-B₁₀₁-C₁₇ (270 ng cm⁻²), because of its greater roughness, which was due to the formation of a greater number of gaps than in the case of the A₄₅-B₁₀₁-C₁₇ copolymer film. Additionally, the same relation can be observed when comparing amount of enzyme adsorbed to A₄₅-B₁₀₁-C₂₇ monolayer and bilayer. Monolayer being rougher was able to adsorb more laccase than bilayer.

A₄₅-B₁₀₁-C₂₇ block copolymer films had the highest monolayer roughness, which enabled adsorption of the highest amount of laccase. For this reason this copolymer was used for further investigations of “active surface”.

3.3.6. Generation of active surfaces

Various methods can be applied for protein immobilization on solid surfaces, including binding to a support (physical adsorption or chemical binding), cross-linking or entrapment.¹⁶⁴ After demonstrating the ability of ABC block copolymer monolayers to adsorb enzymes, A₄₅-B₁₀₁-C₂₇ triblock copolymer was used to generate “active surfaces” by employing two different strategies, based on physical adsorption of laccase, *i.e.*: i) immersion of the ABC solid supported monolayers in an enzyme solution, and ii) spreading of the enzyme solution on ABC monolayer at air-water interface, followed by the transfer of the mixed polymer-enzyme film to silica slide (Figure 3.3-16).

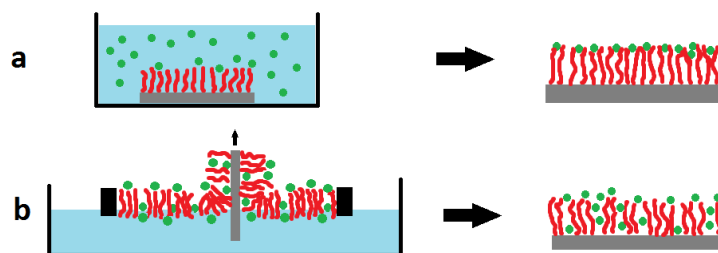


Figure 3.3-16. Strategies for enzyme immobilization: (a) immersion of the ABC solid supported monolayer in the enzyme solution; (b) transfer of mixed polymer-enzyme film to silica substrate; enzyme – green dots.

Laccase immobilization by immersion of PEG₄₅-*b*-PMCL₁₀₁-*b*-PDMAEMA₂₇ solid-supported monolayer in an enzyme solution is a straightforward method due to the electrostatic interactions that occur between the polymer film and enzyme, as described in paragraph 3.3.5. Immersion of the polymer film in enzyme solution was performed for a longer period of time (1 hour), than that used for assessing the capability of the polymer films for enzyme adsorption by QCM-D (approximately 15-30 minutes) to improve the diffusion and stabilization of the enzyme. The presence of laccase after immersion influenced the topography of the A₄₅-B₁₀₁-C₂₇ film. After laccase adsorption, the roughness of the surface increased from 0.6 nm to 1.4 nm (Figure 3.3-17). Since the size of laccase is 6.5 nm x 5.5 nm x 4.5 nm,¹⁶² the bright points, having the approximate height of 5 nm and width of 200 nm, correspond to the adsorbed enzyme agglomerates (Figure 3.3-17 c and d).

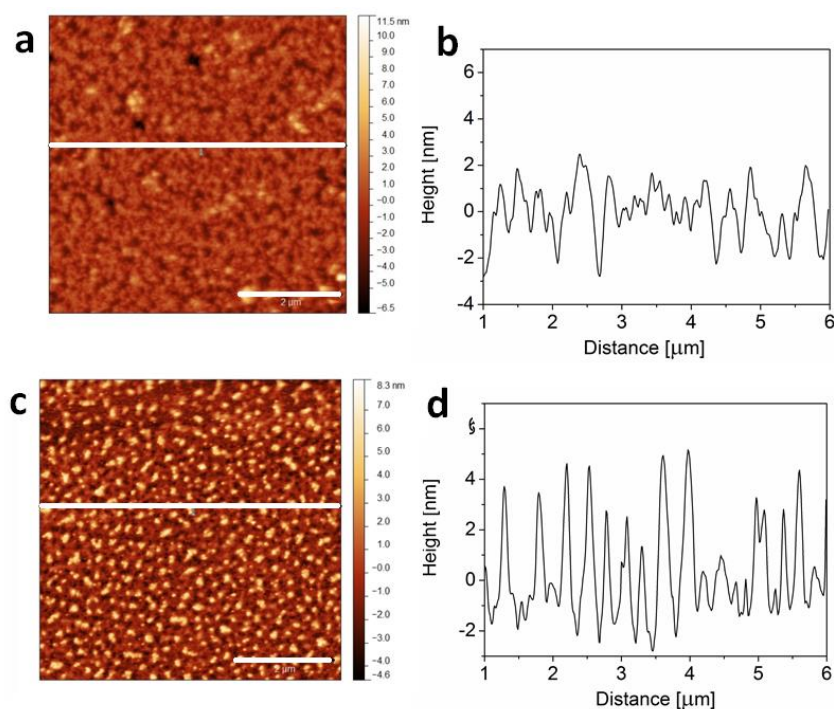


Figure 3.3-17. AFM images of A_{45} - B_{101} - C_{27} monolayers: (a) without laccase and (b) a corresponding profile; (c) after immersion in laccase solution and (d) a corresponding profile; Scale bars: 2 μ m.

In order to achieve enzyme immobilization by transferring the mixed polymer-laccase film onto a solid surface, influence of the enzyme on monolayer formation was studied. For this purpose laccase, prepared in water (pH 7), was spread on PEG_{45} - b - $PMCL_{101}$ - b - $PDMAEMA_{27}$ monolayer at the air-water interface. Addition of the enzyme caused a slight decrease in the surface pressure of the monolayer (Figure 3.3-18). Hydrogen bonding and/or electrostatic interaction between amino groups from the C block of the ABC triblock copolymer, and the reactive groups of the enzyme might have created a more closely packed structure, which reduced the surface pressure, and the mean molecular areas. Introduction of the laccase influenced also the morphology of the monolayer at the air-water interface, which becomes less homogeneous, as revealed by BAM (Figure 3.3-18).

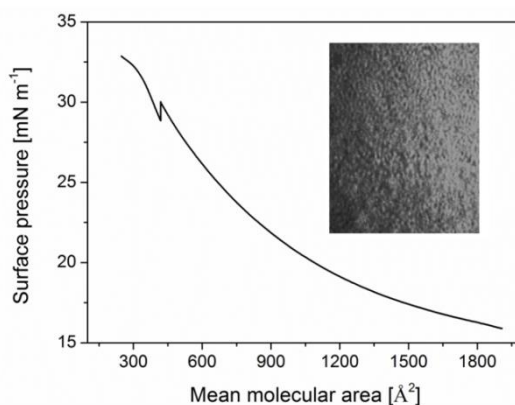


Figure 3.3-18. Surface pressure-area isotherm and BAM image of A₄₅-B₁₀₁-C₂₇ monolayer after addition of 100 µl of laccase (2 mg ml⁻¹).

The mixed A₄₅-B₁₀₁-C₂₇-enzyme films transferred to a solid-support have different roughness, depending on the quantity of the enzyme, which was spread on the monolayer during compression as evaluated by AFM. Spreading low volumes of enzyme solution (25 µl of 2 mg ml⁻¹) induced a decrease in the monolayer roughness to 0.7 nm, compared to the laccase-free A₄₅-B₁₀₁-C₂₇ monolayer with R_a of 1.0 nm at surface pressure of 30 mN m⁻¹ (Figure 3.3-19 a). Higher volume of enzyme solution (100 µl of 2 mg ml⁻¹) spread on the surface induced an increase in roughness of the ABC-enzyme film to 1.8 nm (Figure 3.3-19 b). When a low amount of laccase was spread, the enzyme occupied the free space available between the chains of ABC polymer film, and induced the formation of a more compact film, thus decreasing R_a, in agreement with the values of the immobilization yield. In contrast, spreading a high amount of laccase resulted in the free intra ABC film space being exceeded, and induced an increase of R_a.

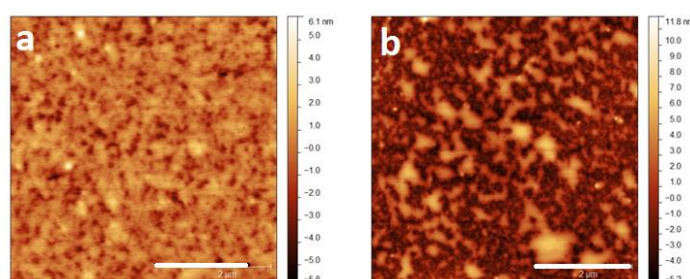


Figure 3.3-19. AFM images of A₄₅-B₁₀₁-C₂₇ monolayers after transfer of polymer-enzyme mixed film from air-water interface, (a) with low and (b) high enzyme concentrations. Scale bars: 2 µm.

3.3.7. Laccase activity assays with DMP

The activity of the laccase was investigated by monitoring the oxidation of phenolic electron mediator, DMP. This compound in presence of active laccase undergo oxidation resulting in the formation of a metastable radical, which gives characteristic absorbance signal at $\lambda = 470$ nm.¹⁰⁵ The radical can further react forming a number of oxidation products, such as 2,6-dimethoxy-p-benzoquinone, C-C and C-O dimers, and oligomers (Figure 3.3-20).¹⁶⁵

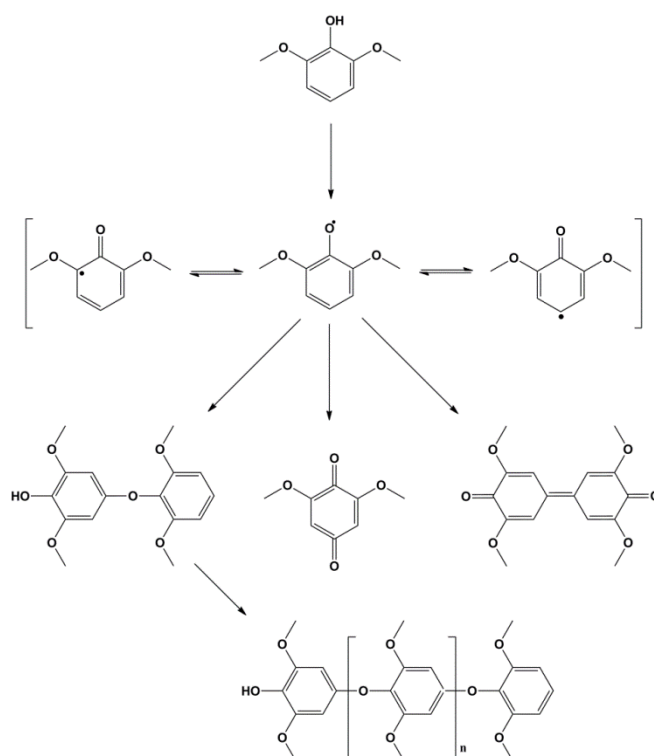


Figure 3.3-20. Possible oxidation products of 2,6-dimethoxyphenol (DMP) in the laccase catalyzed reaction.¹⁶⁵

The enzymatic activity was measured for A₄₅-B₁₀₁-C₂₇ polymer films with laccase immobilized by two methods, described in paragraph 3.3.6. It was assumed that the amount of enzyme immobilized by the immersion strategy should be, in approximation, the same as established by QCM-D measurements (450 ng cm⁻²). For this purpose a solution of free laccase of the same concentration has been used as the reference sample. All the samples were put to the solution of DMP of the same concentration and after 15 hours their absorbance was measured.

The activity of laccase was preserved when adsorbed on A₄₅-B₁₀₁-C₂₇ polymer films, as revealed by the spectrophotometric measurements (Figure 3.3-21). The immobilization techniques did not influence the overall enzymatic activity, *i.e.* the polymer monolayer with laccase immobilized by immersion technique resulted in average absorbance of 0.19 at $\lambda = 470$ nm, while the polymer monolayer with laccase immobilized by transfer technique resulted in an absorbance of 0.21. The higher absorbance value obtained with the active surfaces compared to free laccase ($A = 0.09$) shows that the amount of laccase adsorbed through immersion was higher than that estimated from QCM-D data. Additionally the immobilization process could stabilize the enzyme, and increase the accessibility for substrate. The control sample, *i.e.* pure A₄₅-B₁₀₁-C₂₇ film immersed in DMP solution did not give any absorbance signal at 470 nm indicating that the polymer has no influence on the oxidation of DMP.

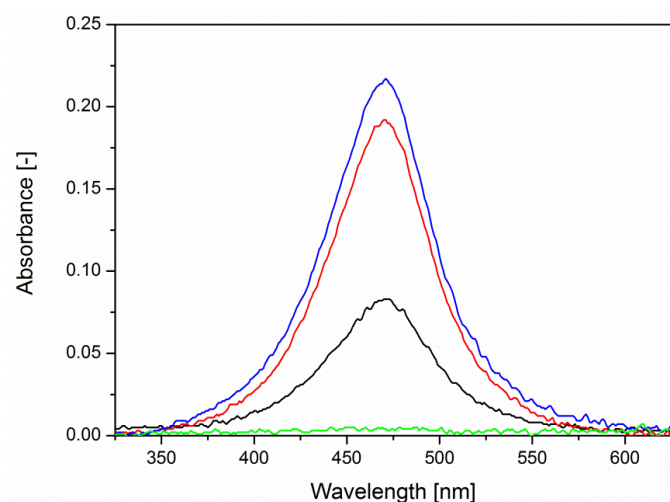


Figure 3.3-21. Spectroscopic evaluation of laccase activity based on formation of the DMP oxidation product ($\lambda = 470$ nm) for a free laccase (black), a polymer monolayer with laccase adsorbed by: immersion (red), and transfer of mixed ABC-laccase film (blue); a polymer monolayer without laccase (green).

3.3.8. Summary

This project presents a strategy for engineering “active surfaces” by immobilization of enzymes on solid-supported films based on PEG₄₅-*b*-PMCL₁₀₁-*b*-PDMAEMA_X asymmetric amphiphilic triblock copolymers. Four polymers varying in the length of the PDMAEMA block were investigated in terms of behavior at the air-water interface,

formation of films on a silica support, and ability to adsorb laccase, which was used as a model enzyme.

During the Langmuir isotherm compression, the PEG₄₅-*b*-PMCL₁₀₁-*b*-PDMAEMA_X block copolymers adopted different arrangements depending on molecular weight of the copolymer. At the air-water interface, films were oriented with PEG in the water subphase and PDMAEMA facing towards air, *i.e.* externally oriented, due to the higher hydrophobicity of this block comparing to PEG. The LB technique was chosen for preparation of uniform ABC block copolymer monolayers on solid supports, favoring a reproducible enzyme immobilization. The properties of LB monolayers, such as thickness, wettability, topography and roughness were established by AFM, ellipsometry, and contact angle. These properties varied with the surface pressure of transfer, ABC composition (hydrophilic/hydrophobic blocks length and active groups), and pH.

All the polymers were able to adsorb the laccase, as established by QCM-D. It was shown that addition of a second polymer layer did not increase the amount of adsorbed enzyme, for this purpose PEG₄₅-*b*-PMCL₁₀₁-*b*-PDMAEMA₂₇ monolayer was chosen as representative and the most suitable for enzyme immobilization, due to formation of rough films with high surface area available for enzyme adsorption.

Two strategies were applied for laccase immobilization: i) immersion of solid-supported polymer films in enzyme solution, and ii) transfer of mixed ABC-enzyme films on silica slides. Both methods resulted in successful immobilization of the enzyme. Obtained solid-supported laccase-polymer films were both stable and active, as measured by QCM-D and activity assays, respectively.

This study represents a strategy for the immobilization of enzymes on a soft asymmetric membrane attached to a solid support. Simple and fast method to obtain well-organized uniform polymer membranes combined with straightforward techniques for enzyme immobilization. This strategy is appealing for applications in the medical or ecological domains where the enzyme activity plays a key role. It should be emphasized that these are preliminary results showing the potential of asymmetric membranes for development of active surfaces however it requires further optimization and investigation.

4. Conclusions and Outlook

This thesis presents three projects, of which the common goal was development of biomimetic solid-supported membranes based on amphiphilic block copolymers. By preparation of different systems, it was shown that amphiphilic block copolymers can form uniform and reproducible membranes when deposited on solid supports and that they can successfully perform as platforms for active compounds.

Firstly, behavior of two groups of block copolymers, PDMS-*b*-PMOXA and PEG-*b*-PMCL-*b*-PDMAEMA, at the air-water interface has been carefully studied. By performing a series of experiments on the Langmuir trough, it was proven that these copolymers form reproducible Langmuir monolayers, which are stable in time, and elastic. The copolymer monolayers have been transferred by Langmuir-Blodgett and Langmuir-Schaefer techniques, which resulted in well-organized and defect-free films deposited on solid supports.

A bilayer formed by PDMS-*b*-PMOXA diblock copolymer had a structure mimicking a natural membrane. Thanks to covalent immobilization of the first layer to the support, the stability of the membrane was increased, while upper layer, attached by hydrophobic interactions, provided the fluidity of the system. The membrane protein was successfully inserted into such a copolymer membrane by employing Bio-Beads, which destabilized the protein and forced it to reconstitute into the membrane. This is the first time Bio-Beads were used for inserting of the membrane proteins into a solid-supported membrane. Such an approach is advantageous, since it allows incorporation of the membrane protein in the planar membrane supported on a slide of unrestricted size and shape. This project proved a concept that solid-supported polymer membrane can host membrane protein however it requires further development in order to make this system more applicable. An interesting strategy would be preparation of such membranes on porous supports, which could provide necessary stability of the system combined with the advantages of freestanding membranes over the pores. Such pore-solid-supported membranes would allow investigation of transport of the matter, or ion flux through the membrane.

A step further in development of functional surfaces was the investigation of mixing properties of three PDMS-*b*-PMOXA diblock copolymers with different lipids, in order to control the distribution of the membrane protein within the membrane. It was shown, that significant factors influencing the phase separation between polymer and lipid are: size, state, and ratio of the mixture's components. In this respect, the biggest domains were formed in mixtures of the longest polymer, having 65 PDMS units, and the rigid, saturated lipids. The distribution of the protein inserted into such binary mixtures depended strongly on the phase state, *i.e.* it was preferentially inserted into a more fluid phase. By choosing appropriate composition of the mixture it was possible to obtain a material with uniform protein distribution within the whole membrane (in mixtures of polymer with unsaturated POPE), or with protein closed in small DOPC domains, *etc.* This systematic study of domain formation and protein distribution enables the design of a new group of multicomponent materials. These systems behave in a similar manner to biological membranes, which is also known to form raft-like domains. A very appealing follow-up of this project will be the comparison of phase separation phenomenon in binary planar and vesicular membranes. Furthermore, it would be interesting to develop more advanced systems by addition of a third component, *e.g.* cholesterol, which is known to increase the fluidity of the biological membranes.

Asymmetric membranes composed of a triblock copolymer were used as cushions for immobilization of laccase. A group of PEG-*b*-PMCL-*b*-PDMAEMA varying with the length of PDMAEMA was investigated in terms of homogeneity of the formed monolayer and ability to adsorbed enzyme. It was shown that with increasing length of the third block the film became more hydrophobic, which resulted in higher amount of laccase adsorbed. Addition of the second layer to the system did not increase the number of immobilized enzymes, as established by QCM-D. Two strategies for enzyme immobilization have been presented: i) immersion of the solid-supported monolayer in an enzyme solution, and ii) spreading of the enzyme solution on an ABC monolayer at the air-water interface, followed by the transfer of the mixed polymer-enzyme film to a silica slide. Activity assays performed by monitoring the oxidation of phenolic mediator (DMP) revealed that transfer of the polymer-enzyme film results in a slightly higher enzyme activity than in the case in the immersion strategy of enzyme immobilization. This could be caused by a higher number of enzymes deposited, and increased stability of the enzyme within the polymer film. This project showed that such asymmetric block

copolymers can preserve the activity of the immobilized enzyme. The next steps for this project would involve: measurement of the immobilized enzyme's kinetics, optimization of the amount of immobilized enzyme, and improvement of the system's stability, *e.g.* by covalent binding of the enzyme to the polymer film.

Active surfaces prepared from block copolymers exhibit high stability, diversity, and possibility of adjusting their properties to the desired functionality. In addition, it was shown that these robust membranes can successfully act as platforms for insertion of the biomolecules, such as membrane proteins and enzymes, with preserving their activity. Such biofunctional membranes mimic natural membranes, and by varying the polymer as well as immobilized biomolecule, tailored membrane properties and functionalities can be achieved. This thesis shows the great potential of the amphiphilic block copolymers in development of systems mimicking biological membranes, which can find applications in various fields, such as medicine, sensing, technology, or packaging.

5. Materials and Methods

5.1. Materials

All chemicals and solvents were purchased from Sigma-Aldrich or Fluka (Sigma Chemical Co., US) and used as received, unless otherwise stated.

5.2. Methods

5.2.1. Polymers

PDMS-*b*-PMOXA was synthesized according to the procedure described by Egli et al.¹⁴ Activated PDMS was used as a macroinitiator for cationic ring-opening polymerization of 2-methyl-2-oxazoline. Polymers with the following compositions were used: PDMS₆₅-*b*-PMOXA₁₂ ($M_w = 5735 \text{ g mol}^{-1}$, PDI = 1.67), PDMS₃₇-*b*-PMOXA₉ ($M_w = 3704 \text{ g mol}^{-1}$, PDI = 1.34), and PDMS₁₆-*b*-PMOXA₉ ($M_w = 2151 \text{ g mol}^{-1}$, PDI = 1.46).

The end-group of PDMS₆₅-*b*-PMOXA₁₂ was oxidized by using a Dess-Martin periodinane.¹²⁴ Polymer (200 mg) and DMP (17 g, 40 μmol) were placed in a two-neck round bottom flask, closed, and degassed. The reaction was performed in anhydrous dichloromethane (10 ml) at room temperature for 24 h. The polymer was purified by dialysis (Spectrapor[®], MWCO 3500 Da) in ethanol for 18 h.

PEG₄₅-*b*-PMCL_X (AB) and PEG₄₅-*b*-PMCL_X-*b*-PDMAEMA_Y (ABC) block copolymers were synthesized as described previously.¹⁵¹ In brief, ring-opening polymerization (ROP) of γ -methyl- ϵ -caprolactone (MCL) was performed using PEG as a macroinitiator. The modified PEG-*b*-PMCL diblock copolymer containing an atom transfer radical polymerization (ATRP)-initiating group was then used for synthesis of the third, PDMAEMA block.

5.2.2. Lipids

DPPC ($M_w = 734 \text{ g mol}^{-1}$, $T_m = 41 \text{ }^\circ\text{C}$), DOPC ($M_w = 786 \text{ g mol}^{-1}$, $T_m = -17 \text{ }^\circ\text{C}$), DPPE ($M_w = 692 \text{ g mol}^{-1}$, $T_m = 63 \text{ }^\circ\text{C}$), and POPE ($M_w = 718 \text{ g mol}^{-1}$, $T_m = 25 \text{ }^\circ\text{C}$) were purchased from Avanti Polar Lipids, Inc. For the experiments lipid solutions of concentration of 1 mg ml^{-1} were prepared. DPPC, DOPC, and POPE were dissolved in chloroform, while DPPE in a mixture of chloroform and methanol (v/v, 9:1).

5.2.3. MloK1 expression, labeling, and purification

Full-length, cyclic nucleotide-modulated potassium channel MloK1 was expressed and purified to homogeneity by Dr. Julia Kowal.¹¹⁹ Briefly, *E. coli* cells containing His-tagged MloK1 construct were grown in LB medium at 37°C . Protein expression was induced with anhydrotetracycline (0.2 mg/ml) for 2h at OD_{600} of 0.7. Bacterial cells were then centrifuged and disrupted by sonication. The membrane fraction was isolated by ultracentrifugation and solubilized for 2.5h at 4°C in buffer containing 1.2% n-decyl- β -D-maltopyranoside (DM; Anatrace), 295 mM NaCl, 5 mM KCl, 20 mM Tris-HCl pH 8.0, 10% glycerol, 1 mM PMSF, 0.2 mM cAMP (Fluka). Insoluble material was removed by ultracentrifugation and extracted MloK1 was purified by Co^{2+} -affinity chromatography in buffer containing 295 mM NaCl, 5 mM KCl, 20 mM Tris-HCl pH 8.0, 10% glycerol, 1 mM PMSF, 40/500 mM (wash/elution) imidazole, 0.2% DM, 0.2 mM cAMP.

MloK1 was labeled at its primary amines with the fluorescent dye DyLight 488 Amine-Reactive (Thermo Fisher Scientific). Tris buffer was not used for labeling, because it is a primary amine which will compete with the protein for reaction with the dye, and instead Bicine (20 mM Bicine pH 7.6, 20 mM KCl, 200 μM cAMP, 0.4 % DM), which is a tertiary amine, was used as the buffer. DyLight 488 (1 mg) was dissolved in DMSO (100 μl), then the dye solution (10 μl) was added to MloK1 (100 μl , 2.7 mg ml^{-1}) dropwise, and stirred for 2 hours. The protein was purified from free dye by dialysis (MWCO 10 kDa) against Bicine buffer for 5 days at $6 \text{ }^\circ\text{C}$.

5.2.4. Surface-pressure – area isotherms

Monolayers at the air-water interface were investigated on a Langmuir Teflon[®] trough (KSV Instruments, Finland), with the area of 420 cm², and equipped with two symmetric, hydrophilic Delrin[®] barriers. Surface pressure was measured by usage of a Wilhelmy plate made of ashless filter paper. Prior to taking the measurements, the trough was cleaned with chloroform and ethanol, and then filled with high purity water. The solution of polymer or polymer-lipid mixture (1 mg ml⁻¹) was spread drop-wise on the subphase. After evaporation of chloroform (15 min) the monolayer compression was performed at a speed of 10 mm min⁻¹. All the measurements were performed in the temperature of 25 °C.

5.2.5. Substrate preparation

Silica wafers (Si-Mat Silicon Materials, Germany), glass cover slips (Menzel-Gläser, Germany), and gold substrates (Ssens, Netherlands) were cleaned ultrasonically in chloroform and ethanol (one hour in each solvent), and prior the use they were placed in UV/ozone chamber for 15 min.

Modification of silica and glass slides with 3-aminopropytriethoxysilane (99%, APTES, Acros Organics) was performed in oxygen-free atmosphere, at room temperature. The slides were placed in the flask, which was then sealed and degassed. The slides were incubated in 5% (v/v) solution of anhydrous toluene and APTES for 3 h, and then washed with ethanol, and dried with a stream of nitrogen.¹³²

Gold substrates were functionalized with 11-amino-1-undecanethiol hydrochloride (AUT) by overnight incubation in 0.5 mM solution of AUT in ethanol, with addition of 3% (v/v) triethylamine. Afterwards the slides were rinsed thoroughly with ethanol, and dried with a stream of nitrogen.¹⁶⁶

5.2.6. Langmuir-Blodgett (LB) and Langmuir-Schaefer (LS) transfers

LB and LS transfers were performed on a Mini-trough (KSV Instruments, Finland) with an area of 242 cm². In order to perform LB transfer, the slide was first placed in the subphase (water), then the chloroform solution of polymer (or polymer-lipid mixture) was

spread drop-wise on the subphase, and the monolayer was formed. After 10 minutes of equilibration the film was transferred with a dipper speed of 0.5 mm min^{-1} .

To transfer the monolayer with addition of the protein, first the polymer-lipid mixture was compressed to the surface pressure of 20 mN m^{-1} and after 10 min of stabilization $5.2 \text{ }\mu\text{g}$ of labeled protein dissolved in Bicine buffer was added dropwise on the monolayer surface (Figure 3.3-19) and allowed to stabilize for 20 min. After this time the monolayer was compressed to 35 mN m^{-1} and it was transferred to glass.

In LS approach, first the monolayer at the air-water interface was formed, and then horizontally placed slide was pressed through the monolayer into the subphase with the constant dipper speed of 50 mm min^{-1} . The water surface was precisely cleaned until the surface pressure was lower than 0.1 mN m^{-1} , and then the slide could be removed from the reservoir and placed in ultra-pure water.

5.2.7. Protein incorporation

Incorporation experiments were performed in Tris buffer (20 mM Tris pH 7.6, 20 mM KCl, 200 μM adenosine 3',5'-cyclic monophosphate (cAMP), 0.4 % *n*-decyl- β -D-maltopyranoside (DM, Affymetrix), 0.02% NaN_3) except experiments with labelled protein, where Bicine buffer (20 mM Bicine pH 7.6, 20 mM KCl, 200 μM cAMP, 0.4 % DM) was used.

A solid-supported membrane was placed in a vessel filled with buffer, then Bio-Beads (SM-2, Bio-Rad, Richmond California) and protein solution (final protein concentration: $14 \text{ }\mu\text{g ml}^{-1}$) were added. The incorporation was performed for 3 h at room temperature and then the substrates were thoroughly washed with detergent-free buffer (20 mM Tris pH 7.6, 20 mM KCl, 200 μM cAMP, 0.02% NaN_3).

5.2.8. Immobilization of the laccase to polymer films

Immobilization of enzymes on polymer films was performed in two different ways: i) before transfer of the films to the solid support, and ii) after film transfer to the solid support. For i), the polymer films were compressed to a surface pressure of 20 mN m^{-1} and then 25 or 100 μl of laccase solution (2 mg ml^{-1} in PBS or bidistilled water) were

spread drop-wise at the air-water interface. After 30 minutes of stabilization, ABC-enzyme films were compressed to 30 mN m^{-1} and then transferred to the silica substrate (indicated as “transfer technique”). For ii), silica slides with transferred polymer monolayers were immersed in enzyme solutions for 30 minutes or 1 hour (0.5 mg ml^{-1} in PBS pH = 4.25), and then rinsed with PBS buffer (indicated as “immersion technique”).

5.2.9. Activity of the immobilized enzyme

Activities of free laccase and laccase immobilized on polymer films were investigated with DMP as the substrate, with a final concentration of 0.06 mM in bidistilled water, at pH 7. The activity of free enzyme was measured after 12 hours with a laccase solution with final concentration of laccase of 500 ng ml^{-1} . Slides with immobilized enzymes were immersed in DMP solutions, also for 12 hours. The UV-Vis spectra were then recorded in the wavelength range of 200 to 800 nm (with an accuracy of 1 nm) using a Thermo Scientific NanoDrop 2000c UV-Vis spectrophotometer (Thermo Fisher Scientific, USA) equipped with a xenon flash lamp.

5.3. Characterization techniques

5.3.1. ^1H NMR

^1H -NMR spectra were recorded with a Bruker DPX-400 spectrometer using deuterated chloroform (99.8 % CDCl_3) as solvent, and analyzed with MestReNova 6.1.1 software. The molecular mass of the polymer and length of the blocks were calculated from the ^1H -NMR spectra.

5.3.2. Brewster angle microscope (BAM)

Compression of the amphiphiles monolayers at the air-water interface was monitored by a Brewster angle microscope (EP³SW system, Nanofilm Technologie GmbH, Göttingen, Germany) equipped with a Nd-YAG laser ($\lambda = 532 \text{ nm}$), long distance objective (Nikon, 20x), and monochrome CCD camera. The size of the Brewster angle microscopy (BAM) image corresponds to $220 \times 250 \text{ }\mu\text{m}^2$, with a resolution of $1 \text{ }\mu\text{m}$.

5.3.3. Atomic force microscopy (AFM)

AFM images were recorded with an Agilent 5100 AFM/SPM microscope (PicoLe System, Molecular Imaging). Measurements carried out in contact mode in the Bicine buffer (20 mM Bicine pH 7.6, 20 mM KCl, 200 μ M cAMP), were performed by using silicon nitride cantilevers (PNP-TR, NanoWorld AG) with a nominal spring constant of 0.32 N m⁻¹. Measurements in the tapping mode in air were carried out using silicon cantilevers (PPP-NCHR, Nanosensors) with a nominal spring constant of 42 N m⁻¹. The images were analyzed with the data analysis software Gwyddion (v. 2.37).

5.3.4. Ellipsometry

Measurements were carried out on an EP³ SW imaging ellipsometer (Nanofilm Technologie GmbH, Göttingen, Germany) with Nd-YAG laser at 532 nm. Measurements (one every 2 degrees) were performed in air for angles of incidence ranging from 55° to 75°. For the silica substrates, the thickness of the layer was estimated by a model which included the silicon dioxide thickness (~ 2 nm). Refractive index values used for modeling were: $n_{\text{APTES}} = 1.465$, and $n_{\text{polymer}} = 1.5$. For all samples prepared on silica the extinction coefficient (k) was equal to 0. For the gold substrates the following parameters were used: $n_{\text{AUT}} = 1.53$, $k_{\text{AUT}} = 0.26$, $n_{\text{polymer}} = 1.52$, and $k_{\text{polymer}} = 0.07$. Each type of sample was measured at least 5 times on two different slides, and average values were calculated for values determined with a mean squared error (MSE) < 1.

5.3.5. Static contact angle

Static contact angle measurements were performed with a contact angle goniometer, CAM 100 (KSV Instruments, Finland) based on a CDD camera with 50 mm optics. Droplets of ultrapure water were placed on the substrates with a micro-syringe, and the contact angle was automatically calculated. Each sample was measured at least 10 times and the average value was calculated.

5.3.6. ATR-Fourier transform infrared spectroscopy (ATR-FTIR)

Attenuated total reflection Fourier transform infrared spectroscopy measurements were performed on a Platinum ATR ALPHA (Bruker, Germany) spectrometer with a single reflection diamond ATR sampling module. All spectra were recorded with a resolution of 2 cm^{-1} in the range $400 - 4000\text{ cm}^{-1}$, with 128 acquisition scans.

5.3.7. Confocal laser scanning microscopy (CLSM)

CLSM measurements were performed on a Zeiss LSM 510-META/Confocor2 (Germany), in LSM mode.

Protein labeled with DyLight 488 was measured with an Ar laser (488 nm) and a 40x water-immersion objective (Zeiss C-Apochromat 40x, NA 1.2) with pinhole adjusted to $78\text{ }\mu\text{m}$. An Ar laser was used as the excitation source with excitation transmission at 488 nm set for 4 %. Samples were prepared on glass cover slips. Before performing the measurements, a small volume of Bicine buffer or water was placed on a cleaned microscope slide and covered with a glass cover slip so that the polymer membrane was enclosed between two slides. Measurements were performed at room temperature, and after adjusting for a sharp image, the sample was scanned randomly throughout the surface.

Mixed polymer-lipid films contained 5% of SRB-labeled polymer and were measured with the HeNe laser (543 nm) as the excitation source, and a 40x water-immersion objective (Zeiss C-Apochromat 40x, NA 1.2). The excitation transmission of HeNe laser was set for 20%. In order to measure the distribution of the protein within the mixed film we prepared films with SRB-labeled polymer and DyLight 488-labeled protein, measurements were performed in two channels. In such way two micrographs of the same area, presenting signals from two different dyes could be overlapped.

For the LSM measurements of the mixtures containing the shortest diblock copolymer (PDMS₁₆-*b*-PMOXA₉), 5% of SRB-labeled PDMS₃₇-*b*-PMOXA₉ was added.

5.3.8. Fluorescence correlation spectroscopy (FCS)

FCS measurements of labeled protein were performed with the same instrument as CLSM measurements. An Ar laser was used as the excitation source with excitation transmission at 488 nm set for 10 % and pinhole adjusted to 78 μm . 10 FCS autocorrelation curves were recorded over 20 s each.

5.3.9. Electrical conductance

Electrical conductance measurements were performed with a source-meter Keithley 2636A (Keithley International, Germany). To carry out these measurements an electric circuit was built and samples were prepared on conductive substrates, *i.e.* gold slides. The gold substrate with polymer membrane was covered with a PDMS liquid chamber (which had a small vertical hole) in order to always have the same measurement area and constant buffer volume. A gold wire was attached with a silver paint to the sample so that the gold substrate was connected to the circuit (Figure 3.1-22).¹¹⁷ The paint was left for 30 minutes to dry but the membrane was still hydrated, and the liquid chamber was then filled with buffer (20 mM Tris pH 7.6, 20 mM KCl, 200 μM cAMP, 0.02% NaN_3) and left for 15 minutes to stabilize. From the top, the liquid chamber was closed with an electrode. A constant voltage of 40 mV was applied to the system, and the current was measured. All devices were controlled by self-made LabView software.

5.3.10. Quartz crystal microbalance with dissipation (QCM-D)

QCM-D measurements were performed with the system Q-Sense E1 (Biolin Scientific, Sweden). The polymer film was first transferred by the LB technique to the silica QCM-sensor on the Mini-trough, and placed in the QCM chamber. After 1 hour in PBS buffer for stabilization, the enzyme solution (0.5 mg ml^{-1}) was introduced into the QCM chamber with a flow speed of 100 $\mu\text{l min}^{-1}$, and then allowed to stabilize for approximately 15-30 minutes, before washing thoroughly with buffer. Measurements with laccase were performed at pH 4.25.

5.3.11. Circular dichroism (CD)

CD spectra were recorded with a Chirascan Circular Dichroism Spectrometer (Applied Biophysics Ltd, Leatherhead, UK) equipped with a peltier temperature control device (Alpha Omega Instruments, Cumberland, USA). CD measurements were performed using a spectral bandwidth of 0.2 nm and a step resolution of 0.2 nm. A Quartz cell with a path length of 2 mm was used.

6. Appendix

^1H -NMR and ATR-FTIR spectra of the polymers used in this thesis, whose characterization was now shown in the main text (Figures 6-1 – 6-11).

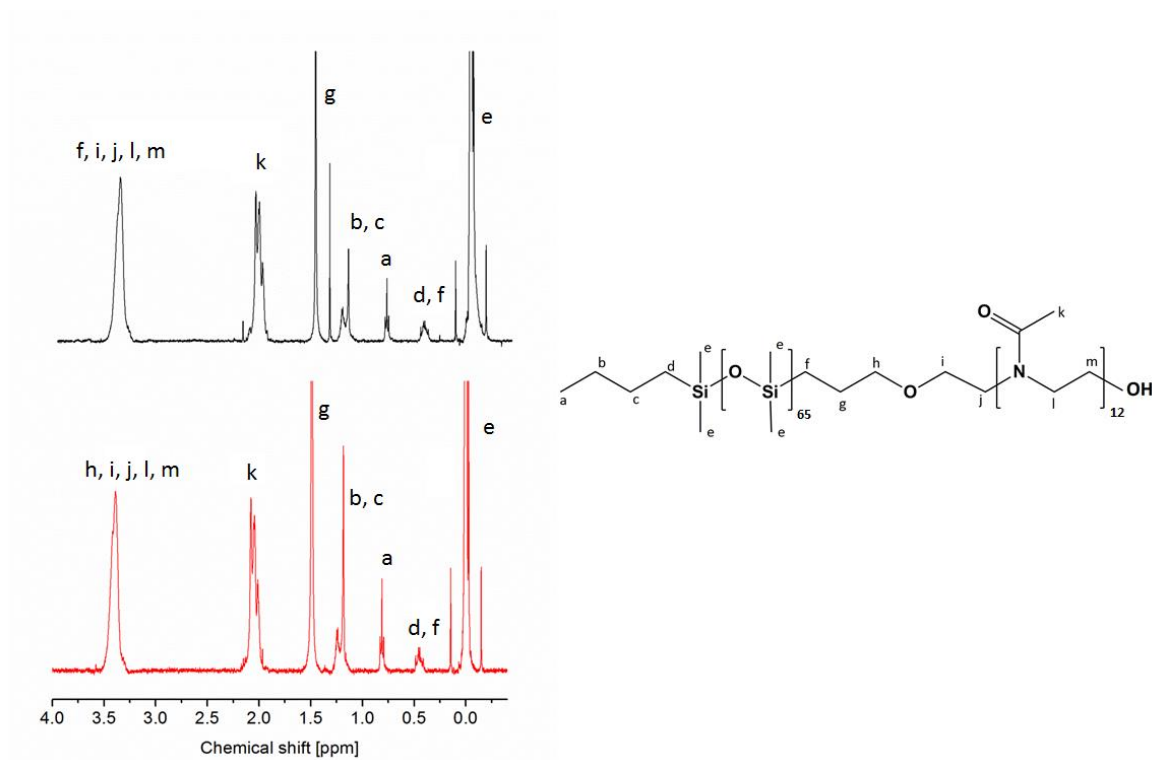


Figure 6-1. ^1H NMR spectrum of pure (in black) and SRB-labeled (in red) PDMS₆₅-*b*-PMOXA₁₂ diblock copolymer.

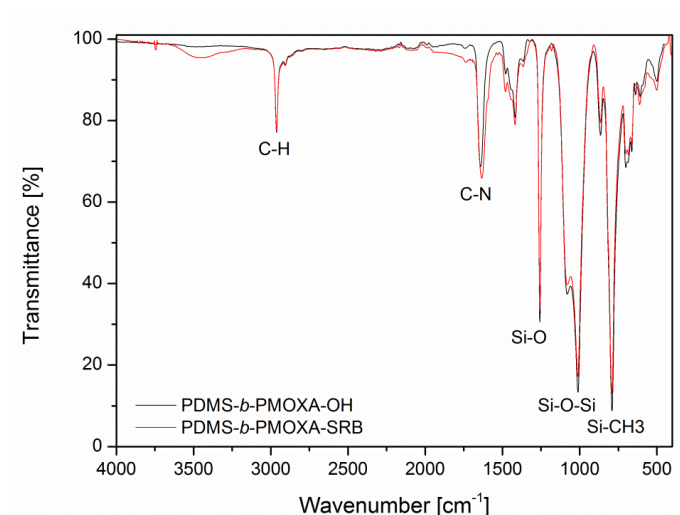


Figure 6-2. ATR-IR spectra of pure (in black) and SRB-labeled (in red) PDMS₆₅-*b*-PMOXA₁₂ diblock copolymer.

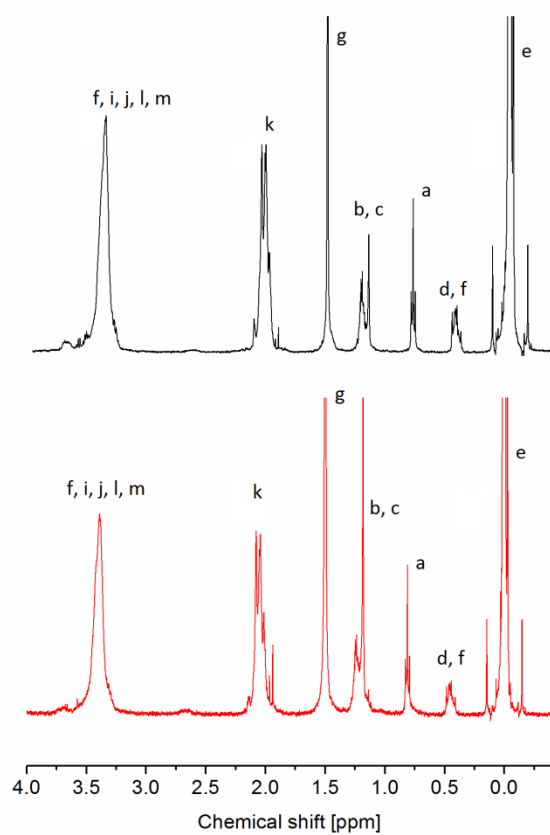


Figure 6-3. ¹H NMR spectrum of pure (in black) and SRB-labeled (in red) PDMS₃₇-*b*-PMOXA₉ diblock copolymer. Assignment of the peaks as in figure 6-1.

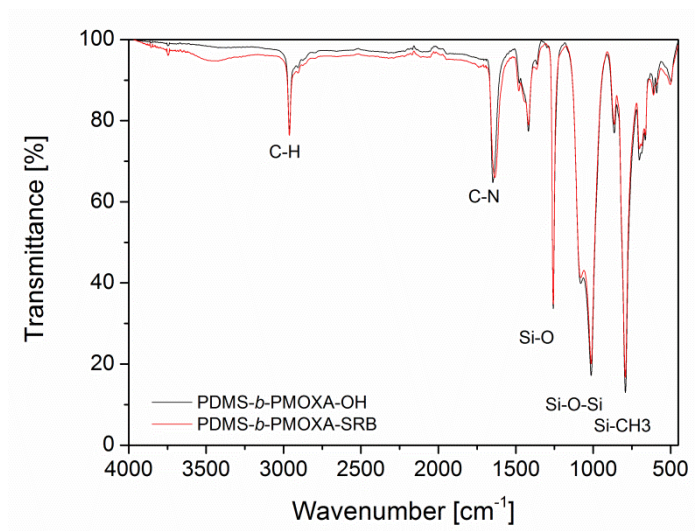


Figure 6-4. ATR-IR spectra of pure (in black) and SRB-labeled (in red) PDMS₃₇-*b*-PMOXA₉ diblock copolymer.

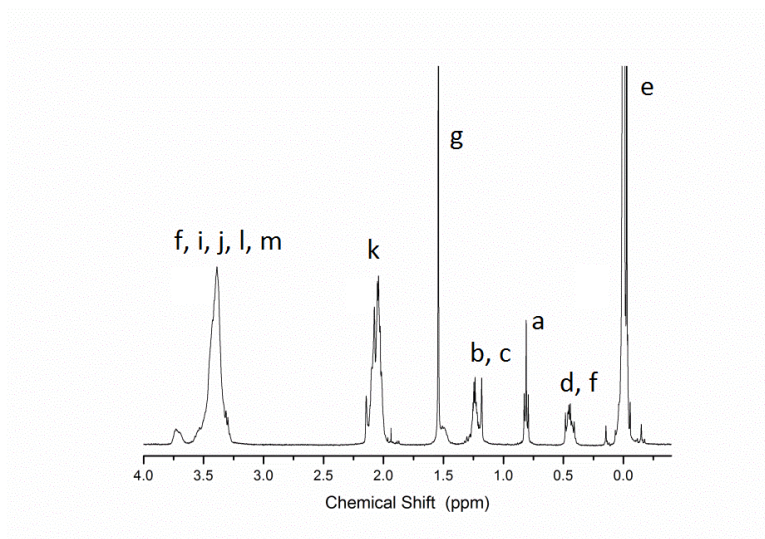


Figure 6-5. ¹H NMR spectrum of pure (in black) and SRB-labeled (in red) PDMS₁₆-*b*-PMOXA₉ diblock copolymer. Assignment of the peaks as in figure 6-1.

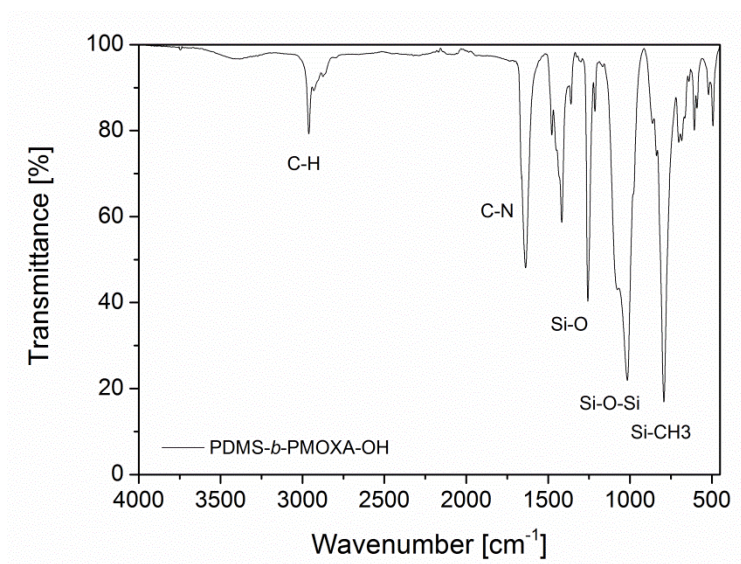


Figure 6-6. ATR-IR spectrum of pure PDMS₁₆-*b*-PMOXA₉ diblock copolymer.

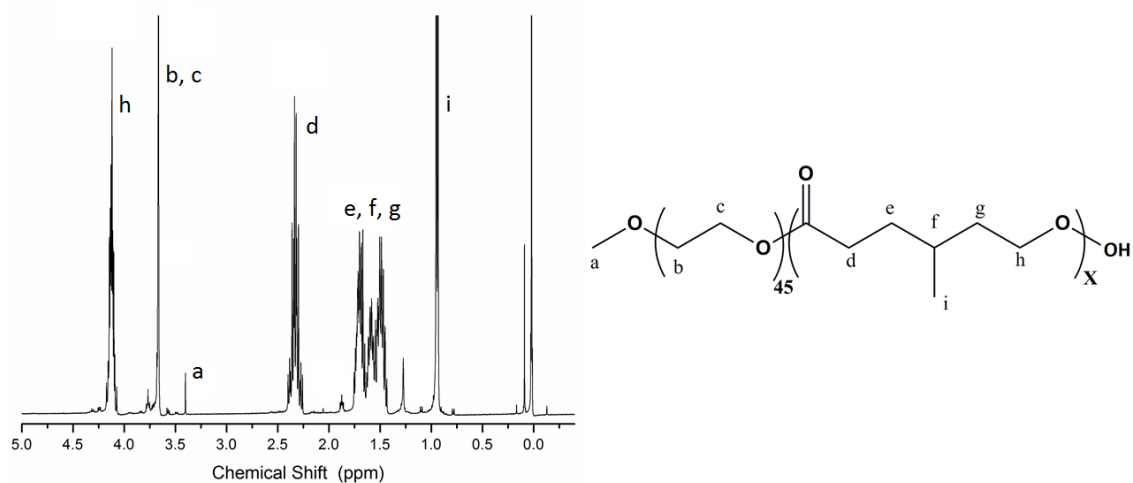


Figure 6-7. ¹H-NMR spectrum and structure of PEG₄₅-*b*-PMCL₁₀₁ diblock copolymer.

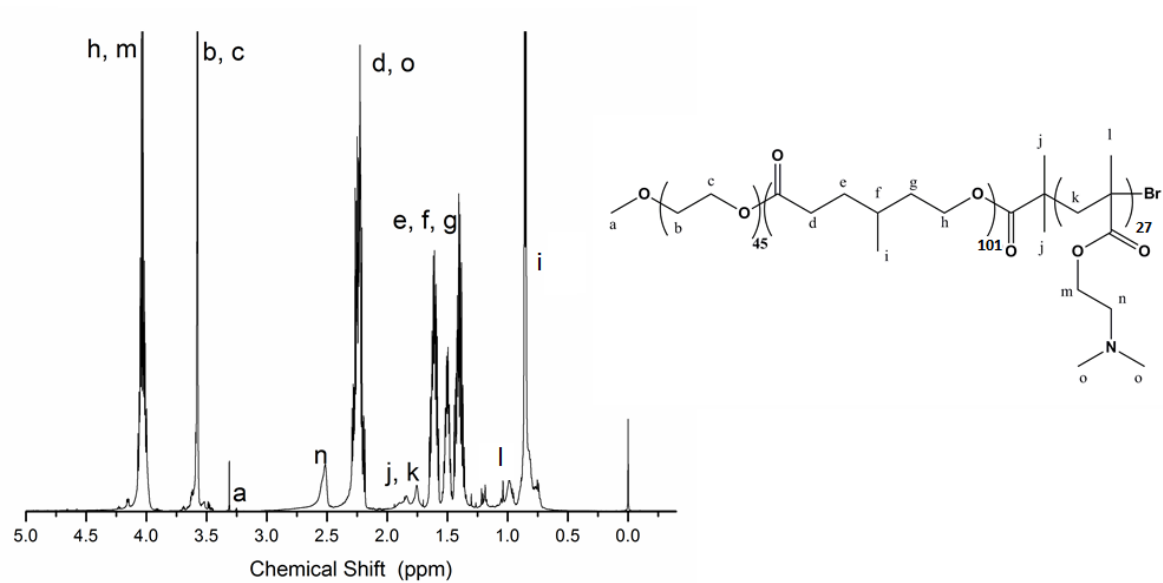


Figure 6-8. ^1H -NMR spectrum and structure of $\text{PEG}_{45}\text{-}b\text{-PMCL}_{101}\text{-}b\text{-PDMAEMA}_{27}$ triblock copolymer.

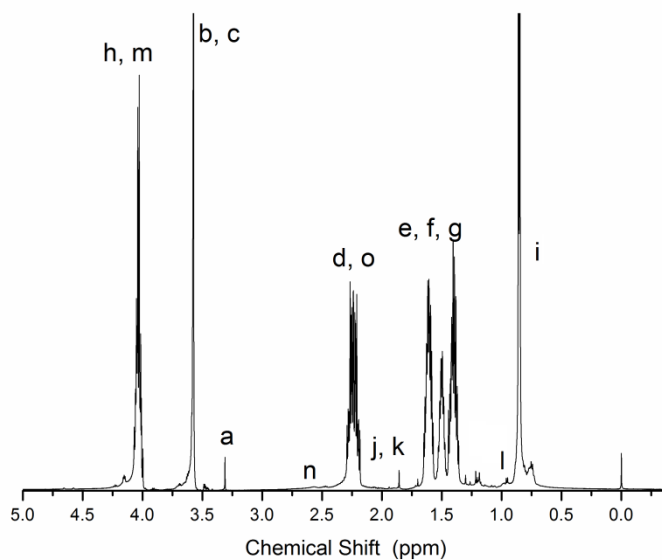


Figure 6-9. ^1H -NMR spectrum and structure of $\text{PEG}_{45}\text{-}b\text{-PMCL}_{101}\text{-}b\text{-PDMAEMA}_3$ triblock copolymer. Assignment of the peaks as in figure 6-8.

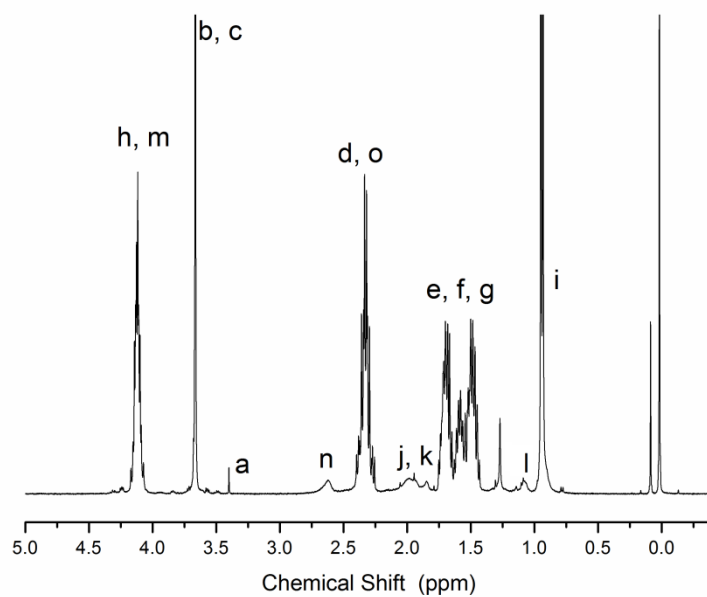


Figure 6-10. ^1H -NMR spectrum and structure of $\text{PEG}_{45}\text{-}b\text{-PMCL}_{101}\text{-}b\text{-PDMAEMA}_{12}$ triblock copolymer. Assignment of the peaks as in figure 6-8.

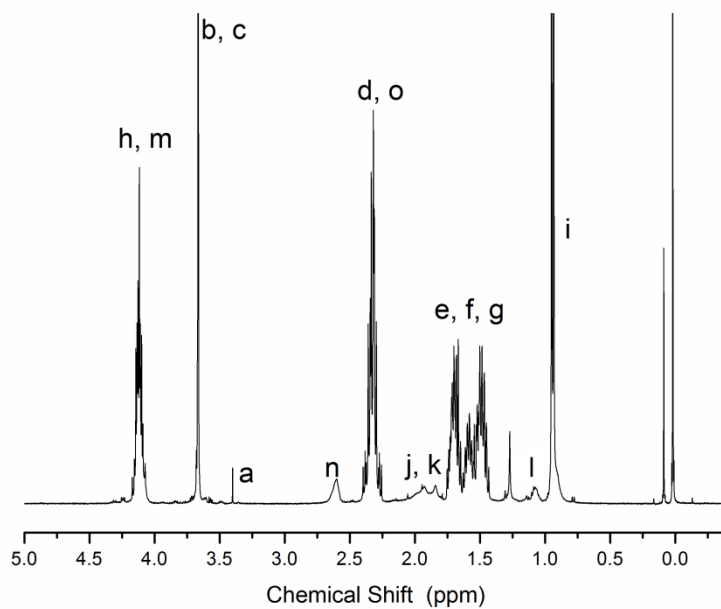


Figure 6-11. ^1H -NMR spectrum and structure of $\text{PEG}_{45}\text{-}b\text{-PMCL}_{101}\text{-}b\text{-PDMAEMA}_{17}$ triblock copolymer. Assignment of the peaks as in figure 6-8.

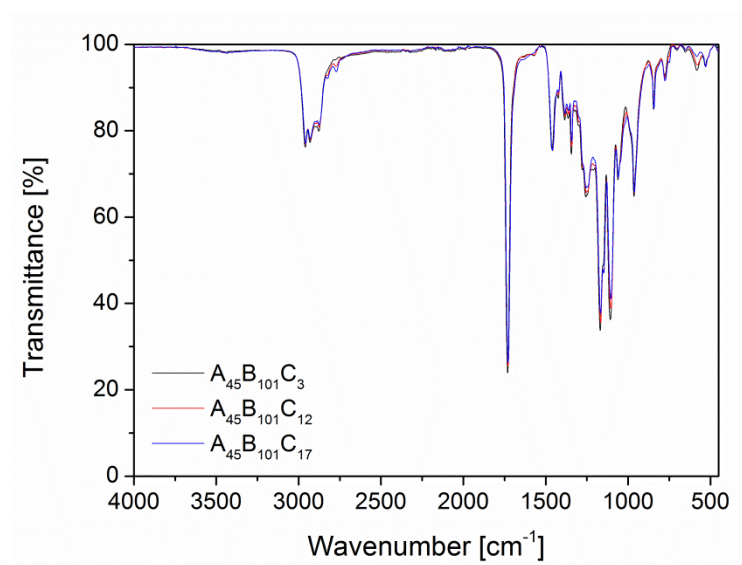


Figure 6-11. ATR-FTIR spectrum of PEG₄₅-*b*-PMCL₁₀₁-*b*-PDMAEMA₃ (black), PEG₄₅-*b*-PMCL₁₀₁-*b*-PDMAEMA₁₂ (red), and PEG₄₅-*b*-PMCL₁₀₁-*b*-PDMAEMA₁₇ (blue) triblock copolymer. Assignment of the peaks as in the paragraph 3.3.1.

7. References

- (1) Cooper, G. M.; Hausman, R. E. *The cell*; Sinauer Associates Sunderland, 2000.
- (2) Singer, S. J.; Nicolson, G. L. The Fluid Mosaic Model of the Structure of Cell Membranes. *Science (New York, N.Y.)* **1972**, *175*, 720-731.
- (3) Nagarajan, R.; Ruckenstein, E. Theory of Surfactant Self-Assembly - a Predictive Molecular Thermodynamic Approach. *Langmuir* **1991**, *7*, 2934-2969.
- (4) Timberlake, K. C.; *Chemistry: An introduction to general, organic, and biological chemistry*; Pearson Prentice Hall, 2009.
- (5) Nielsen, C. H. Biomimetic Membranes for Sensor and Separation Applications. *Anal. Bioanal. Chem.* **2009**, *395*, 697-718.
- (6) Zhang, X. Y.; Tanner, P.; Graff, A.; Palivan, C. G.; Meier, W. Mimicking the Cell Membrane with Block Copolymer Membranes. *J. Polym. Sci. Pol. Chem.* **2012**, *50*, 2293-2318.
- (7) Wasankar, S. R.; Deshmukh, A. D.; Ughade, M. A.; Burghat, R. M.; Gandeche, D. P.; Meghwani, R. R.; Faizi, S. M. Liposome as a Drug Delivery System-A Review. *Research Journal of Pharmaceutical Dosage Forms and Technology* **2012**, *4*, 104-112.
- (8) Nam, J.; Beales, P. A.; Vanderlick, T. K. Giant Phospholipid/Block Copolymer Hybrid Vesicles: Mixing Behavior and Domain Formation. *Langmuir* **2011**, *27*, 1-6.
- (9) Broz, P.; Driamov, S.; Ziegler, J.; Ben-Haim, N.; Marsch, S.; Meier, W.; Hunziker, P. Toward Intelligent Nanosize Bioreactors: A pH-Switchable, Channel-Equipped, Functional Polymer Nanocontainer. *Nano Lett.* **2006**, *6*, 2349-2353.
- (10) Discher, D. E.; Eisenberg, A. Polymer Vesicles. *Science* **2002**, *297*, 967-973.
- (11) Blanz, A.; Armes, S. P.; Ryan, A. J. Self-Assembled Block Copolymer Aggregates: From Micelles to Vesicles and their Biological Applications. *Macromol. Rapid. Comm.* **2009**, *30*, 267-277.
- (12) Chen, Q.; de Groot, G. W.; Schonherr, H.; Vancso, G. J. Patterns of Surface Immobilized Block Copolymer Vesicle Nanoreactors. *Europ. Polym. J.* **2011**, *47*, 130-138.
- (13) LoPresti, C.; Lomas, H.; Massignani, M.; Smart, T.; Battaglia, G. Polymersomes: Nature Inspired Nanometer Sized Compartments. *J. Mater. Chem.* **2009**, *19*, 3576-3590.
- (14) Egli, S.; Nussbaumer, M. G.; Balasubramanian, V.; Chami, M.; Bruns, N.; Palivan, C.; Meier, W. Biocompatible Functionalization of Polymersome

- Surfaces: A New Approach to Surface Immobilization and Cell Targeting Using Polymersomes. *J. Am. Chem. Soc.* **2011**, *133*, 4476-4483.
- (15) Graff, A.; Fraysse-Ailhaas, C.; Palivan, C. G.; Grzelakowski, M.; Friedrich, T.; Vebert, C.; Gescheidt, G.; Meier, W. Amphiphilic Copolymer Membranes Promote NADH:Ubiquinone Oxidoreductase Activity: Towards an Electron-Transfer Nanodevice. *Macromol. Chem. Phys.* **2010**, *211*, 229-238.
 - (16) Grzelakowski, M.; Onaca, O.; Rigler, P.; Kumar, M.; Meier, W. Immobilized Protein-Polymer Nanoreactors. *Small* **2009**, *5*, 2545-8.
 - (17) Langowska, K.; Palivan, C. G.; Meier, W. Polymer Nanoreactors Shown to Produce and Release Antibiotics Locally. *Chem. Commun.* **2013**, *49*, 128-130.
 - (18) Rutnakornpituk, M.; Ngamdee, P.; Phinyocheep, P. Preparation and Properties of Polydimethylsiloxane-Modified Chitosan. *Carbohydr. Polym.* **2006**, *63*, 229-237.
 - (19) Schlaad, H.; Diehl, C.; Gress, A.; Meyer, M.; Demirel, A. L.; Nur, Y.; Bertin, A. Poly(2-oxazoline)s as Smart Bioinspired Polymers. *Macromol. Rapid Comm.* **2010**, *31*, 511-525.
 - (20) Hoogenboom, R.; Schlaad, H. Bioinspired Poly(2-oxazoline)s. *Polymers* **2011**, *3*, 467-488.
 - (21) Antonietti, M.; Forster, S. Vesicles and liposomes: A self-assembly Principle Beyond Lipids. *Adv. Mater.* **2003**, *15*, 1323-1333.
 - (22) Gaucher, G.; Dufresne, M. H.; Sant, V. P.; Kang, N.; Maysinger, D.; Leroux, J. C. Block Copolymer Micelles: Preparation, Characterization and Application in Drug Delivery. *J. Controlled Release* **2005**, *109*, 169-188.
 - (23) Wang, Z. G. Curvature Instability of Diblock Copolymer Bilayers. *Macromolecules* **1992**, *25*, 3702-3705.
 - (24) Wu, D.; Spulber, M.; Itel, F.; Chami, M.; Pfohl, T.; Palivan, C. G.; Meier, W. Effect of Molecular Parameters on the Architecture and Membrane Properties of 3D Assemblies of Amphiphilic Copolymers. *Macromolecules* **2014**, *47*, 5060-5069.
 - (25) Brinkhuis, R. P.; Rutjes, F. P. J. T.; van Hest, J. C. M. Polymeric Vesicles in Biomedical Applications. *Polym. Chem.* **2011**, *2*, 1449-1462.
 - (26) Yan, Y.; Xiong, W.; Li, X. S.; Lu, T.; Huang, J. B.; Li, Z. C.; Fu, H. L. Molecular Packing Parameter in Bolaamphiphile Solutions: Adjustment of Aggregate Morphology by Modifying the Solution Conditions. *J. Phys. Chem. B* **2007**, *111*, 2225-2230.
 - (27) Jagoda, A.; Kowal, J.; Delcea, M.; Palivan, C. G.; Meier, W. Polymer Vesicles on Surfaces. In *Biomaterials Surface Science*; Wiley-VCH Verlag GmbH & Co. KGaA, 2013; pp 159-203.
 - (28) Dynarowicz-Łątka, P.; Dhanabalan, A.; Oliveira, O. N. Modern Physicochemical Research on Langmuir Monolayers. *Adv. Colloid Interface Sci.* **2001**, *91*, 221-293.

- (29) Ries, R. S.; Choi, H.; Blunck, R.; Bezanilla, F.; Heath, J. R. Black Lipid Membranes: Visualizing the Structure, Dynamics, and Substrate Dependence of Membranes. *J. Phys. Chem. B* **2004**, *108*, 16040-16049.
- (30) Sackmann, E. Supported Membranes: Scientific and Practical Applications. *Science* **1996**, *271*, 43-48.
- (31) Van Gelder, P.; Dumas, F.; Winterhalter, M. Understanding the Function of Bacterial Outer Membrane Channels by Reconstitution into Black Lipid Membranes. *Biophys. Chem.* **2000**, *85*, 153-167.
- (32) Wong, D.; Jeon, T. J.; Schmidt, J. Single Molecule Measurements of Channel Proteins Incorporated into Biomimetic Polymer Membranes. *Nanotechnology* **2006**, *17*, 3710-3717.
- (33) Winterhalter, M. Black Lipid Membranes. *Curr. Opin. Colloid. In.* **2000**, *5*, 250-255.
- (34) Kowal, J.; Zhang, X.; Dinu, I. A.; Palivan, C. G.; Meier, W. Planar Biomimetic Membranes Based on Amphiphilic Block Copolymers. *ACS Macro Letters* **2014**, *3*, 59-63.
- (35) Jones, M. C.; Leroux, J. C. Polymeric Micelles - a New Generation of Colloidal Drug Carriers. *Eur. J. Pharm. Biopharm.* **1999**, *48*, 101-111.
- (36) Torchilin, V. P. Recent Advances with Liposomes as Pharmaceutical Carriers. *Nat. Rev. Drug Discov.* **2005**, *4*, 145-160.
- (37) Tanner, P.; Baumann, P.; Enea, R.; Onaca, O.; Palivan, C.; Meier, W. Polymeric Vesicles: From Drug Carriers to Nanoreactors and Artificial Organelles. *Acc. Chem. Res.* **2011**, *44*, 1039-1049.
- (38) Renggli, K.; Baumann, P.; Langowska, K.; Onaca, O.; Bruns, N.; Meier, W. Selective and Responsive Nanoreactors. *Adv. Funct. Mat.* **2011**, *21*, 1241-1259.
- (39) Gonzalez-Perez, A.; Stibius, K. B.; Vissing, T.; Nielsen, C. H.; Mouritsen, O. G. Biomimetic Triblock Copolymer Membrane Arrays: A Stable Template for Functional Membrane Proteins. *Langmuir* **2009**, *25*, 10447-10450.
- (40) Langowska, K.; Kowal, J.; Palivan, C. G.; Meier, W. A General Strategy for Creating Self-Defending Surfaces for Controlled Drug Production for Long Periods of Time. *J. Mater. Chem. B* **2014**, *2*, 4684 - 4693.
- (41) Stoenescu, R.; Meier, W. Vesicles with Asymmetric Membranes from Amphiphilic ABC Triblock Copolymers. *Chem. Commun.* **2002**, 3016-3017.
- (42) Stoenescu, R.; Graff, A.; Meier, W. Asymmetric ABC-Triblock Copolymer Membranes Induce a Directed Insertion of Membrane Proteins. *Macromol. Biosci.* **2004**, *4*, 930-935.
- (43) Torchilin, V. P. Structure and Design of Polymeric Surfactant-Based Drug Delivery Systems. *J. Controlled Release* **2001**, *73*, 137-172.

- (44) Chemin, M.; Brun, P.-M.; Lecommandoux, S.; Sandre, O.; Le Meins, J.-F. Hybrid Polymer/Lipid Vesicles: Fine Control of the Lipid and Polymer Distribution in the Binary Membrane. *Soft Matter* **2012**, *8*, 2867-2874.
- (45) Le Meins, J. F.; Schatz, C.; Lecommandoux, S.; Sandre, O. Hybrid Polymer/Lipid Vesicles: State of the Art and Future Perspectives. *Mater. Today* **2013**, *16*, 397-402.
- (46) Chang, L. C.; Chang, Y. Y.; Gau, C. S. Interfacial Properties of Pluronics and the Interactions between Pluronics and Cholesterol/DPPC Mixed Monolayers. *J. Colloid Interface Sci.* **2008**, *322*, 263-273.
- (47) Leiske, D. L.; Meckes, B.; Miller, C. E.; Wu, C.; Walker, T. W.; Lin, B. H.; Meron, M.; Ketelson, H. A.; Toney, M. F.; Fuller, G. G. Insertion Mechanism of a Poly(ethylene oxide)-Poly(butylene oxide) Block Copolymer into a DPPC Monolayer. *Langmuir* **2011**, *27*, 11444-11450.
- (48) Nam, J.; Vanderlick, T. K.; Beales, P. A. Formation and Dissolution of Phospholipid Domains with Varying Textures in Hybrid Lipo-Polymersomes. *Soft Matter* **2012**, *8*, 7982-7988.
- (49) Schulz, M.; Glatte, D.; Meister, A.; Scholtysek, P.; Kerth, A.; Blume, A.; Bacia, K.; Binder, W. H. Hybrid Lipid/Polymer Giant Unilamellar Vesicles: Effects of Incorporated Biocompatible PIB-PEO Block Copolymers on Vesicle Properties. *Soft Matter* **2011**, *7*, 8100-8110.
- (50) Schulz, M.; Werner, S.; Bacia, K.; Binder, W. H. Controlling Molecular Recognition with Lipid/Polymer Domains in Vesicle Membranes. *Angew. Chem. Int. Edit.* **2013**, *52*, 1829-1833.
- (51) Thoma, J.; Belegirinou, S.; Rossbach, P.; Grzelakowski, M.; Kita-Tokarczyk, K.; Meier, W. Membrane Protein Distribution in Composite Polymer-Lipid Thin Films. *Chem. Commun.* **2012**, *48*, 8811-8813.
- (52) Franklin, B.; Brownrigg, W.; Farish, M. Of the Stilling of Waves by Means of Oil. Extracted from Sundry Letters between Benjamin Franklin, LL. DFRS William Brownrigg, MDRS and the Reverend Mr. Farish. *Philosophical Transactions* **1774**, *64*, 445-460.
- (53) Langmuir, I.: The constitution and fundamental properties of solids and liquids. II. Liquids. 1. *J. Am. Chem. Soc.* **1917**, *39*, 1848-1906.
- (54) Langmuir, I. The Mechanism of the Surface Phenomena of Flotation. *Trans. Faraday Soc.* **1920**, *15*, 62-74.
- (55) Ybert, C.; Lu, W. X.; Moller, G.; Knobler, C. M. Collapse of a Monolayer by Three Mechanisms. *J. Phys. Chem. B* **2002**, *106*, 2004-2008.
- (56) Girard-Egrot, A. P.; Godoy, S.; Blum, L. J. Enzyme Association with Lipidic Langmuir-Blodgett Films: Interests and Applications in Nanobioscience. *Adv. Colloid Interface Sci.* **2005**, *116*, 205-225.
- (57) Johann, R.; Vollhardt, D.; Mohwald, H. Shifting of Fatty Acid Monolayer Phases due to Ionization of the Headgroups. *Langmuir* **2001**, *17*, 4569-4580.

- (58) Kanicky, J. R.; Shah, D. O. Effect of Degree, Type, and Position of Unsaturation on the pK_a of Long-Chain Fatty Acids. *J. Colloid Interf. Sci.* **2002**, *256*, 201-207.
- (59) Marsden, J.; Rideal, E. K. On Monolayers of Isomeric Unsaturated Compounds. *J. Chem. Soc.* **1938**, 1163-1171.
- (60) Dynarowicz-Lątka, P.; Hąc-Wydro, K. Interactions Between Phosphatidylcholines and Cholesterol in Monolayers at the Air/Water Interface. *Colloids Surf. B* **2004**, *37*, 21-25.
- (61) Vié, V.; Van Mau, N.; Lesniewska, E.; Goudonnet, J. P.; Heitz, F.; Le Grimellec, C. Distribution of Ganglioside GM1 between Two-Component, Two-Phase Phosphatidylcholine Monolayers. *Langmuir* **1998**, *14*, 4574-4583.
- (62) Ma, G.; Allen, H. C. DPPC Langmuir Monolayer at the Air–Water Interface: Probing the Tail and Head Groups by Vibrational Sum Frequency Generation Spectroscopy. *Langmuir* **2006**, *22*, 5341-5349.
- (63) Haefele, T.; Kita-Tokarczyk, K.; Meier, W. Phase Behavior of Mixed Langmuir Monolayers from Amphiphilic Block Copolymers and an Antimicrobial Peptide. *Langmuir* **2006**, *22*, 1164-1172.
- (64) Baker, S. M.; Leach, K. A.; Devereaux, C. E.; Gragson, D. E. Controlled Patterning of Diblock Copolymers by Monolayer Langmuir-Blodgett Deposition. *Macromolecules* **2000**, *33*, 5432-5436.
- (65) Matmour, R.; Joncheray, T. J.; Gnanou, Y.; Duran, R. S. Two-Dimensional Polymeric Nanomaterials through Cross-Linking of Polybutadiene-*b*-Poly(ethylene oxide) Monolayers at the Air/Water Interface. *Langmuir* **2007**, *23*, 649-658.
- (66) Rosenholm, J. B.; Ihalainen, P.; Peltonen, J. Thermodynamic Characterization of Langmuir Monolayers of Thiolipids: A Conceptual Analysis. *Colloids Surf. A* **2003**, *228*, 119-130.
- (67) Tanaka, M.; Sackmann, E. Polymer-Supported Membranes as Models of the Cell Surface. *Nature* **2005**, *437*, 656-663.
- (68) Zhao, B.; Brittain, W. J. Polymer Brushes: Surface-Immobilized Macromolecules. *Prog. Polym. Sci.* **2000**, *25*, 677-710.
- (69) Barbey, R.; Lavanant, L.; Paripovic, D.; Schüwer, N.; Sugnaux, C.; Tugulu, S.; Klok, H.-A. Polymer Brushes via Surface-Initiated Controlled Radical Polymerization: Synthesis, Characterization, Properties, and Applications. *Chem. Rev.* **2009**, *109*, 5437-5527.
- (70) Zdyrko, B.; Luzinov, I. Polymer Brushes by the "Grafting to" Method. *Macromol. Rapid. Comm.* **2011**, *32*, 859-869.
- (71) Belegriinou, S.; Menon, S.; Dobrunz, D.; Meier, W. Solid-Supported Polymeric Membranes. *Soft Matter* **2011**, *7*, 2202-2210.
- (72) Matyjaszewski, K.; Xia, J. Atom Transfer Radical Polymerization. *Chem. Rev.* **2001**, *101*, 2921-2990.

- (73) Rakhmatullina, E.; Manton, A.; Bürgi, T.; Malinova, V.; Meier, W. Solid-Supported Amphiphilic Triblock Copolymer Membranes Grafted from Gold Surface. *J. Polym. Sci. A* **2009**, *47*, 1-13.
- (74) Boxer, S. G. Molecular Transport and Organization in Supported Lipid Membranes. *Curr. Opin. Chem. Biol.* **2000**, *4*, 704-709.
- (75) Kalb, E.; Frey, S.; Tamm, L. K. Formation of Supported Planar Bilayers by Fusion of Vesicles to Supported Phospholipid Monolayers. *Biochim. Biophys. Acta* **1992**, *1103*, 307-316.
- (76) Richter, R.; Mukhopadhyay, A.; Brisson, A. Pathways of Lipid Vesicle Deposition on Solid Surfaces: A Combined QCM-D and AFM Study. *Biophys. J.* **2003**, *85*, 3035-3047.
- (77) Richter, R. P.; Berat, R.; Brisson, A. R. Formation of Solid-Supported Lipid Bilayers: An Integrated View. *Langmuir* **2006**, *22*, 3497-3505.
- (78) Dorn, J.; Belegriou, S.; Kreiter, M.; Sinner, E.-K.; Meier, W. Planar Block Copolymer Membranes by Vesicle Spreading. *Macromol. Biosci.* **2011**, *11*, 514-525.
- (79) Rakhmatullina, E.; Meier, W. Solid-Supported Block Copolymer Membranes through Interfacial Adsorption of Charged Block Copolymer Vesicles. *Langmuir* **2008**, *24*, 6254-6261.
- (80) Richter, R. P.; Brisson, A. R. Following the Formation of Supported Lipid Bilayers on Mica: A Study Combining AFM, QCM-D, and Ellipsometry. *Biophys. J.* **2005**, *88*, 3422-3433.
- (81) Richter, R. P.; Him, J. L. K.; Brisson, A. Supported Lipid Membranes. *Mater. Today* **2003**, *6*, 32-37.
- (82) Itami, K.; Fujitani, H. Charge Characteristics and Related Dispersion/Flocculation Behavior of Soil Colloids as the Cause of Turbidity. *Colloids Surf. A* **2005**, *265*, 55-63.
- (83) Lee, S. W.; Laibinis, P. E. Protein-Resistant Coatings for Glass and Metal Oxide Surfaces Derived from Oligo(ethylene glycol)-Terminated Alkyltrichlorosilanes. *Biomaterials* **1998**, *19*, 1669-1675.
- (84) Lopez-Salido, I.; Lim, D. C.; Kim, Y. D. Ag Nanoparticles on Highly Ordered Pyrolytic Graphite (HOPG) Surfaces Studied using STM and XPS. *Surf. Sci.* **2005**, *588*, 6-18.
- (85) Belegriou, S.; Dorn, J.; Kreiter, M.; Kita-Tokarczyk, K.; Sinner, E.-K.; Meier, W. Biomimetic Supported Membranes from Amphiphilic Block Copolymers. *Soft Matter* **2010**, *6*, 179-186.
- (86) Girard-Egrot, A.; Blum, L. Langmuir-Blodgett Technique for Synthesis of Biomimetic Lipid Membranes. In *Nanobiotechnology of Biomimetic Membranes*; Martin, D., Ed.; Springer US, 2007; Vol. 1; pp 23-74.
- (87) Agarwal, V. K.: Langmuir-Blodgett Films. *Physics Today* **1988**, *41*, 40-46.

- (88) Brosseau, C. L.; Leitch, J.; Bin, X.; Chen, M.; Roscoe, S. G.; Lipkowski, J. Electrochemical and PM-IRRAS a Glycolipid-Containing Biomimetic Membrane Prepared Using Langmuir-Blodgett/Langmuir-Schaefer Deposition. *Langmuir* **2008**, *24*, 13058-13067.
- (89) Kita-Tokarczyk, K.; Junginger, M.; Belegirinou, S.; Taubert, A. Amphiphilic Polymers at Interfaces. *Self Organized Nanostructures of Amphiphilic Block Copolymers II* **2011**, *242*, 151-201.
- (90) Schwartz, D. K. Langmuir-Blodgett Film Structure. *Surf. Sci. Rep.* **1997**, *27*, 245-334.
- (91) Albertorio, F.; Diaz, A. J.; Yang, T. L.; Chapa, V. A.; Kataoka, S.; Castellana, E. T.; Cremer, P. S. Fluid and Air-Stable Lipopolymer Membranes for Biosensor Applications. *Langmuir* **2005**, *21*, 7476-7482.
- (92) Castellana, E. T.; Cremer, P. S. Solid Supported Lipid Bilayers: From Biophysical Studies to Sensor Design. *Surf. Sci. Rep.* **2006**, *61*, 429-444.
- (93) Holden, M. A.; Jung, S. Y.; Yang, T. L.; Castellana, E. T.; Cremer, P. S. Creating Fluid and Air-Stable Solid Supported Lipid Bilayers. *J. Am. Chem. Soc.* **2004**, *126*, 6512-6513.
- (94) Tanaka, M. Polymer-Supported Membranes: Physical Models of Cell Surfaces. *Mrs Bull* **2006**, *31*, 513-520.
- (95) Kita-Tokarczyk, K.; Grumelard, J.; Haefele, T.; Meier, W. Block Copolymer Vesicles—Using Concepts from Polymer Chemistry to Mimic Biomembranes. *Polymer* **2005**, *46*, 3540-3563.
- (96) Wang, J. Nanomaterial-Based Electrochemical Biosensors. *Analyst* **2005**, *130*, 421-426.
- (97) Natrajan, N.; Sheldon, B. W. Efficacy of Nisin-Coated Polymer Films to Inactivate Salmonella Typhimurium on Fresh Broiler Skin. *J. Food Protect.* **2000**, *63*, 1189-1196.
- (98) Fadnavis, N. W.; Bhaskar, V.; Kantam, M. L.; Choudary, B. M. Highly Efficient “Tight Fit” Immobilization of α -Chymotrypsin in Mesoporous MCM-41: A Novel Approach Using Precursor Immobilization and Activation. *Biotechnol. Progr.* **2003**, *19*, 346-351.
- (99) Bornscheuer, U. T. Immobilizing Enzymes: How to Create more Suitable Biocatalysts. *Angew. Chem. Int. Edit.* **2003**, *42*, 3336-3337.
- (100) Garcia-Galan, C.; Berenguer-Murcia, A.; Fernandez-Lafuente, R.; Rodrigues, R. C. Potential of Different Enzyme Immobilization Strategies to Improve Enzyme Performance. *Adv. Synth. Catal.* **2011**, *353*, 2885-2904.
- (101) Sheldon, R. A. Enzyme Immobilization: The Quest for Optimum Performance. *Adv. Synth. Catal.* **2007**, *349*, 1289-1307.

- (102) Gormally, M. V.; McKibben, R. K.; Johal, M. S.; Selassie, C. R. D. Controlling Tyrosinase Activity on Charged Polyelectrolyte Surfaces: A QCM-D Analysis. *Langmuir* **2009**, *25*, 10014-10019.
- (103) Kumar, M.; Grzelakowski, M.; Zilles, J.; Clark, M.; Meier, W. Highly Permeable Polymeric Membranes Based on the Incorporation of the Functional Water Channel Protein Aquaporin Z. *Proc. Natl. Acad. Sci.* **2007**, *104*, 20719-20724.
- (104) Hudson, S.; Cooney, J.; Magner, E. Proteins in Mesoporous Silicates. *Angew. Chem. Int. Edit.* **2008**, *47*, 8582-8594.
- (105) Qiu, H. J.; Xu, C. X.; Huang, X. R.; Ding, Y.; Qu, Y. B.; Gao, P. J. Immobilization of Laccase on Nanoporous Gold: Comparative Studies on the Immobilization Strategies and the Particle Size Effects. *J. Phys. Chem. C* **2009**, *113*, 2521-2525.
- (106) Zhou, X. Q.; Yu, T.; Zhang, Y. H.; Kong, J. L.; Tang, Y.; Marty, J. L.; Liu, B. H. Nanozeolite-Assembled Interface Towards Sensitive Biosensing. *Electrochem. Commun.* **2007**, *9*, 1525-1529.
- (107) Arica, M. Y.; Altintas, B.; Bayramoglu, G. Immobilization of Laccase onto Spacer-Arm Attached Non-Porous Poly(GMA/EGDMA) Beads: Application for Textile Dye Degradation. *Bioresour. Technol.* **2009**, *100*, 665-669.
- (108) Caseli, L.; Furriel, R. P. M.; de Andrade, J. F.; Leone, F. A.; Zaniquelli, M. E. D. Surface Density as a Significant Parameter for the Enzymatic Activity of Two Forms of Alkaline Phosphatase Immobilized on Phospholipid Langmuir–Blodgett Films. *J. Colloid Interface Sci.* **2004**, *275*, 123-130.
- (109) Kowal, J. Ł.; Kowal, J. K.; Wu, D.; Stahlberg, H.; Palivan, C. G.; Meier, W. P. Functional Surface Engineering by Nucleotide-Modulated Potassium Channel Insertion into Polymer Membranes Attached to Solid Supports. *Biomaterials* **2014**, *35*, 7286-7294.
- (110) Goennenwein, S.; Tanaka, M.; Hu, B.; Moroder, L.; Sackmann, E. Functional Incorporation of Integrins into Solid Supported Membranes on Ultrathin Films of Cellulose: Impact on Adhesion. *Biophys. J.* **2003**, *85*, 646-655.
- (111) Naumann, C. A.; Prucker, O.; Lehmann, T.; Ruhe, J.; Knoll, W.; Frank, C. W. The Polymer-Supported Phospholipid Bilayer: Tethering as a New Approach to Substrate-Membrane Stabilization. *Biomacromolecules* **2002**, *3*, 27-35.
- (112) Naumann, R.; Jonczyk, A.; Hampel, C.; Ringsdorf, H.; Knoll, W.; Bunjes, N.; Gräber, P. Coupling of Proton Translocation through ATPase Incorporated into Supported Lipid Bilayers to an Electrochemical Process. *Bioelectroch. Bioener.* **1997**, *42*, 241-247.
- (113) Gritsch, S.; Nollert, P.; Jähnig, F.; Sackmann, E. Impedance Spectroscopy of Porin and Gramicidin Pores Reconstituted into Supported Lipid Bilayers on Indium–Tin-Oxide Electrodes. *Langmuir* **1998**, *14*, 3118-3125.

- (114) Knoll, W.; Köper, I.; Naumann, R.; Sinner, E.-K. Tethered Bimolecular Lipid Membranes—A Novel Model Membrane Platform. *Electrochim. Acta* **2008**, *53*, 6680-6689.
- (115) Graneli, A.; Rydstrom, J.; Kasemo, B.; Hook, F. Formation of Supported Lipid Bilayer Membranes on SiO₂ from Proteoliposomes Containing Transmembrane Proteins. *Langmuir* **2003**, *19*, 842-850.
- (116) Discher, B. M.; Hammer, D. A.; Bates, F. S.; Discher, D. E. Polymer Vesicles in Various Media. *Curr. Opin. Colloid Interface Sci.* **2000**, *5*, 125-131.
- (117) Zhang, X. Y.; Fu, W. Y.; Palivan, C. G.; Meier, W. Natural Channel Protein Inserts and Functions in a Completely Artificial, Solid-Supported Bilayer Membrane. *Sci. Rep.* **2013**, *3*.
- (118) Chiu, P.-L.; Pagel, M. D.; Evans, J.; Chou, H.-T.; Zeng, X.; Gipson, B.; Stahlberg, H.; Nimigean, C. M. The Structure of the Prokaryotic Cyclic Nucleotide-Modulated Potassium Channel MloK1 at 16 Å Resolution. *Structure* **2007**, *15*, 1053-1064.
- (119) Kowal, J.; Chami, M.; Baumgartner, P.; Arheit, M.; Chiu, P.-L.; Rangl, M.; Scheuring, S.; Schröder, G. F.; Nimigean, C. M.; Stahlberg, H. Ligand-Induced Structural Changes in the Cyclic Nucleotide-Modulated Potassium Channel MloK1. *Nat. Commun.* **2014**, *5*, 3106.
- (120) Kaupp, U. B.; Seifert, R. Molecular Diversity of Pacemaker Ion Channels. *Annu. Rev. Physiol.* **2001**, *63*, 235-257.
- (121) Kaupp, U. B.; Seifert, R. Cyclic Nucleotide-Gated Ion Channels. *Physiol. Rev.* **2002**, *82*, 769-824.
- (122) Robinson, R. B. Hyperpolarization-Activated Cation Currents: From Molecules to Physiological Function. *Annu. Rev. Physiol.* **2003**, *65*, 453-480.
- (123) Rigaud, J.-L.; Lévy, D. Reconstitution of Membrane Proteins into Liposomes. In *Methods in Enzymology*; Nejat, D., Ed.; Academic Press, 2003; Vol. Volume 372; pp 65-86.
- (124) Dess, D. B.; Martin, J. C. Readily Accessible 12-I-5 Oxidant for the Conversion of Primary and Secondary Alcohols to Aldehydes and Ketones. *J. Org. Chem.* **1983**, *48*, 4155-4156.
- (125) Dunn, M. J.; Bradd, S. J. Separation and Analysis of Membrane Proteins by SDS-Polyacrylamide Gel Electrophoresis. In *T Biomembrane Protocols*, 1993; Vol. 19; pp 203-210.
- (126) Rath, A.; Glibowicka, M.; Nadeau, V. G.; Chen, G.; Deber, C. M. Detergent Binding Explains Anomalous SDS-PAGE Migration of Membrane Proteins. *Proc. Natl. Acad. Sci.* **2009**, *106*, 1760-1765.
- (127) Joncheray, T. J.; Bernard, S. A.; Matmour, R.; Lepoittevin, B.; El-Khoury, R. J.; Taton, D.; Gnanou, Y.; Duran, R. S. Polystyrene-b-poly(tert-butyl acrylate) and Polystyrene-b-poly(acrylic acid) Dendrimer-Like Copolymers: Two-Dimensional Self-Assembly at the Air-Water Interface. *Langmuir* **2007**, *23*, 2531-2538.

- (128) Kita-Tokarczyk, K.; Itel, F.; Grzelakowski, M.; Egli, S.; Rossbach, P.; Meier, W. Monolayer Interactions between Lipids and Amphiphilic Block Copolymers. *Langmuir* **2009**, *25*, 9847-9856.
- (129) Russell, T. P.: Copolymers at surfaces and interfaces. *Curr. Opin. Colloid Interface Sci.* **1996**, *1*, 107-115.
- (130) Ma, H.; Li, D.; Sheng, X.; Zhao, B.; Chilkoti, A. Protein-Resistant Polymer Coatings on Silicon Oxide by Surface-Initiated Atom Transfer Radical Polymerization. *Langmuir* **2006**, *22*, 3751-3756.
- (131) Domes, S.; Filiz, V.; Nitsche, J.; Frömsdorf, A.; Förster, S. Covalent Attachment of Polymersomes to Surfaces. *Langmuir* **2010**, *26*, 6927-6931.
- (132) Böhmeler, J.; Ploux, L.; Ball, V.; Anselme, K.; Ponche, A. Necessity of a Thorough Characterization of Functionalized Silicon Wafers before Biointerface Studies. *J. Phys. Chem. C* **2011**, *115*, 11102-11111.
- (133) Pasternack, R. M.; Rivillon Amy, S.; Chabal, Y. J.: Attachment of 3-(Aminopropyl)triethoxysilane on Silicon Oxide Surfaces: Dependence on Solution Temperature. *Langmuir* **2008**, *24*, 12963-12971.
- (134) Love, J. C.; Estroff, L. A.; Kriebel, J. K.; Nuzzo, R. G.; Whitesides, G. M. Self-Assembled Monolayers of Thiolates on Metals as a Form of Nanotechnology. *Chem. Rev.* **2005**, *105*, 1103-1169.
- (135) Seelig, A.; Gerebtzoff, G. Enhancement of Drug Absorption by Noncharged Detergents Through Membrane and P-glycoprotein Binding. *Expert Opin. Drug Metab. Toxicol.* **2006**, *2*, 733-752.
- (136) Itel, F.; Chami, M.; Najer, A.; Lorcher, S.; Wu, D. L.; Dinu, I. A.; Meier, W. Molecular Organization and Dynamics in Polymersome Membranes: A Lateral Diffusion Study. *Macromolecules* **2014**, *47*, 7588-7596.
- (137) Craven, K. B.; Zagotta, W. N. CNG and HCN Channels: Two Peas, One Pod. *Annu. Rev. Physiol.* **2006**, *68*, 375-401.
- (138) DeGrip, W. J.; VanOostrum, J.; Bovee-Geurts, P. H. M. Selective Detergent-Extraction from Mixed Detergent/Lipid/Protein Micelles, Using Cyclodextrin Inclusion Compounds: a Novel Generic Approach for the Preparation of Proteoliposomes. *Biochem. J.* **1998**, *330*, 667-674.
- (139) Knol, J.; Sjollem, K.; Poolman, B. Detergent-Mediated Reconstitution of Membrane Proteins. *Biochemistry* **1998**, *37*, 16410-16415.
- (140) Ritchie, T. K.; Grinkova, Y. V.; Bayburt, T. H.; Denisov, I. G.; Zolneric, J. K.; Atkins, W. M.; Sligar, S. G. Chapter 11 Reconstitution of Membrane Proteins in Phospholipid Bilayer Nanodiscs. In *Methods in Enzymology*; Nejat, D., Ed.; Academic Press, 2009; Vol. Volume 464; pp 211-231.
- (141) Shenoy, D. K.; Barger, W. R.; Singh, A.; Panchal, R. G.; Misakian, M.; Stanford, V. M.; Kasianowicz, J. J. Functional Reconstitution of Protein Ion Channels into Planar Polymerizable Phospholipid Membranes. *Nano Lett.* **2005**, *5*, 1181-1185.

- (142) Mari, S. A.; Pessoa, J.; Altieri, S.; Hensen, U.; Thomas, L.; Morais-Cabral, J. H.; Muller, D. J. Gating of the MlotiK1 Potassium Channel Involves Large Rearrangements of the Cyclic Nucleotide-Binding Domains. *Proc. Natl. Acad. Sci. USA* **2011**, *108*, 20802-20807.
- (143) Nimigean, C. M.; Shane, T.; Miller, C. A Cyclic Nucleotide Modulated Prokaryotic K⁺ Channel. *J. Gen. Physiol.* **2004**, *124*, 203-210.
- (144) Wydro, P.; Hąc-Wydro, K. Thermodynamic Description of the Interactions between Lipids in Ternary Langmuir Monolayers: the Study of Cholesterol Distribution in Membranes. *J. Phys. Chem. B* **2007**, *111*, 2495-2502.
- (145) Aroti, A.; Leontidis, E.; Maltseva, E.; Brezesinski, G. Effects of Hofmeister Anions on DPPC Langmuir Monolayers at the Air–Water Interface. *J. Phys. Chem. B* **2004**, *108*, 15238-15245.
- (146) Domenech, O.; Ignes-Muollol, J.; Montero, M. T.; Hernandez-Borrell, J. Unveiling a Complex Phase Transition in Monolayers of a Phospholipid from the Annular Region of Transmembrane Proteins. *J. Phys. Chem. B* **2007**, *111*, 10946-10951.
- (147) Amado, E.; Kerth, A.; Blume, A.; Kressler, J. Infrared Reflection Absorption Spectroscopy Coupled with Brewster Angle Microscopy for Studying Interactions of Amphiphilic Triblock Copolymers with Phospholipid Monolayers. *Langmuir* **2008**, *24*, 10041-10053.
- (148) Amado, E.; Blume, A.; Kressler, J.: Novel Non-Ionic Block Copolymers Tailored for Interactions with Phospholipids. *React. Funct. Polym.* **2009**, *69*, 450-456.
- (149) Korchowiec, B.; Paluch, M.; Corvis, Y.; Rogalska, E. A Langmuir Film Approach to Elucidating Interactions in Lipid Membranes: 1,2-dipalmitoyl-sn-glycero-3-phosphoethanolamine/Cholesterol/Metal Cation Systems. *Chem. Phys. Lipids* **2006**, *144*, 127-136.
- (150) Jagoda, A.; Zinn, M.; Meier, W.; Kita-Tokarczyk, K. Head Group Influence on Lipid Interactions With a Polyhydroxyalkanoate Biopolymer. *Macromol. Chem. Phys.* **2012**, *213*, 1922-1932.
- (151) Matter, Y.; Enea, R.; Casse, O.; Lee, C. C.; Baryza, J.; Meier, W. Amphiphilic PEG-b-PMCL-b-PDMAEMA Triblock Copolymers: From Synthesis to Physico-Chemistry of Self-Assembled Structures. *Macromol. Chem. Phys.* **2011**, *212*, 937-949.
- (152) Madhavi, V.; Lele, S. S. Laccase: Properties and Applications. *Bioresources* **2009**, *4*, 1694-1717.
- (153) Couto, S. R.; Herrera, J. L. T. Industrial and Biotechnological Applications of Laccases: A review. *Biotechnol. Adv.* **2006**, *24*, 500-513.
- (154) Bourbonnais, R.; Paice, M. G.; Reid, I. D.; Lanthier, P.; Yaguchi, M. Lignin Oxidation by Laccase Isozymes from *Trametes Versicolor* and Role of the Mediator 2,2'-Azinobis(3-Ethylbenzthiazoline-6-Sulfonate) in Kraft Lignin Depolymerization. *Appl. Environ. Microb.* **1995**, *61*, 1876-1880.

- (155) Howarter, J. A.; Youngblood, J. P. Self-Cleaning and Anti-Fog Surfaces via Stimuli-Responsive Polymer Brushes. *Adv. Mater.* **2007**, *19*, 3838-+.
- (156) Gupta, S.; Agrawal, M.; Conrad, M.; Hutter, N. A.; Olk, P.; Simon, F.; Eng, L. M.; Stamm, M.; Jordan, R. Poly(2-(dimethylamino)ethyl methacrylate) Brushes with Incorporated Nanoparticles as a SERS Active Sensing Layer. *Adv. Funct. Mater.* **2010**, *20*, 1756-1761.
- (157) Mahltig, B.; Gohy, J. F.; Antoun, S.; Jerome, R.; Stamm, M. Adsorption and Structure Formation of the Weak Polyelectrolytic Diblock Copolymer, PVP-b-PDMAEMA. *Colloid Polym. Sci.* **2002**, *280*, 495-502.
- (158) Wang, M. F.; Zou, S.; Guerin, G.; Shen, L.; Deng, K. Q.; Jones, M.; Walker, G. C.; Scholes, G. D.; Winnik, M. A. A Water-Soluble pH-Responsive Molecular Brush of Poly(N,N-dimethylaminoethyl methacrylate) Grafted Polythiophene. *Macromolecules* **2008**, *41*, 6993-7002.
- (159) Vogt, B. D.; Lin, E. K.; Wu, W. L.; White, C. C. Effect of Film Thickness on the Validity of the Sauerbrey Equation for Hydrated Polyelectrolyte Films. *J. Phys. Chem. B* **2004**, *108*, 12685-12690.
- (160) Mazur, M.; Krysiński, P.; Michota-Kamińska, A.; Bukowska, J.; Rogalski, J.; Blanchard, G. J. Immobilization of Laccase on Gold, Silver and Indium Tin Oxide by Zirconium-Phosphonate-Carboxylate (ZPC) Coordination Chemistry. *Bioelectrochem.* **2007**, *71*, 15-22.
- (161) Fogel, R.; Limson, J. L. Probing Fundamental Film Parameters of Immobilized Enzymes—Towards Enhanced Biosensor Performance. Part I—QCM-D Mass and Rheological Measurements. *Enzyme Microb. Technol.* **2011**, *49*, 146-152.
- (162) Piontek, K.; Antorini, M.; Choinowski, T. Crystal Structure of a Laccase from the Fungus *Trametes versicolor* at 1.90-Å Resolution Containing a Full Complement of Coppers. *J. Biol. Chem.* **2002**, *277*, 37663-37669.
- (163) Deere, J.; Magner, E.; Wall, J. G.; Hodnett, B. K. Mechanistic and Structural Features of Protein Adsorption onto Mesoporous Silicates. *J. Phys. Chem. B* **2002**, *106*, 7340-7347.
- (164) Hartmann, M.; Jung, D. Biocatalysis with Enzymes Immobilized on Mesoporous Hosts: the Status quo and Future Trends. *J. Mater. Chem.* **2010**, *20*, 844-857.
- (165) Kallio, J. P.; Auer, S.; Jänis, J.; Andberg, M.; Kruus, K.; Rouvinen, J.; Koivula, A.; Hakulinen, N. Structure-Function Studies of a *Melanocarpus albomyces* Laccase Suggest a Pathway for Oxidation of Phenolic Compounds. *J. Mol. Biol.* **2009**, *392*, 895-909.
- (166) Wang, H.; Chen, S.; Li, L.; Jiang, S. Improved Method for the Preparation of Carboxylic Acid and Amine Terminated Self-Assembled Monolayers of Alkanethiolates. *Langmuir* **2005**, *21*, 2633-2636.

Curriculum Vitae

PERSONAL DATA

Name	Justyna Kowal
Date and place of Birth	28 th February 1986 in Kraków, Poland
Nationality	Polish

EDUCATION

10.2010 – 02.2015	PhD in Physical Chemistry, Supervisor: Prof. Dr. Wolfgang Meier Department of Chemistry, University of Basel, Basel, Switzerland <i>“Solid-supported biomimetic membranes based on amphiphilic block copolymers”</i>
10.2005 – 06.2010	MSc in Chemistry, Supervisor: Prof. Dr. Szczepan Zapotoczny Department of Chemistry, Jagiellonian University, Kraków, Poland <i>“Synthesis and characterization of conductive polymer brushes by self-templating surface-initiated polymerization”</i>
09.2002 – 06.2005	Secondary School, Jan III Sobieski 2 nd General College, Kraków, Poland

EXPERIENCE

10.2010 – 02.2015	Research Assistant, University of Basel, Switzerland Group of Prof. Dr. Wolfgang Meier
01.2011 – 12.2014	Teaching Assistant, University of Basel, Switzerland
09.2009	Intern, Polish Academy of Science, Kraków, Poland
03.2009 – 08.2010	Research Assistant, Jagiellonian University, Kraków, Poland Group of Prof. Dr. Szczepan Zapotoczny
10.2008 – 02.2009	Erasmus Fellow, EPFL, Lausanne, Switzerland Group of Prof. Dr. Harm-Anton Klok

PUBLICATIONS

1. **Justyna Kowal**, Dalin Wu, Viktoria Mikhalevich, Cornelia G. Palivan, Wolfgang Meier, *Hybrid polymer-lipid films as platforms for directed membrane protein insertion*, accepted in Langmuir (**2015**)
2. **Justyna Kowal**, Julia Kowal, Dalin Wu, Henning Stahlberg, Cornelia G. Palivan, and Wolfgang Meier, *Functional surface engineering by nucleotide-modulated potassium channel insertion into polymer membranes attached to solid supports* Biomaterials **2014**, 35, 7286-94
3. Karolina Langowska, **Justyna Kowal**, Cornelia G. Palivan, and Wolfgang Meier, *A general strategy for creating self-defending surfaces for controlled drug production for long periods of time* Journal of Materials Chemistry B **2014**, 2, 4684-93
4. Camelia L. Draghici*, **Justyna Kowal***, Alina Darjan, Wolfgang Meier, and Cornelia Palivan, "Active surfaces" formed by immobilization of enzymes on solid-supported polymer membranes Langmuir **2014**, 30 (39), p 11660–9
5. **Justyna Kowal***, Xiaoyan Zhang*, Ionel A. Dinu, Cornelia G. Palivan, and Wolfgang Meier, *Planar biomimetic membranes based on amphiphilic block copolymers* ACS Macro Letters **2014**, 3, 59-63
6. Michał Szuwarzyński, **Justyna Kowal**, and Szczepan Zapotoczny, *Self-templating surface-initiated polymerization: a route to synthesize conductive brushes* Journal of Materials Chemistry **2012**, 22, 20179-81
7. Marc A. Gauthier, Maxime Ayer, **Justyna Kowal**, Frederik R. Wurm, and Harm-Anton Klok, *Arginine-specific protein modification using α -oxo-aldehyde functional polymers prepared by atom transfer radical polymerization* Polymer Chemistry **2011**, 2, 1490-8

* Authors contributed equally

BOOK CHAPTER

1. Agnieszka Jagoda, **Justyna Kowal**, Mihaela Delcea, Cornelia G. Palivan, and Wolfgang Meier, *Polymer vesicles on surfaces* in Biomaterials Surface Science, 159-203 (Wiley-VCH Verlag GmbH & Co. KGaA, **2013**)

ORAL AND POSTER PRESENTATIONS

Oral talks

1. Justyna Kowal, Wolfgang Meier, 7th Swiss Soft Days, Lausanne, 13th February 2012
2. Justyna Kowal, Julia Kowal, Dalin Wu, Henning Stahlberg, Cornelia G. Palivan, Wolfgang Meier, Swiss Chemical Society Fall Meeting 2014, Zürich, Switzerland, 11th September 2014
3. Justyna Kowal, Julia Kowal, Dalin Wu, Henning Stahlberg, Cornelia G. Palivan, Wolfgang Meier, 2nd International Conference on Biobased and Bioinspired Chemistry and Materials, Nice, France, 15th – 17th October 2014

Poster presentations

1. Justyna Kowal, Karolina Langowska, Wolfgang Meier, inet, NanoEvent “NextNanoStars”, Basel, Switzerland, 21st March 2013
2. Justyna Kowal, Wolfgang Meier, PolyColl, Basel, Switzerland, 7th June 2013
3. Justyna Kowal, Wolfgang Meier, European Polymer Congress, Pisa, Italy, 16th – 21st June 2013
4. Justyna Kowal, Wolfgang Meier, Swiss Chemical Society Fall Meeting 2013, Lausanne, Switzerland, 6th September 2013
5. Justyna Kowal, Julia Kowal, Dalin Wu, Henning Stahlberg, Cornelia G. Palivan, Wolfgang Meier, 13th Swiss Soft Day, Basel, 6th June 2014
6. Justyna Kowal, Julia Kowal, Dalin Wu, Henning Stahlberg, Cornelia G. Palivan, Wolfgang Meier, Swiss Chemical Society Fall Meeting 2014, Zürich, Switzerland, 11th September 2014
7. Justyna Kowal, Camelia Draghici, Alina Darjan, Wolfgang Meier, and Cornelia Palivan, 15th Swiss Soft Day, Lausanne, 2nd October 2014